

University of Southern Queensland
Faculty of Health, Engineering & Sciences

**Compressive Behaviour of Short Engineered Cementitious Composite Columns
Containing Recycled Polyethylene Terephthalate Aggregate**

A dissertation submitted by

Thomas Gough

in fulfilment of the requirements of

ENG4111 and ENG4112 Research Project

towards the degree of

Bachelor of Engineering (Honours) (Civil)

Submitted: October 2022

ABSTRACT

Polyethylene terephthalate (PET) plastic waste is a significant environmental problem. Research has shown that sequestering this waste as a lightweight recycled aggregate in conventional concrete is promising. However, conventional concrete is brittle and has a durability problem.

Engineered cementitious composites (ECC) also known as bendable concrete are a highly durable and ductile fibre-reinforced concrete construction material, typically requiring ultra-fine manufactured sand with high cement contents. Consequently, it is costly to produce and has a significant environmental impact. Recycled aggregates can reduce environmental impacts and could help reduce costs.

This study is the first to evaluate the performance of new high fly ash composites utilising locally available natural sand and recycled PET granule aggregates. A control using natural sand was compared to trials volumetrically replacing sand with 10%, 30% and 50% PET granules. A three-step mixing process and a high-shear pan mixer were used to optimise the performance of the composites.

Flexural beams were formed to assess flexural strength and briquette specimens were formed to assess the uniaxial tensile strength of each trial. Cylinder test specimens were formed to evaluate the indirect tensile strength as well as the glass fibre confined and unconfined strength of short columns.

The results indicate that a lightweight strain-hardening composite is achievable using locally available sand and PET granules. Generally, the tensile strain capacity and ultimate strength were reduced as the PET content increased. The compressive strength was reduced by more than 20% with PET granules but an increase in strength with the replacement ratio was observed. The ductility of the columns was increased by 48% with PET granules and a single layer of confinement equalised the ductility between all PET replacement ratios.

Natural sand and recycled PET granules were found to produce a high fly ash ECC with acceptable mechanical properties and short columns with low weight and excellent ductility. Adequate mixing and tailoring of the mixture design would assist researchers to realise the full potential of these new more environmentally friendly engineered composites.

University of Southern Queensland
Faculty of Health, Engineering & Sciences

ENG4111 & ENG4112 Research Project

Limitations of Use

The Council of the University of Southern Queensland, its Faculty of Health, Engineering & Sciences, and the staff of the University of Southern Queensland do not accept any responsibility for the truth, accuracy or completeness of material contained within or associated with this dissertation.

Persons using all or any part of this material do so at their own risk, and not at the risk of the Council of the University of Southern Queensland, its Faculty of Health, Engineering & Sciences, or the staff of the University of Southern Queensland.

This dissertation reports an educational exercise and has no purpose or validity beyond this exercise. The sole purpose of the course pair entitled "Research Project" is to contribute to the overall education within the student's chosen degree program. This document, the associated hardware, software, drawings, and other material set out in the associated appendices should not be used for any other purpose: if they are so used, it is entirely at the risk of the user.

University of Southern Queensland
Faculty of Health, Engineering & Sciences

ENG4111 & ENG4112 Research Project

Certification of Dissertation

I certify that the ideas, designs and experimental work, results, analyses, and conclusions set out in this dissertation are entirely my own effort, except where otherwise indicated and acknowledged.

I further certify that the work is original and has not been previously submitted for assessment in any other course or institution, except where specifically stated.

THOMAS GOUGH



ACKNOWLEDGMENTS

I would like to thank my supervisor Prof. Weena Lokuge for her guidance, support, and assistance throughout the project.

Thanks also to Wayne Crowell, from the University of Southern Queensland for his valuable guidance and assistance throughout the testing phase of the project. Thank you to the University of Southern Queensland for providing access to testing laboratories and equipment.

This project would not have been possible without the generous assistance from Wagners, who provided the laboratory access, equipment, raw materials, and assistance necessary to carry out the experimental phase of the project.

Finally, I would like to thank my family for their loving support throughout this research project, and my engineering journey at the University of Southern Queensland.

TABLE OF CONTENTS

Abstract.....	i
Acknowledgments	iv
Table of Contents	v
List of Figures.....	ix
List of Tables	xii
NOMENCLATURE.....	xiii
CHAPTER 1. Introduction	15
1.2 The Problem	18
1.3 Research Objectives	18
1.4 Expected Outcomes.....	19
1.5 Thesis Outline	20
CHAPTER 2. Literature Review.....	21
2.1 Background	21
2.2 ECC Using Alternate Materials.....	23
2.3 PET Aggregate Concrete Performance	25
2.4 PET Aggregate Concrete Properties	26
2.4.1 PET-Cement Interaction	26
2.4.2 Workability	27
2.4.3 Compressive Strength	28
2.4.4 Splitting Tensile Strength and Uniaxial Tensile Strength.....	30
2.4.5 Flexural Strength.....	31
2.5 Improving the properties of PET-ECC.....	32
2.5.1 Mixture Design	33
2.5.2 Mixing Methods.....	34
2.5.3 Curing	35

2.6	GFRP Confined Concrete and Composites	36
2.7	Numerical Investigation and Modelling.....	37
2.8	Summary	38
2.8.1	Knowledge Gaps	39
CHAPTER 3.	Methodology.....	40
3.1	Outline.....	40
3.2	Assumptions	41
3.3	Limitations	41
3.4	ECC Matrix	41
3.5	Fine Aggregate Selection	42
3.6	Producing Laboratory Specimens	43
3.6.1	ECC Mixing	43
3.6.2	Specimen Details	44
3.6.3	Specimen Casting.....	46
3.6.4	Curing Conditions.....	46
3.7	Experimental Testing	47
3.7.1	Assessing Rheological Properties	47
3.7.2	Tensile Testing.....	49
3.7.3	Flexural Testing	50
3.7.4	Compression Testing	51
3.8	Numerical Modelling	53
CHAPTER 4.	Experimental Investigation.....	54
4.1	Materials.....	54
4.2	Particle Size Distribution	58
4.3	Material Quantities.....	61
4.4	Sample Preparation	63
4.4.1	Trial Batch	63

4.4.2	Mixing and Casting.....	63
4.4.3	End Grinding.....	67
4.4.4	GFRP Wrapping.....	69
4.4.5	Attaching Lateral Strain Gauges	70
4.5	Experimental Testing	71
4.5.1	Tensile Testing.....	71
4.5.2	Flexural Testing	74
4.5.3	Compression Testing	76
CHAPTER 5. Numerical Investigation.....		79
5.1	Model Development.....	79
5.2	Material Simulation.....	80
5.2.1.	Concrete Damaged Plasticity	80
CHAPTER 6. Results and Discussion		83
6.1	Limitations	83
6.2	Fresh Concrete Testing.....	83
6.2.1	Mortar Rheology	83
6.2.2	ECC Matrix Rheology	86
6.3	ECC Density.....	87
6.4	Tensile Testing	87
6.4.1	Uniaxial Tensile Strength	87
6.4.2	Splitting Tensile Strength	90
6.5	Flexural Strength	92
6.6	Compression Testing.....	96
6.6.1	Compressive Strength	96
6.6.2	Stress-Strain Behaviour	98
6.6.3	Column Ductility	104
6.6.4	Modulus of Elasticity	106

6.7	Scanning Electron Microscopy (SEM) Investigation.....	107
6.8	Numerical Investigation	110
CHAPTER 7. Conclusion.....		111
7.1	Summary	111
7.2	Future Research.....	113
List of References.....		115
Appendix A – Project Specification.....		122
Appendix B – Risk Management		123
Appendix C – Consequences and Ethics.....		126
Appendix D – Material Test Report.....		127
Appendix E – Experimental Data.....		128
Appendix F – Project Plan		133

LIST OF FIGURES

Figure 1.1 – Tensile stress vs strain for common cementitious materials (Ma et al. 2021)	16
Figure 1.2 – HFA-ECC residual crack width to fly ash content (Yang et al. 2007).....	17
Figure 2.1 – Typical Bridging Stress vs Crack Opening Curve for Strain Hardening Composites (Wang & Li 2007).....	22
Figure 2.2 - PET Concrete Compressive Strength Variation at 28 days	29
Figure 2.3 – PET Concrete Splitting Tensile Strength Variation at 28 days	30
Figure 2.5 – Compressive Strength of HFA-ECC given Fly Ash Content and Age (Yang et al. 2007)	34
Figure 3.1 – Bennett equipment pan mixer.....	44
Figure 3.2 – Briquette gang mould (1) and individual mould dimensions in inches (The American Society for Testing and Materials, 1999).....	45
Figure 3.3 – Typical sump flow test (Standards Australia, 2015)	47
Figure 3.4 – Custom made flow funnel used to indicate plastic viscosity.....	48
Figure 3.5 – Typical indirect tensile test jig arrangement (Standards Australia, 2000b)	49
Figure 3.6 – Uniaxial testing apparatus	50
Figure 3.7 – Suitable flexure testing apparatus governed by clause 5 measurements (Standards Australia, 2000a).....	51
Figure 3.8 – Compression testing setup.....	52
Figure 4.1 – Example particle sizes of the fine PET aggregate fraction.....	54
Figure 4.2 – RECS15 PVA fibre.....	55
Figure 4.3 – Grade 1 fly ash.....	56
Figure 4.4 –Rockwell medium quartz sand	57
Figure 4.5 – Separation of PET granules into three size fractions.....	59
Figure 4.6 – Particle size distribution sampling of fine PET	59
Figure 4.7 – Particle size distribution of PET and medium sand.....	60
Figure 4.8 – ECC slump flow tests a) 0% PET-ECC, b) 50% PET-ECC.....	64
Figure 4.9 – Flexural specimens cast and covered in custom made form ply moulds	65
Figure 4.10 – Cylinder and briquette specimens’ initial cure	65
Figure 4.11 – Control batch cylinder paste loss and table accumulation.....	66
Figure 4.12 – Several PET-ECC specimens in the UniSQ fog room	66
Figure 4.13 – Average cylinder heights and standard deviation before end grinding	67
Figure 4.14 – Cylinder bleeding defect in 10% PET-ECC.....	68

Figure 4.15 – Cylinder height variations in the control batch	68
Figure 4.16 – a) top, b) side of all cylinders cut level to 170 mm height	69
Figure 4.17 – GFRP wrapped cylinders.....	70
Figure 4.18 – Compression cylinders ready for testing	71
Figure 4.19 – Batch 1 control splitting tensile testing	72
Figure 4.20 – Hounsfield H5KS testing machine	73
Figure 4.21 – Equipment validation of flexural testing apparatus	74
Figure 4.22 – Flexural test data validation.....	75
Figure 4.23 – Equilibrium forces acting on beam specimen	75
Figure 4.24 – Control GFRP cylinder under compression with centralized fibre rupture.....	77
Figure 4.25 – Typical curves for ductility factor measurement (Lokuge & Karunasena 2016)	78
Figure 5.1 – GFRP (S4R) wrapped cylinder with infill protrusion	79
Figure 5.2 – ABAQUS model development	80
Figure 5.3 – Stress-strain and damage-strain relationships for the control ECC.....	81
Figure 5.4 – Behaviour of column infill under a) tension and b) compression (Otoom et al. 2021)	82
Figure 6.1 – Indicative mortar rheological properties	83
Figure 6.2 – 50% PET-ECC mortar aggregates stuck in flow cone	84
Figure 6.3 – Mortar matrix mini-slump tests: a) 30% PET content, b) 50% PET content	85
Figure 6.4 – In pan mortar reaction with 50% PET content	85
Figure 6.5 – Mini-slump tests: a) control, b) 10%, c) 30% and d) 50% PET	86
Figure 6.6 – Average density results.....	87
Figure 6.7 – Tensile stress-strain curve of PET-ECC at 28 days.....	88
Figure 6.8a – Stereo microscope image of a control briquet with residual cracks highlighted	89
Figure 6.8b – Cracking of a control briquet at failure	89
Figure 6.9 – Cracking of 50% PET at failure with visible cracks highlighted	90
Figure 6.10 – Comparison of splitting tensile strength.....	91
Figure 6.11 – Strongest specimen cracks at failure	92
Figure 6.12 – Comparison of all flexural load-deflection behaviours	92
Figure 6.13 – Characteristic flexural tension failure a) control, b) 30% PET-ECC	93
Figure 6.14 – Residual beam failure patterns with fibre bridging highlighted.....	94
Figure 6.15 – Comparison of all flexural results	95

Figure 6.17 – Compressive strength of confined and unconfined short ECC columns	97
Figure 6.18 – Unconfined and confined control stress-strain behaviour	99
Figure 6.19 – Unconfined and confined control failure patterns	99
Figure 6.20 – Unconfined and confined 10% PET-ECC stress-strain behaviour.....	100
Figure 6.21 – Unconfined and confined 10% PET-ECC failure patterns.....	100
Figure 6.22 – Unconfined and confined 30% PET-ECC stress-strain behaviour.....	101
Figure 6.23 – Unconfined and confined 30% PET-ECC failure patterns.....	101
Figure 6.25 – Unconfined and Confined 50% PET-ECC failure patterns	102
Figure 6.26 – Comparison of all unconfined column tests	103
Figure 6.27 – Comparison of unconfined tests	104
Figure 6.28 – Comparison of column ductility	104
Figure 6.29 – Comparison of all GFRP confined column tests	105
Figure 6.30 – Modulus of elasticity values	106
Figure 6.31 – Degraded PET granule surface at: a) 200 times magnification, and b) 500 times magnification	107
Figure 6.32 – Relatively smooth and intact PET surface at 300 times magnification.....	107
Figure 6.33 – Fibre matrix interface of 50% PET-ECC at 32 days	108
Figure 6.34 – PET matrix interface of 50% PET-ECC at 32 days	109
Figure 6.35 – Control stress-strain FE model validation	110
Figure D-1 – Millmerran fly ash testing report.....	127

LIST OF TABLES

Table 4.1 – PET granule properties	54
Table 4.2 – Standard RECS 15 properties	55
Table 4.3 – Typical Millmerran grade 1 fly ash quality parameters.....	56
Table 4.4 –Medium quartz sand properties.....	57
Table 4.5 – Medium sand PSD and grading limits	58
Table 4.6 – Fine PET granules PSD	60
Table 4.7 – ECC volume calculations.....	61
Table 4.8 – HFA-ECC mixture proportions	61
Table 4.9 – PET-ECC mixture proportions	62
Table 4.10 – PET-ECC material quantity	62
Table 4.11 – WEST SYSTEM 105 epoxy resin and 206 slow hardener properties	70
Table 5.1 – CDP model elasticity input parameters	81
Table B-1 – Risk matrix.....	123
Table B-2 – Experimental risk assessment	124
Table B-3 – Project risk assessment	125
Table E.1 – Cylinder height results.....	128
Table E.2 – Fresh testing	129
Table E.3 – Uniaxial tensile test data.....	130
Table E.4 – Splitting tensile test data.....	130
Table E.5 – Flexural beam properties	131
Table E.6 – Flexural beam test data.....	131
Table E.7 – Compressive column properties	132
Table E.8 – Compression testing results and analysis	132
Table F-1 – Project plan.....	133

NOMENCLATURE

ECC – Engineered Cementitious Composite

FEM – Finite element model

FRP – Fibre reinforced polymer

GFRP – Glass fibre-reinforced polymer

HFA-ECC – High fly ash ECC

HRWR – High Range Water Reducer

ITZ – Interfacial Transition Zone

NA – Natural Aggregate

OPC – Ordinary Portland Cement

PET – Polyethylene Terephthalate

PET-ECC – SEQ-ECC with Recycled PET Aggregates

PSD – Particle size distribution

SEQ-ECC – HFA-ECC with Natural Southeast Queensland Sand Aggregate

USS – Ultrafine silica sand

W/b – Ratio of water to binder (I.e., cement + fly ash)

W/c – Ratio of water to cement

CHAPTER 1. INTRODUCTION

The origins of modern Portland cement are often traced back to the year 1824 when British bricklayer Joseph Aspdin formalised his experimental heating of limestone and clay until they were calcined. When crushed into a fine powder the mix reacted with water through hydration and he observed significant hardening. Due to similarities with stone quarried on the Isle of Portland, Aspdin named his finding ‘Portland Cement’ (Nobis 2022). What Aspdin found in 1824 has evolved to become the main component in a highly utilised construction material, concrete.

Concrete typically utilises ordinary Portland cement (OPC) as a binder of fine and coarse aggregates. Different proportions and additives can be used to maximise the desired hardened properties. Globally, the production of concrete is the third largest single source of carbon dioxide emissions, representing 8% of total global emissions (Andrew 2018). To meet the goals of net zero emissions by 2050, this source of emission requires significant action.

Plastic waste is also a significant environmental problem. In 2018 alone, Australia consumed more than 350,000 metric tons of polyethylene terephthalate (PET) plastics, of which only 21% was recovered (O'Farrell 2020). The quantity of inappropriately disposed plastics is expected to grow and can have dramatic impacts on ecosystems and human health. For this reason, research has focused on sequestering this potential source of lightweight aggregate in ordinary concrete. There have been several promising results (Silva et al. 2013; Bamigboye et al. 2021; Kangavar et al. 2022).

Emissions of concrete are linked to the production of OPC and a lesser extent, the sourcing of natural aggregates. To this end, many areas of research exist to find greener production methods. Critically, the reduction or removal of the reliance on OPC through the utilisation of industrial waste products such as fly ash and slag has been well studied (Wang & Li 2007; Lokuge & Karunasena 2016; Zhang et al. 2020; Chithambar Ganesh et al. 2021). Secondly, the reduction or substitution of natural aggregates with waste or recycled sources such as PET flakes and granules has also been studied (Choi et al. 2005; Saikia & de Brito 2012; Ataei et al. 2017; Bamigboye et al. 2021; Tayeh et al. 2021; Kangavar et al. 2022).

Engineered cementitious composites (ECC), also known as bendable concrete, are a unique type of high-performance fibre-reinforced concrete (FRC) that has been optimised for high performance based on micromechanical principles (Li et al. 2001; Li 2003). Unlike ordinary

concrete or other types of FRC, ECC develops a metal-like pseudo strain hardening behaviour and is characterised by multiple cracking with a tensile strain capacity of 1-8% (Li et al. 2001; Li 2003; Wang & Li 2007; Nawy 2008; Ma et al. 2021). This key difference is highlighted in Figure 1.1.

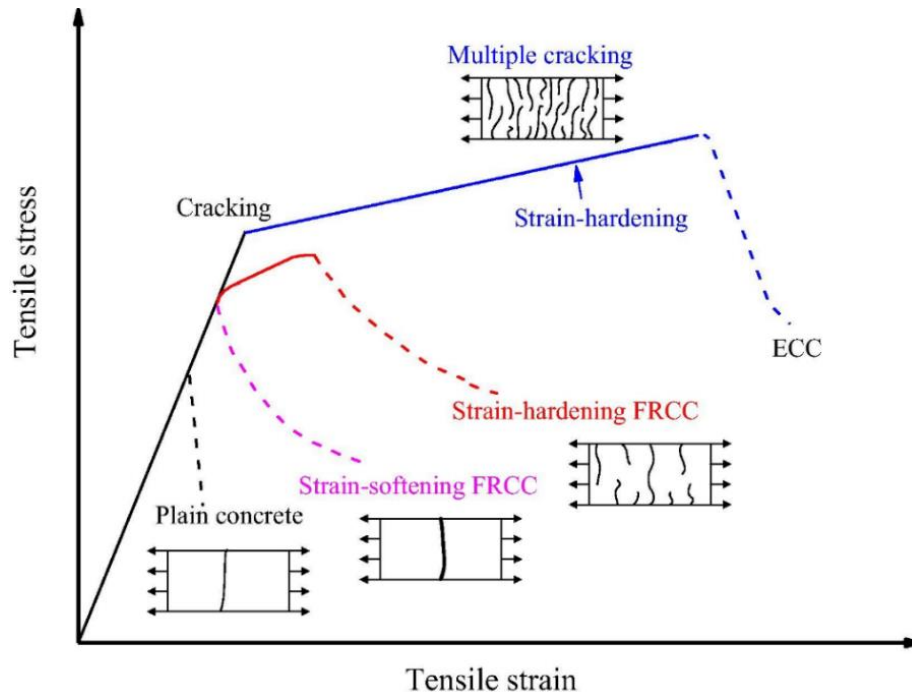


Figure 1.1 – Tensile stress vs strain for common cementitious materials (Ma et al. 2021)

Over the life cycle of a reinforced concrete structure, ECC could drastically improve durability and tensile loading capacity (Sahmaran et al. 2007; Nawy 2008; Şahmaran & Li 2008). Conventional concrete can achieve high durability but is typically more brittle due to a higher strength requirement. By contrast, ECC has high durability and self-healing ability by design because of controlled microcracking under tensile loads (Nawy 2008; Nicolaidis et al. 2015). Many benefits and reasons for structural implementation exist, namely ECC can overcome several long-term durability issues common to reinforced concrete structures today (Guan et al. 2018).

The trade-off for this high ductility and durable cementitious material is high economic and environmental costs as well as production quality assurance challenges (Yang et al. 2009). ECC generally requires expensive ultrafine silica sand (USS), admixtures, polyvinyl alcohol (PVA)

fibres, and a cement content two to three times higher than normal structural concrete. The cement content and types of fibre used in ECC are a large source of emissions (Ohno & Li 2018).

To combat these emissions, research into the development of high fly ash green ECC (HFA-ECC) has found several benefits beyond recycling an industrial waste source and its associated environmental impacts (Yang et al. 2007; Zhu et al. 2014; Shoji et al. 2022). Due to a weakening of the interfacial transition zone (ITZ) fly ash can improve strain hardening potential, and durability (Wang & Li 2007; Yang et al. 2007). Figure 1.2 shows the correlation between residual crack width (μm) and the fly ash-to-cement ratio as observed by Yang et al. (2007).

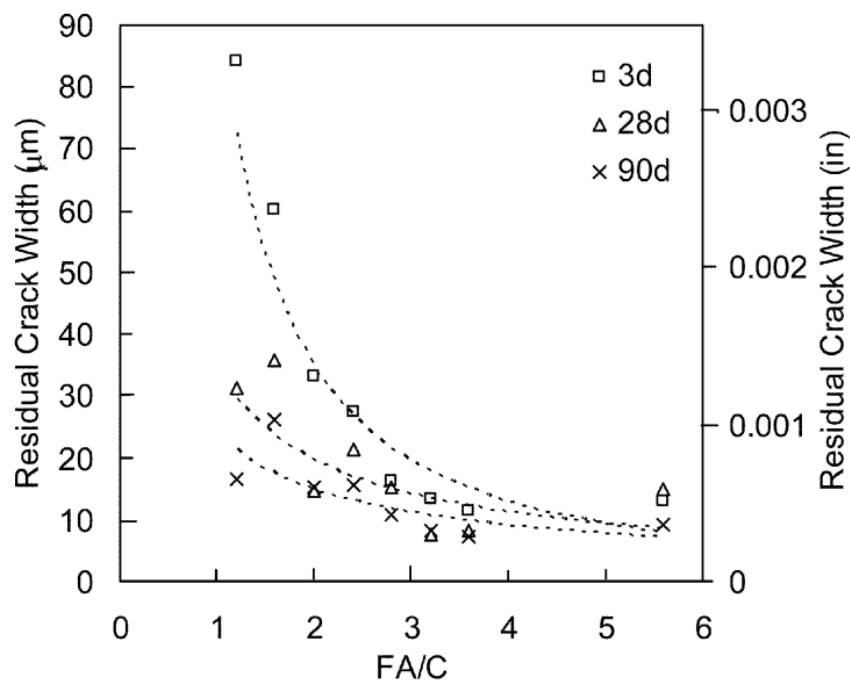


Figure 1.2 – HFA-ECC residual crack width to fly ash content (Yang et al. 2007)

Utilising fly ash in ECC reduces the amount of cement required and has a positive greening environmental impact (Yang et al. 2007). However, it has been found the compressive strength of HFA-ECC can decrease (Yang et al. 2007; Zhu et al. 2014). To address this reduction, FRP wrapping will be explored in this project (Lokuge & Karunasena 2016; Kissman & Sundar 2020; Otoom et al. 2021).

ECC is being extensively researched and is a vital civil engineering material (Shanmugasundaram & Praveenkumar 2021). Beyond utilising fly ash, there are gaps in the literature exploring additional greening methods in ECC. No published research could be found that substitutes natural or processed sand aggregate for PET granules. This would lower overall ECC emissions and sequester part of the growing plastic waste problem (Kangavar et al. 2022). There is a significant gap in the application of recycled greening aggregates which this project strives to address.

1.2 The Problem

To combat climate change, a reduction in construction-related greenhouse gas emissions is necessary. HFA-ECC has been shown to possess desirable construction properties and may contribute to lower lifetime emissions through superior durability. Previous research has also demonstrated that partial natural aggregate replacement with PET granules can lessen emissions and recycle waste while providing good mechanical properties in ordinary concrete.

No research has been conducted with PET or locally available Southeast Queensland sand in HFA-ECC. Thus, a composite using locally available sand as a replacement for USS in HFA-ECC is proposed (SEQ-ECC). The effect of recycled PET plastics on this composite will be studied by volumetrically replacing sand with 10%, 30% and 50% PET granules (PET-ECC). These new composites would divert waste from landfill and could lower overall emissions in the production of high-performance concrete.

An inherent weakness of conventional HFA-ECC is reduced compressive strength. One method of increasing the compressive strength of a concrete member is GFRP confinement. This project seeks to evaluate the performance of GFRP confined and unconfined SEQ-ECC and PET-ECC columns under compression. The results will ultimately contribute to the knowledge of greening aggregates in ECC by providing base knowledge of the relationships between recycling volume, fresh rheological properties, and the hardened mechanical properties of the newly developed ECCs.

1.3 Research Objectives

This research is proposed to bridge a knowledge gap by identifying the mechanical properties of greener short ECC columns using recycled aggregates. The main objective of this project is to develop a new high fly ash ECC using locally available sand and PET aggregate with a

tensile strain capacity larger than 1%. Successful results are expected to indicate the potential for greener ECC and whether PET-ECC is mechanically viable.

To achieve these goals the following targets have been identified:

1. Source or produce PET granules with similar PSD to locally available sand.
2. Produce high ductility HFA-ECC using locally available sand (SEQ-ECC).
3. Produce PET-ECC with sand replaced with PET by 10%, 30% and 50% volume.
4. Produce GFRP confined and unconfined specimens and evaluate the compressive strength, tensile strength, flexural strength, and matrix properties.
5. Evaluate the use of PET granules in ECC.
6. Further develop PET-ECC knowledge with numerical modelling using ABAQUS.
7. Contribute to the field of research into the viability of alternative green ECC aggregates.

1.4 Expected Outcomes

Typical ECC is costly, both economically and to the environment. Green recycled aggregates can reduce environmental impacts and could reduce costs. The project aims to further the body of research surrounding the mechanical properties of green aggregate in ECC. Initial laboratory trials are seen as necessary to begin to understand the proposed new material. To realise the full potential of PET-ECC it is hoped this project provides foundational knowledge for future research.

The project will endeavour to deliver the following outcomes:

1. Characterise the mechanical properties of HFA-ECC developed using locally available natural aggregate.
2. Identify the effects of PET recycling on the mechanical properties of PET-ECC.
3. Develop base fundamental knowledge to conduct future research into ECC substitutes.

1.5 Thesis Outline

This project dissertation contains seven chapters, as outlined below:

- | | |
|------------------|--|
| Chapter 1 | introduces the project topic, the problem, and the objectives. |
| Chapter 2 | is a collation of past and current research related to the project in a literature review. The research and ideas presented in this chapter are used to develop background theory and the project methodology. |
| Chapter 3 | details the methodology, experimental processes and relevant standards required to perform the experimental investigation. |
| Chapter 4 | outlines the tasks undertaken in the experimental investigation. The sourcing of materials, their properties, mixture design and testing are discussed. Challenges encountered throughout the process are identified and mitigation methods are presented. |
| Chapter 5 | outlines the development of the numerical model and investigates material properties within ABAQUS software. The developed compressive model can simulate the unconfined experimental results. |
| Chapter 6 | presents results and evaluates the mechanical properties of PET-ECC. The numerical results are validated against experimental findings. |
| Chapter 7 | concludes the project and provides a summary of key findings while suggesting further research opportunities. |

CHAPTER 2. LITERATURE REVIEW

A literature review has been undertaken to identify gaps in current knowledge as well as develop the background theory, mixture design, and methodology for the project.

2.1 Background

ECC is gaining prominence due to its unique properties. In some cases, the use of this material can improve the sustainability of structural concrete by addressing the durability problem (Sahmaran et al. 2007; Şahmaran & Li 2008).

ECC micromechanical design theory centres around the criteria that steady-state crack propagation is necessary to promote saturated multiple cracking and strain hardening (Kanda & Li 1999; Li et al. 2002; Li 2003; Wang & Li 2007; Yang et al. 2008). In other words, the steady-state crack stress σ_{ss} must satisfy Equation 2.1.

$$\sigma_{ss}\delta_{ss} - \int_0^{\delta_{ss}} \sigma(\delta)d\delta = J_{tip} \quad (2.1) \text{ (Wang \& Li 2007)}$$

Where, δ_{ss} is the steady state crack opening, and the crack tip toughness J_{tip} is approximated by the fracture toughness K_m and elastic modulus E_m : $J_{tip} = \frac{K_m^2}{E_m}$ (Wang & Li 2007).

Equation 2.2 expresses the condition for which steady-state cracking occurs and is the fundamental energy criterion ensuring multiple cracking in ECC.

$$J_{tip} \leq \sigma_0\delta_0 - \int_0^{\delta_0} \sigma(\delta)d\delta \equiv J_b' \quad (2.2) \text{ (Wang \& Li 2007)}$$

Where the right-hand side J_b' is the complementary energy governed by the maximum crack opening δ_0 , and the corresponding crack opening stress σ_0 . From equation 2.2 the J_{tip} value should fundamentally not exceed J_b' . When larger aggregates are used (increasing J_{tip}) an

increase in w/b ratio or use of inert filler can be useful to then decrease J_{tip} and insure multiple cracking (Wang & Li 2007).

The second fundamental theory to realise strain hardening and multiple cracking is the strength criterion (Equation 2.3). That is, the governing theory of crack initiation. The first crack strength σ_{fc} of the matrix should not be greater than the maximum fibre-bridging stress σ_0 .

$$\sigma_{fc} \leq \sigma_0 \quad (2.3) \text{ (Yang et al. 2008)}$$

The fundamental ECC design theory is easier interpreted as illustrated by the typical bridging stress versus crack opening width curve shown in Figure 2.1.

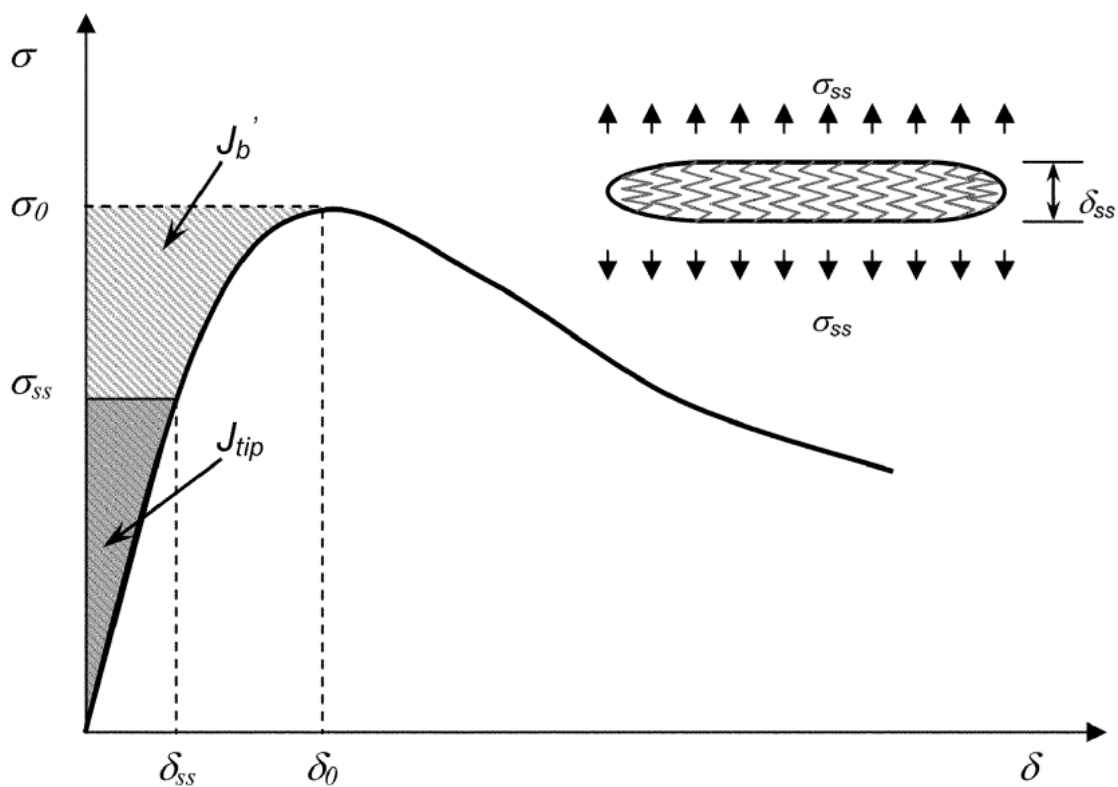


Figure 2.1 – Typical Bridging Stress vs Crack Opening Curve for Strain Hardening Composites
(Wang & Li 2007)

The study of micromechanical theory also includes how the bridging behaviour $\sigma(\delta)$ is influenced by fibre/interface properties and the links between composite ductility, matrix toughness and the flaw size distribution (Kanda & Li 1999).

In essence, for strain hardening behaviour it is beneficial to have a lower tensile first cracking strength and lower matrix toughness. It is commonly believed high content or larger-sized aggregate negatively influences the matrix toughness and decreases interfacial friction. Thus, ECC generally uses ultrafine silica sand (USS).

PET particles inherently form weaker bonds and provide additional flaws due to their hydrophobic nature (Kangavar et al. 2022). When implemented correctly, it could be hypothesised that this behaviour could offset some of the negative impacts larger aggregates impose and benefit the fundamental micromechanical properties of ECC.

2.2 ECC Using Alternate Materials

Micromechanical design theory has generally limited the production of ECC to include less sustainable and relatively expensive materials. Yet, researchers continue to endeavour to find more cost-effective, locally available, and sustainable substitutes that maintain or enhance the mechanical properties of ECC.

Careful consideration of ECC design theory and mixture components has developed and verified the performance of HFA-ECC (Wang & Li 2007; Yang et al. 2007). Greening of ECC, that is, a reduction in greenhouse gas emissions, is achieved by HFA-ECC (Yang et al. 2007). For a fly ash-to-cement (FA/c) ratio of 1.2 and above, adequate interface and matrix properties can be reached (Wang & Li 2007; Yang et al. 2007). In ECC design the use of fly ash can lead to a desirable weakening of the interface and matrix properties, encouraging saturated multiple cracking and strain hardening. Changes in these properties are likely due to differences in the chemical composition of the matrix and the inert coating of the PVA fibre provided by the fly ash (Wang & Li 2007).

Non-published findings presented at a postgraduate conference by Pourfalah and Suryanto (2013) investigated the use of locally available fly ash materials in the UK. Two types of fly ash were studied. It was observed that the size of the fly ash particles significantly affected the plastic viscosity and saturation dosages of HRWR in fresh ECC mortar (Pourfalah & Suryanto 2013). While the impacts on plastic viscosity in HFA-ECC were not studied by other peer-

reviewed researchers (Wang & Li 2007; Yang et al. 2007), the use of finer fly ash is likely to provide a better coating of fibres and flow of particles throughout the matrix.

However, it is important to balance the use of mineral admixtures such as fly ash. Increases in fly ash content can cause early strength retardation and reductions in compressive strength (Yang et al. 2007; Sahmaran et al. 2009; Zhu et al. 2014). Several options of reinforcement do exist to address the loss of compressive strength for HFA-ECC. FRP and glass fibre reinforced polymer (GFRP) wrapping has been found to improve the compressive performance of ordinary cement and conventual ECC (Otoom et al. 2021; Yuan et al. 2021). GFRP wrapping on PET-ECC has not been previously studied.

Within the literature, PVA fibre is most widely used in ECC (Wang & Li 2007; Yang et al. 2007; Ma et al. 2021). However, more research is needed to elucidate the extent of environmental impacts (Ohno & Li 2018). It is known that PVA fibre forms strong bonds to cement hydration products hindering strain-hardening potential if untreated (Li et al. 2002). Alternate fibres are an area for additional research and may increase performance. Yu et al. (2017) developed an ultra-high ductility cementitious material with the mechanical characteristics of ECC and polyethylene fibre. Ultra-high-performance or normal ECC using alternate fibres are promising but not as well studied and were not considered in this project.

Sahmaran et al. (2009) were one of the earliest to study the mechanical performance of different aggregate types and sizes in HFA-ECC. Crushed and gravelly dolomitic limestone sand with nominal maximum sizes of 1.19 mm and 2.38 mm was compared to ECC with USS. It was found that the aggregates did not negatively impact the ductility of ECC so long as uniform fibre distribution was achieved (Sahmaran et al. 2009). The results also indicate that the tensile ductility of the ECC is dependent on the surface texture and bonding of the aggregate. A lower matrix toughness was likely achieved with gravelly sand hence a slightly higher tensile strain capacity was observed (Sahmaran et al. 2009). Researchers have also investigated natural aggregates up to 4.75 mm as a means of addressing the practical limitations of ECC requiring USS. Guan et al. (2019) observed good durability (crack width control) and a tensile strain capacity well above 5% is possible with natural river sand. Similar findings by Li et al. (2020) using coarse river sand demonstrate the ability of ECC to be developed with robust multiple cracking and tensile strain capacity with the sand beneficially providing effective flaws (Li et al. 2020). Both these studies provide a new understanding of the fundamental ECC design principles.

Research has also been focused on substituting USS for materials with further sustainability improvements. Siad et al. (2017) successfully developed ECC using recycled glass sand with an average grain size of $110\ \mu\text{m}$, slightly larger than the conventional USS. It was found that the replacement of USS with between 25% and 50% recycled glass exceeded or was comparable to the reference ECC in terms of durability and mechanical performance (Siad et al. 2017). Adesina and Das (2021a) as part of a long-term research program at the University of Winsor successfully utilised relatively larger (average grain size of $210\ \mu\text{m}$) recycled asphalt aggregate up to a 50% replacement of USS in ECC without compromising mechanical properties (Adesina & Das 2021a). The authors conducted a further study suggesting it is sustainably and mechanically feasible to replace up to 75% of USS in ECC with recycled concrete aggregates (Adesina & Das 2021b).

No research has utilised locally available Southeast Queensland Sand or PET granules. This is a knowledge gap.

2.3 PET Aggregate Concrete Performance

For ordinary cement and mortars, research regarding PET replacement can be generalised into two categories: those replacing aggregates with flaky particles, and those with granular particles. Poorer mechanical properties have been well documented for concrete with natural aggregate (NA) replaced with PET flakes (Albano et al. 2009; Silva et al. 2013; Saikia & de Brito 2014). While increases to or similar compressive strength, tensile strength and workability have been reported when replacing NA with PET granules at quantities of 5% and up to 40% in some cases (Bamigboye et al. 2021; Dawood et al. 2021; Tayeh et al. 2021; Kangavar et al. 2022).

Kangavar et al. (2022) studied the effect of a similar PET aggregate used in this study. This is important because while granular-type particles consistently outperform flaky particles, the generalisation of increased or similar mechanical properties at lower replacement volumes does not always hold. This is due to differences in PET granules, but also mix proportions, size distribution and processing. The main point of difference in mix proportions is the replacement methodology. These variations can lead to performance disparities. For PET granules the volumetric design approach as used by (Kangavar et al. 2022) should be adopted due to the difference in specific gravity between PET and natural sand.

Saikia & de Brito (2014) reported reductions in compressive and tensile strength of more than 10% for just 15% volume PET replacement. Marzouk et al. 2007 observed an 11.6% reduction in mechanical properties at a 70% replacement percentage. This represents a large variation between researchers and is attributable to different PET size distributions and particle properties. Kangavar et al. (2022) suggested that the aggregates used in this project can increase the mechanical properties of ordinary cement at 10% replacement and possess similar properties up to 30% replacement. After 30% larger reductions were observed.

When replacing sand with PET granules in geopolymer concrete Chithambar Ganesh et al. (2021) found a reduction in workability but increased compressive and tensile strengths up to a 10% PET replacement. This was due to the increased surface area and specific gravity of replacement PET granules vs sand. This suggests that ordinary cement and geopolymer concrete based on fly ash and ground granulated blast furnace slag polymerization demonstrate similar mechanical properties with PET substitution. No adverse effects in fresh or hardened properties were reported with PET substitution.

No published research has been found on the effect of PET granular replacement of fine aggregate in ECC. However, the use of PET fibres has been explored to further decrease the cost and emissions of ECC (Yu et al. 2018). Yu et al. (2018) found that the interfacial bond was low due to the smooth surface of PET fibres used and as a result, tensile strength and stain capacity were reduced. There has been no indication of an adverse reaction of ECC or high fly ash geopolymer concretes to the addition of PET. Thus, the project has grounding and there is a research gap in the performance of PET-ECC.

2.4 PET Aggregate Concrete Properties

2.4.1 PET-Cement Interaction

For ordinary concrete, it has been documented by scanning electron microscopy (SEM) that the matrix aggregate adhesion is good for PET aggregate but does weaken further as the replacement percentage is increased (Marzouk et al. 2007; Kangavar et al. 2022).

Marzouk et al. 2007 found that the adhesion did not vary with the types of substituted PET aggregate studied. However, it was found that the compactness in samples below 50% replacement volume was high and then voids high in samples above 50% replacement. Similar findings have also been observed in increased absorption and a reduction in ultrasonic pulse

velocity as the proportion of PET increases (Almeshal et al. 2020; Dawood et al. 2021). This difference in structure helps to explain some of the large decreases in mechanical properties and bulk densities of higher substitution percentages. At ultimate tensile strength, Saikia & de Brito (2014) documented that rather than the failure of the plastic aggregate it was a failure of the bond between PET and cement paste in the ITZ.

Hardened properties of mixes containing PET aggregate are variable due to the type of aggregate used. Kangavar et al. 2022 uses similar PET granules as this project and found non-uniform distribution of PET aggregate and larger voids occurred with substituted volumes greater than 30%. This contradicts research that suggests a 50% replacement volume causes this instability. Regardless, all research into ordinary cement PET aggregate replacement agrees with the general relationship of increased PET replacement volume to increased voids, larger ITZ and weaker mechanical properties.

No published research has been found on the effect of PET granular aggregate in ECC. There is a research gap for the properties of PET-ECC.

2.4.2 Workability

The workability in ordinary cement and mortar with PET aggregate replacement is variable on the type of PET used. The behavioural variations are likely caused by differences in internal friction and the binding mass (Saikia & de Brito 2012).

Decreases in workability as percentage PET increases have been well documented (Albano et al. 2009; Ferreira et al. 2012; Rahmani et al. 2013; Saikia & de Brito 2014; Almeshal et al. 2020; Dawood et al. 2021; Kangavar et al. 2022). Differences between these studies include using percentage weight not volume and or use of non-uniform, irregularly shaped PET flakes versus granules.

Increases in workability have also been documented with varying percentage substitution (Choi et al. 2005; Choi et al. 2009; Ferreira et al. 2012; Saikia & de Brito 2014; Bamigboye et al. 2021; Tayeh et al. 2021). This is attributable to the types of PET aggregate being used I.e., they are smoother than sand. Ferreira et al. (2012) used 3 different types of aggregate observing increased workability for the more regular and spherical-shaped PET aggregate and decreases for coarse, irregular PET aggregate particles.

Bamigboye et al. (2021) found increased workability up to 40% volume replacement using heat-treated, ground PET aggregates and demonstrated the difference to flaked aggregates without heat treatment. Kangavar et al. (2022) use the same PET aggregate as this project and observed minor reductions in workability. This contrasted with other findings in that the value remained insignificant up to the maximum 50% volume replacement studied.

No published research has been found on the effect of PET granular aggregate substitution on the workability of ECC. Workability via slump test is a useful technique in ensuring optimal PVA fibre distribution within ECC (Yang et al. 2009). Changes due to PET need to be studied and this is a knowledge gap.

2.4.3 Compressive Strength

The characteristic strength of an ordinary concrete batch is typically given by its compressive strength in megapascals (MPa) at 28 days of curing time. An ordinary concrete characteristic strength is a result of several factors including age, curing conditions and w/c ratio. Crucially there is a direct relationship between the fresh w/c ratio and strength (Gagg 2014).

This characteristic strength of ordinary cement has been well documented to reduce as PET replacement percentage increases towards 100 % (Choi et al. 2005; Rahmani et al. 2013; Silva et al. 2013; Saikia & de Brito 2014; Kangavar et al. 2022). Others such as Dawood et al. (2021) only examined smaller replacement percentages and did not see large reductions. Rahmani et al. (2013), Dawood et al. (2021) and Kangavar et al. (2022) observed initial improvements in compressive strength at lower substitution levels while others note the addition of any PET causes a reduction (Choi et al. 2005; Silva et al. 2013). No two studies use the same PET aggregates or processes.

Interestingly Kangavar et al. (2022) found a 10% increase in the compressive strength for 10% PET aggregate replacement. This was a larger increase than the findings of most others and is likely due to the methodology and materials used. Kangavar et al. (2022) volumetrically replace river sand with PET granules aligning with the PSD of the sand. This methodology is similar to Choi et al. (2005), Rahmani et al. (2013) and Saikia and de Brito (2014) but in contrast to Silva et al. (2013) and Dawood et al. (2021) who replaced PET with percentage weight.

As shown in Figure 2.2, Kangavar et al. (2022), Choi et al. (2005), Silva et al. (2013) and Saikia and de Brito (2014) saw significant variations in compressive strength depending on the aggregate shape and sizing used.

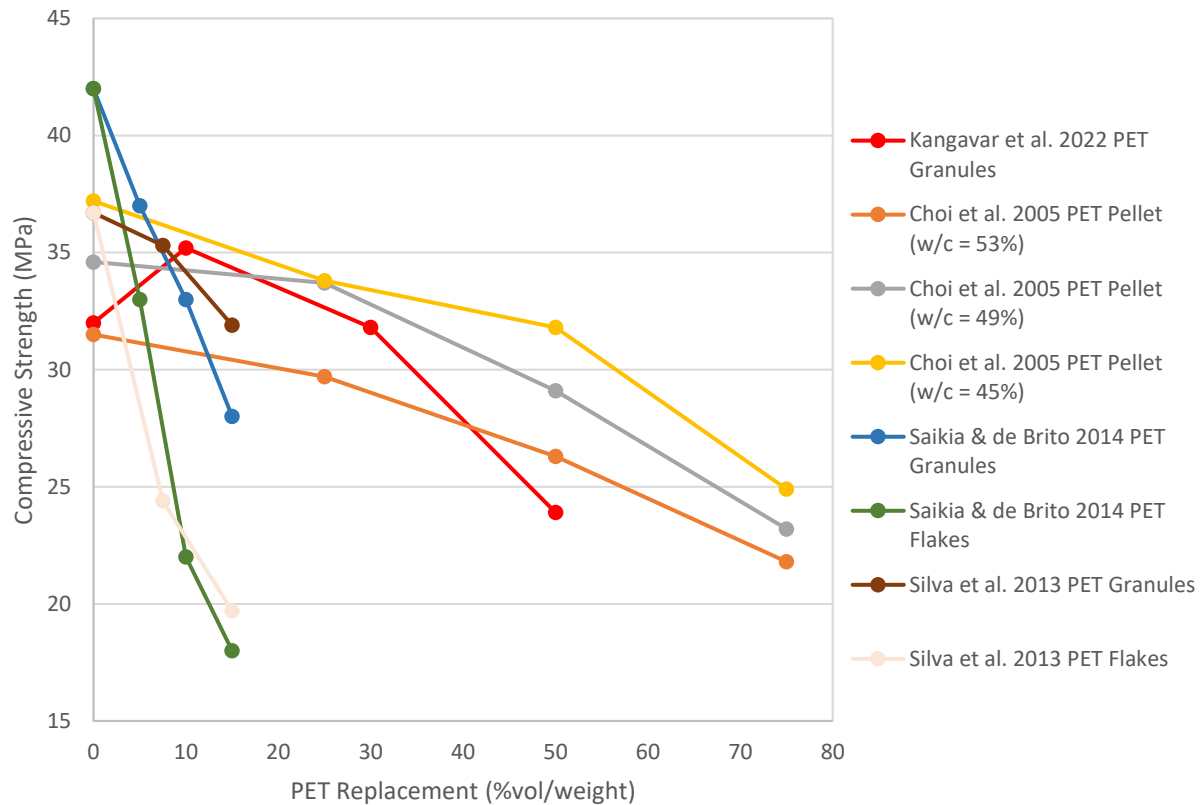


Figure 2.2 - PET Concrete Compressive Strength Variation at 28 days

Choi et al. (2005) observed reductions in compressive strength regardless of the w/c ratios or surface treatment used on PET granules. This was inline but not as significant as Saikia and de Brito (2014) and Silva et al. (2013).

Kangavar et al. (2022) and others all observed a decrease in the modulus of elasticity for increasing PET replacement albeit at varying rates. It was theorised this was attributed to the decrease in density (Kangavar et al. 2022).

No published research has been found on the effect of PET granular aggregate substitution on the compressive strength of ECC. This is a knowledge gap.

2.4.4 Splitting Tensile Strength and Uniaxial Tensile Strength

The splitting tensile strength of ordinary concrete can often be estimated at 8% to 14% of its compressive strength (Hanson 1968). Research into this relationship has also been undertaken to predict splitting tensile strength given age, w/b ratio and type of specimen by developing polynomial equations (Bin Ahmed et al. 2021).

It follows then that research into PET aggregate substitution has found similar relationships to compressive strength. Studies observing increases in compressive strength can observe increases in splitting tensile strength (Kangavar et al. 2022) and vice versa (Choi et al. 2005; Silva et al. 2013; Saikia & de Brito 2014). However, the relationship is not always clear as shown in Figure 2.3.

Saikia & de Brito (2014) found the difference in compressive strength between flakes and pellets to be more than 30% at 5% PET substitution. The difference in splitting tensile strength was found to be less than 3%.

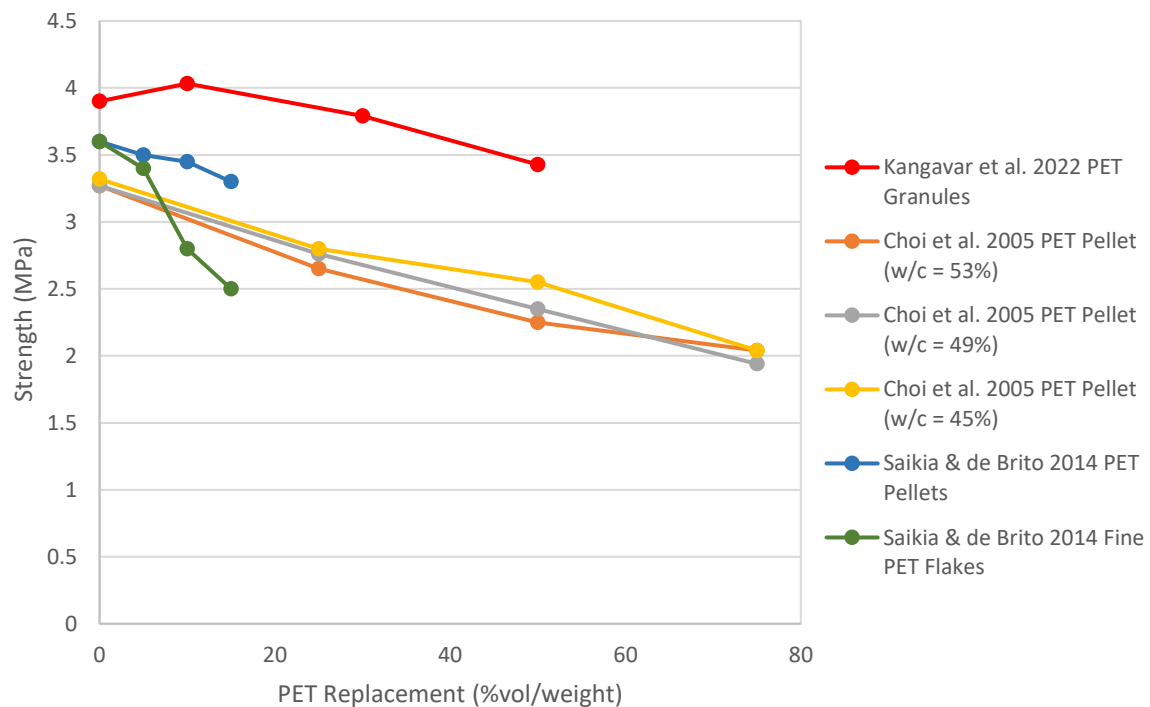


Figure 2.3 – PET Concrete Splitting Tensile Strength Variation at 28 days

Choi et al. (2005) again found reductions compared to the control sample, but the difference was less pronounced, and with a w/c ratio of 53% the tensile strength matched the sample with the highest compressive strength. Variations are likely possible due to PET-cement paste interactions and the various PET particle types, sizes, and surface treatments. The generally increased performance difference compared to compressive strength reflects the well-documented more ductile behaviour of concrete containing PET aggregate (Frigione 2010; Rahmani et al. 2013; Ataei et al. 2017; Kangavar et al. 2022).

For cementitious materials, the splitting tensile test method is often the most accurate strength determination (Zhu et al. 2014). Attempting uniaxial testing can induce compression at the point of contact between the specimen and the gripping method. A combination of compression and tension has been shown to reduce the failure stress in concrete (Yan & Lin 2006). Thus, this is not a common method used to test ordinary concrete, and no research was found on the uniaxial tension of PET concrete.

However, the uniaxial tension test has been widely utilised to indicate the ultimate strength, crack propagation and strain hardening potential of ECC specimens (Yang et al. 2007; Sahmaran et al. 2009; Yang et al. 2009; Li & Li 2011, 2012). When the same method is used, a uniaxial test can be a precise measure of tensile strength and strain hardening so that researchers can evaluate changes in mixture parameters. No published research has been found on the effect of PET granular aggregate substitution on the splitting tensile strength or strain-hardening behaviour of ECC. This is a knowledge gap.

2.4.5 Flexural Strength

The flexural strength of PET granules in ordinary cement has seen variations similar to the compressive strength and splitting tensile strength. Kangavar et al. (2022) found 10% PET replacement to have a slightly higher load-bearing capacity, with 30% and 50% replacement volumes 7.2% and 16.2% lower in comparison to the reference concrete. This contrasts with Saikia and de Brito (2014) who found reductions in flexural strength for all replacement percentages.

Kangavar et al. (2022) also observed optimal post-crack performance, toughness, and ductility for 10% PET cement. This increase is likely explained by the flexible nature of PET within the

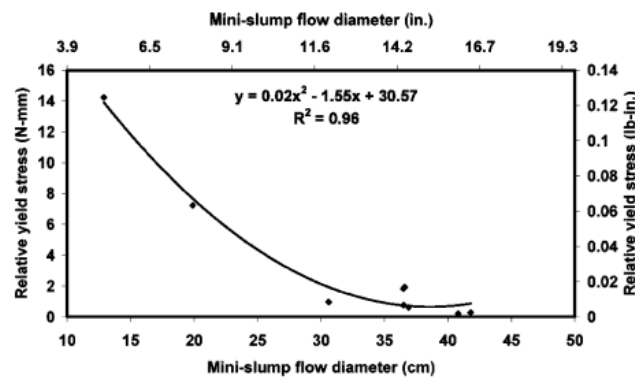
mixture (Kangavar et al. 2022). It was theorised reductions for higher percentage replacements could be caused by the ununiform distribution of PET due to its lower density.

No published research has been found on the effect of PET granular aggregate substitution on the flexural strength or strain-hardening behaviour of ECC. This is a knowledge gap.

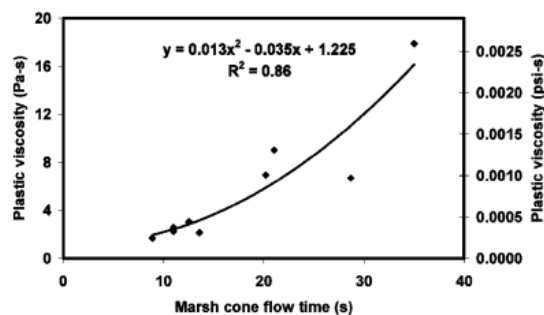
Importantly, a four-point bending test can be used as an indirect assessment of the strain-hardening properties of ECC (Cai & Xu 2010; Guan et al. 2018). This provides a measure independent of the potential compressive forces in uniaxial tensile testing.

2.5 Improving the properties of PET-ECC

The best way to ensure the structural performance of ECC is by providing optimum rheological properties before the addition of reinforcing fibre (Yang et al. 2009; Li & Li 2012). Yang et al. (2009) demonstrate the marsh cone and mini-slump flow tests can indirectly characterise the rheological properties of ECC mortar (without fibres) as shown in Figure 2.4.



(a) Relative yield stress versus mini-slump flow



(b) Plastic viscosity versus Marsh cone flow time

Figure 2.4 – a) mini-slump and b) marsh cone flow time to relative yield stress and plastic viscosity (Yang et al. 2009)

Li and Li (2012) present a guide to optimal plastic viscosity by systematically verifying the correlations between rheological properties, fibre dispersion and mechanical properties. It was observed uniform fibre distribution throughout the matrix is reproducible and hardened tensile properties can be maximised through rheological control of the mortar. A marsh cone flow time and mini slump test serve as reliable measures to insure rheology control (Li & Li 2012). However, the optimal properties of the mortar vary depending on the ingredients, composition, quantity of fibre, mixing procedure and mixer type. This makes it very difficult to judge a new ECC mixture or process before testing the hardened mechanical properties. The current study strives to address these problems.

Generally, to ensure fibre uniformity, it is recommended that a w/b ratio of between 0.25 ± 0.5 be adopted with high plastic viscosity, and low yield stress (Yang et al. 2009; Li & Li 2012). Superplasticiser (HRWR) and viscosity modifying agent (VMA) is highly useful in achieving this.

Non-peer-reviewed research by van Zijl and Stander (2005) has suggested that hardened properties are more sensitive to the use of VMA and that superior ECC ductility results from mixes with the highest flow ability and no segregation. This was supported by Yang et al. (2009) that also found VMA to improve fresh properties but noted ECC with adequate rheological properties and fibre uniformity was attainable through the control of w/b and HRWR dosage without requiring expensive VMA. VMA could be considered if PET granules hurt the rheological properties of fresh PET-ECC. This could be caused by excessive free water not absorbed by the substituted PET aggregate.

No studies were found for the rheological control of PET-ECC. An optimal range of plastic viscosity, and thus admixture dosage for PET-ECC has not yet been established. This is a knowledge gap.

2.5.1 Mixture Design

Generally, any component of ECC mixture design is determined from the micromechanical design principles and previous experience (Li et al. 2020). Due to limited experience, two existing ECC mixtures were considered for PET-ECC development. Firstly, conventional M45-ECC as studied by Wang & Li (2007) with a fly ash-to-cement ratio of 1.2. Secondly, an HFA-ECC with robust strain hardening and desirable mechanical properties was first reported

by (Yang et al. 2007). In ECC mixture designs, it has been observed that high fly ash content and the resulting weakening of the fibre ITZ bond can improve strain hardening potential and ECC performance (Wang & Li 2007; Yang et al. 2007; Sahmaran et al. 2009). The relationship between fly ash, cement and compressive strength is shown in Figure 2.5.

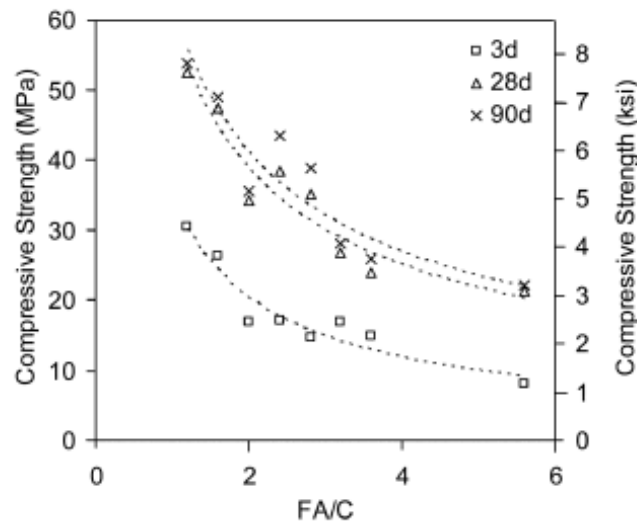


Figure 2.5 – Compressive Strength of HFA-ECC given Fly Ash Content and Age (Yang et al. 2007)

HFA-ECC generally contains fly ash-to-cement ratios greater than two. This increase in fly ash can lead to further greening improvements to ECC through a reduction in OPC while providing good mechanical properties (Liu et al. 2016; Xu et al. 2021).

The use of HFA-ECC in studying increased aggregate size is not new (Guan et al. 2019; Li et al. 2020; Adesina & Das 2021b) and it can be hypothesised that the fracture toughness and matrix properties of PET-ECC will benefit from high quantities of fly ash. No research could be found that utilises locally available Southeast Queensland sand or PET granules in HFA-ECC, and this is a knowledge gap.

2.5.2 Mixing Methods

For ordinary concrete utilising the same PET granules, Kangavar et al. (2022) found success with the mixing methods as outlined in AS 1012.8.1 and AS 1012.2. This indicates the PET granule will behave and mix with OPC similarly to the sand it replaces. It is hoped that this behaviour is also similar when interacting with PVA fibres in ECC. No studies have been found

that combine PVA fibre with PET granules. However, similarly hydrophobic PET fibre has been successfully substituted with PVA (Yu et al. 2018) and no adverse reactions were reported.

In ECC mixing we must account for the specific use of PVA fibre. A mixer with a high shear action is required to distribute fibres uniformly and avoid clumping. The AS 1012.2 mixing sequence was not designed for ECC and variations to the sequence shall be recorded.

Two mixing methods have been identified from the literature. A standard ECC mixing method would generally follow three steps with mixture time dependent on the type of mixer used (Wang & Li 2007; Yang et al. 2009; Zhou et al. 2012; Yu et al. 2018):

- 1) Combine and mix all dry materials,
- 2) Add and mix all liquid materials,
- 3) Add and mix fibre.

The plastic viscosity before fibre addition determines the fibre distribution matrix (Zhou et al. 2012). Even with correct mix proportions, if the mixture's plastic viscosity is not optimal before fibre addition, hardened properties can be negatively impacted. To adapt to a range of w/b ratios Zhou et al. (2012) propose an adjusted mixing sequence. They found the fibre distribution, tensile strain capacity and tensile strength were improved by adjusting the standard ECC mixing process.

The proposed mixture sequence is as follows (Zhou et al. 2012):

- 1) Mix the optimal quantity of dry materials.
- 2) Add and mix the optimal quantity of liquid materials.
- 3) Add and mix fibres.
- 4) Add and mix the remaining dry and liquid materials.

If the w/b ratio is controlled there is no indication that the substitution of PET in the fresh matrix would require an adjusted mixing technique. However, there is also no published data for PET-ECC mixing, this is a knowledge gap.

2.5.3 Curing

For ordinary concrete utilising the same PET granules, Kangavar et al. (2022) found success by curing in a dedicated room at between 20-27 Celsius and 50% relative humidity for 28 days.

Ferreira et al. (2012) found that the mechanical properties of PET-substituted concrete could be influenced by curing conditions. The best compressive strength was found under drier curing conditions and the greatest splitting tensile strength and modulus for elasticity occurred under the 100% relative humidity chamber regime (Ferreira et al. 2012). The curing conditions used by Kangavar et al. (2022) were in line with the driest lab conditions studied by Ferreira et al. (2012). The reductions in the modulus of elasticity, and tensile and flexural strength reported by Kangavar et al. (2022) may partly be attributable to the curing conditions.

The findings of Ferreira et al. (2012) differ from Xu et al. (2021) who conducted research into the impacts of relative humidity on the tensile properties of ECC. Xu et al. (2021) found that ECC with a high fly ash content cured in high relative humidity increased both ultimate tensile strength and compressive strength versus curing in lower relative humidity environments (Xu et al. 2021).

While increases in ultimate tensile strength were observed for higher relative humidity the tensile strain capacity was found to be reduced. Regardless of fly ash content all specimens cured in 25%-95% relative humidity developed robust strain-hardening with multiple cracking (Xu et al. 2021).

There is no indication that PET-ECC would require specific curing techniques to achieve good mechanical properties. There is also no published data for PET-ECC curing, this is a knowledge gap.

2.6 GFRP Confined Concrete and Composites

FRP is a method to increase the strength and durability of concrete members (Kissman & Sundar 2020; Ootom et al. 2021; Yuan et al. 2021). GFRP is a cost-effective type of FRP utilising glass fibres. Combining GFRP and PET-ECC could address the sustainability, ductility, and durability limitations of ordinary concrete in construction applications.

For maximum performance and an even confining pressure, a good mechanical bond between the confined concrete and FRP is vital (Mirmiran et al. 1998). Vacuum consolidation is one way to increase the bonding performance and consistency of FRP in concrete applications (Hadigheh & Kashi 2018). It is less common for researchers into civil infrastructure materials to adopt this method. This has likely been due to the additional complexity and low feasibility of the rehabilitation of existing structures. For construction convenience, the same resin has

been used as the matrix and adhesive resin in FRP bonding systems without the use of vacuum consolidation (Hadigheh et al. 2017; Xin et al. 2017; Ribeiro et al. 2018).

Using Pilemedic™ GFRP composite Ootom et al. (2021) observed a 149% strength increase in ordinary concrete infills. This contrasted with Mohammed et al. (2018), which observed 105% to 523% increases. The properties of concrete infill, type of GFRP, and bonding techniques can lead to significant variations in confinement performance. Mohammed et al. (2018) concluded the behaviour of GFRP wrapping is highly affected by the modulus of elasticity and compressive strength of the infill materials. It is expected that these properties would be affected by the substitution of PET aggregate in PET-ECC.

Previous studies have found unconstrained ECC fails under compression by major oblique shear (Zhou et al. 2015; Yuan et al. 2021). GFRP can greatly improve axial deformation and the compressive strength of ECC (Yuan et al. 2021), which was consistent with (Dang et al. 2020). However, Dang et al. (2020) observed good crack control and local crushing of ECC after FRP rupture while Yuan et al. (2021) observed that GFRP ECC specimens maintained their integrity after the rupture of the FRP wrapping system.

Potential greening could occur by utilising less material for the same structural mechanical properties. GFRP offers good compressive strength improvements. Other methods of confinement such as large rupture strain (LRS) FRP may be more suitable if higher ductility is required (Yuan et al. 2021). No published research has been found on the effect of PET granular aggregate substitution on the GFRP-confined strength of ECC. There is a research gap in using PET-ECC infill material.

2.7 Numerical Investigation and Modelling

The use of ABAQUS allows researchers to calibrate material properties. By tailoring column infill properties to PET-ECC the resulting model could be used to validate experimental results and explore the influence of confinement.

Numerical evaluation of the compression behaviour of GFRP-wrapping and GFRP-wrapped infill of ordinary concrete has been explored previously (Mohammed et al. 2018; Ootom et al. 2021). The use of ABAQUS software to model ordinary concrete is also well documented (Godat et al. 2020; Raza et al. 2020; Ootom et al. 2021). These studies utilise the concrete damaged plastic (CDP) models within ABAQUS to good effect.

To understand the basic, mostly linear properties of ECC several experimental and numerical investigations have also been carried out (Xu & Cai 2010; Zhou et al. 2015; Cai et al. 2020; Yuan et al. 2021). The use of ABAQUS's CDP has been usefully utilised but to less extent compared with ordinary concrete (Cai et al. 2020). No models have been developed for PET-ECC infills and this is a research gap.

Otoom et al. (2021) developed a 3-D finite element model to predict the behaviour of loading GFRP-wrapped ordinary concrete columns. The CDP model is validated by experimental results and used to investigate the influence of confinement. The CDP behavioural model was also used by Cai et al. (2020) for ECC. The methodology of both these studies is useful in the numerical investigation of PET-ECC and is discussed further in Chapter 5. The proposed investigation builds upon the work of Otoom et al. (2021) in GFRP and Cai et al. (2020) in ECC to help fill the research gap of GFRP-wrapped PET-ECC.

2.8 Summary

PET recycling via fine aggregate substitution shows promising results in ordinary concrete. It has been found the use of PET granules sourced in Brisbane by Kangavar et al. (2022) can demonstrate good performance and mechanical properties, particularly at a replacement volume of 10%. However, no research has been conducted to evaluate PET granule recycling in ECC.

HFA-ECC is unique in its strength and durability characteristics. Its usefulness in the construction industry could be extended using GFRP. For construction convenience, the same resin can be used as the matrix and adhesive resin in GFRP bonding systems.

With FE modelling, the mechanical properties and influence of confinement parameters could be predicted. Knowledge of the basic performance and mechanical properties of any concrete substitution is needed to assess its viability.

Variations and contradictions in the literature have been observed. For PET substitution in ordinary concrete, this is at least partially due to the type of particle used. Variations in the development of ECC are more complex. This is due to the susceptibility of ECC to variations in materials, mixing methods and equipment. Hence the problem of quality assurance for ECC in structural applications is realised. This makes it very difficult to judge new ECC mixture designs or processes before having tested the hardened mechanical properties. As such, this

project aims to provide a basis for the mechanical properties of the mixture designs and processes outlined in the following chapters.

The literature review highlights several items that could maximise the performance and mechanical properties of the proposed PET-ECC. These findings include but are not limited by:

- a) HFA-ECC mix design proportions can maximise greenness and the fibre interface performance.
- b) For w/b of 0.25 ± 0.5 , PET-ECC can be mixed using the standard process. If w/b is greater than 0.3 PET-ECC should be mixed using a 4-step adjusted process.
- c) Curing conditions for PET-ECC are flexible ranging from 25% to 95% relative humidity.

2.8.1 Knowledge Gaps

PET aggregates have not been previously studied in ECC. PET-ECC has the potential to improve sustainability, recycle plastic, and provide a concrete alternative to address brittleness durability issues. There is a knowledge and research gap in the effects of recycled aggregate on the mechanical properties of ECC. This project will help to bridge this gap by substituting sand in HFA-ECC with PET granules by up to 50% volume.

CHAPTER 3. METHODOLOGY

3.1 Outline

To help bridge the knowledge gap in the mechanical properties and performance of PET-ECC an experimental and numerical investigation will be performed. Natural quartz sand will be substituted by volume with PET in a new HFA-ECC. The fresh and mechanical properties will be compared with a focus on the compressive strength of confined and unconfined short-column samples. With these results, an evaluation of PET recycling in the newly developed ECC can be performed providing a basis for further investigations.

To this end the following methodology has been adopted:

1. Source all materials and equipment to conduct experiments.
2. Finalise PET-ECC mix design.
3. Prepare one control batch of HFA-ECC and three batches of PET-ECC by substituting sand by volume with 10%, 30%, and 50% PET.
4. Assess the rheological matrix properties of batches using a mini-slump cone and adapted marsh funnel. Assess ECC workability using mini-slump cone and slump flow test.
5. For each batch, prepare several cylindrical specimens to test for compressive and splitting tensile strength, briquets for uniaxial tensile strength, and beams for flexural strength.
6. Conduct laboratory testing to determine the mechanical properties of HFA-ECC and PET-ECC.
7. Conduct numerical investigation.
8. Analyse and discuss experimental and numerical results.
9. Assess the mechanical viability of PET aggregate recycling in ECC.

3.2 Assumptions

In the completion of this project the following key assumptions have been made (but are not limited by):

1. The recycled PET aggregate used for the project is representative of PET granules that could be obtained for general use.
2. The PSD of the quartz sand provided by the supplier is representative of the PSD of the sand used in PET-ECC.
3. The PET aggregate is of similar material properties as those previously reported in the literature.
4. The characteristics of the remaining materials are broadly in line with those reported in the literature for micromechanical mixture design, rheological control, and mixing methods.

3.3 Limitations

The critical limitation of the project was the available size and quantity of PET aggregate. The methodology attempted to address this limitation within the budget and with available equipment. USS was ultimately replaced with locally available medium sand. Due to time and resource restrictions, a conventional HFA-ECC batch was not undertaken as initially planned. Without a conventional control ECC, it was critical to characterise the strain-hardening potential of the new composites with a uniaxial tension test so that comparisons could be drawn from studies using similar mixture designs.

3.4 ECC Matrix

Several HFA-ECC mixes were discovered in the literature. As validated by Yang et al. (2007) a fly ash content of two to three times cement has the unique potential to improve greenness and develop robust multiple cracking and tensile strain hardening. An HFA-ECC with a fly ash-to-cement ratio of 2.4 and a sand-to-binder ratio of 0.37 was adopted in this project based on the work of Yang et al. (2007). Without the time or resources to conduct micromechanical

testing and optimisation, a standard HFA-ECC mixture was adopted with medium sand as a direct replacement for USS. This is a starting point for the research into the new ECC with tailoring based on desired strengths possible with further research (Nawy 2008).

The literature revealed that the fibre-matrix interaction is critical in encouraging the uniform distribution of fibres and the development of strain hardening (Li et al. 2001; Li et al. 2002). For this reason, the project adopted well-known RECS15 PVA fibre.

It has also been found that large river sand aggregates can provide beneficial flaws to the matrix (Li et al. 2020). However, no research has utilised locally available natural Queensland sand. A medium, natural quartz sand from Rockwell Quarries was adopted in this project with a maximum size aligning with Li et al. (2020).

The hydrophobic nature of PET and the interaction of the flaws created has not yet been studied. Thus, the adoption of untreated PET was seen as a good knowledge bridging starting point and sufficient for this project. Additional surface treatments of the PET aggregate or PVA fibre were not considered in the scope of this work.

3.5 Fine Aggregate Selection

Fine aggregates had a particle size distribution as per the limits of deviation in AS 2758.1-2014. It was found that the PET granules available from local recycling companies were significantly larger in fraction size than the available fine and medium sands. Therefore, it was difficult to collect the necessary fractions to replace fine sand and medium sand to match the largest size was adopted.

To align the PET granules with the PSD of medium sand the granules were sieved using available sieves at the Z1 laboratory at the University of Southern Queensland. A similar method was adopted by Kangavar et al. (2022) to achieve a closer replacement characteristic of the substituted PET granules in ordinary concrete. This is vital in mitigating the impacts of varied grading on the matrix and interface properties of concrete (Kangavar et al. 2022) or ECC.

To ensure a representative sample, sampling of processed PET granules smaller than 4.75 mm was undertaken according to AS 1141.3.1-2021. The results of the sieved samples demonstrated larger fraction sizes but were processed within the range of limits of deviation

for fine aggregates in AS 2758.1-2014. The methods of separating and remixing aggregates have been used by other researchers to limit the grading effect of recycled aggregate (Ghorbani et al. 2019; Kangavar et al. 2022).

3.6 Producing Laboratory Specimens

3.6.1 ECC Mixing

The earliest developments of HFA-ECC utilise a three-stage mixing process (Wang & Li 2007; Yang et al. 2007). All dry contents are firstly mixed followed by liquids and lastly fibres (Wang & Li 2007). Yang et al. (2009) later reported that providing optimum rheological matrix properties before fibre addition encourages uniform fibre distribution and reproducible hardened properties. It was recommended that a water-to-binder ratio of between 0.25 ± 0.5 be adopted with high plastic viscosity, low yield stress and no segregation. This has been widely implemented and generally demonstrates good performance as validated by Ranade et al. (2014) and others (Wang & Li 2007; Yang et al. 2009; Zhou et al. 2012; Yu et al. 2018). PET aggregate neither adds nor absorbs water in fresh PET-ECC. A w/b ratio of 0.26 as used by Ranade et al. (2014) ensures optimum rheological properties will not be exceeded theoretically if the free water content and absorption of the sand are accounted for.

For ECC, a high-shear mixer is desirable to encourage the uniform distribution of fibres. As per AS 1012.2-2014, the size of mixing batches exceeded 10% of the volume of test specimens. As ECC is not considered in the AS 1012.2-2014 mixing sequence all variations shall be recorded, and the mixture sequence will align with the available literature.

Detailed mixing sequence:

1. Hand load mixer, with sand and PET, and mix for 30 seconds. No aggregate wetting.
2. Add cement and fly ash and mix slowly for 2 minutes.
3. Add water and admixtures (following manufacturer specifications), mix for 3-5 minutes or until consistent and uniform, and scrape sides as needed.
4. Perform mini-slump cone test and marsh cone test on ECC matrix.
5. Gradually add PVA fibre and mix for 5-8 minutes until all fibres are evenly distributed

Concrete mixing was undertaken at Wagners Precast Laboratory in Wacol, Brisbane. To mix the required quantity and to achieve a higher shear mixing action, a Bennett Equipment planetary pan mixer was used as shown in Figure 3.1. The casting of specimens was completed within 20 minutes aligning with AS 1012.2-2014.



Figure 3.1 – Bennett equipment pan mixer

3.6.2 Specimen Details

Two specimens were cast for each test. This was necessary to remain within the time and budget requirements for the project.

Compression and splitting tensile specimens were cast in cylinders with a diameter-to-height ratio of 1:2 as specified by AS 1012.8.1-2014. Standard steel moulds with 100 mm diameter and 200 mm height were used.

Flexural beams were cast as specified in AS 1012.8.2-2014. The cross-section was 100 mm by 100 mm with a length of 400 mm to comply with the testing requirements of AS 1012.11-2000. Several moulds were made to measure from form ply to remain within budget restrictions.

ECC is typically characterised by its tensile strain capacity using relatively large coupon specimens such as those detailed in ASTM D638 (Li et al. 2001; Wang & Li 2007; Yang et al.

2007). For this project uniaxial tensile testing was not possible to Australian or ASTM D638 Standards at the University of Southern Queensland. To overcome this, and due to the absence of coarse aggregates, an innovative method was adopted. It utilises relatively small and cost-effective briquet specimens according to ASTM C307.

A 3D-printed gang mould developed for ASTM C307-99 was used to cast briquette specimens for uniaxial tension testing as shown in Figure 3.2. ASTM C307-99 is a tensile strength testing method for mortars, grouts, and monolithic surfacing with small aggregate. The length of the PVA fibres used are eight millimetres and exceed the recommended aggregate size of six millimetres. This is a novel testing method for ECC and is only expected to provide an indicative characterisation of the tensile strain capacity. The briquette may be insufficient to measure the tensile strength of PET-ECC precisely or accurately and requires further validation beyond to scope of this project.

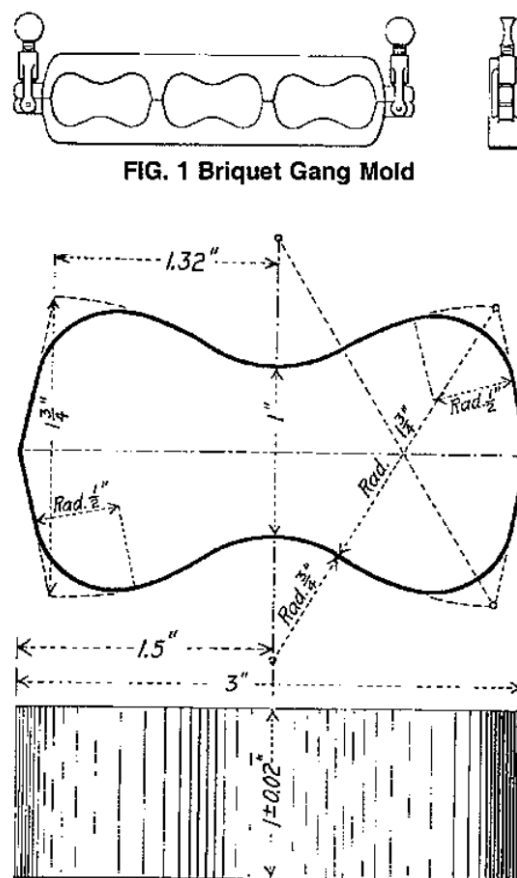


Figure 3.2 – Briquette gang mould (1) and individual mould dimensions in inches (The American Society for Testing and Materials, 1999)

3.6.3 Specimen Casting

Flexural and briquette specimens were cast ensuring symmetrical distribution within the moulds according to AS 1012.8.2-2014. The moulds were tapped with a mallet to remove entrapped air and the top surface was struck off, smoothed, and covered.

Compressive specimens were not easily externally vibrated. The vibrating table was not large enough for all specimens and hand vibration with the mallet was slow to visibly move entrapped air. To address this, cylinders were compacted by rodding aligning with clause 7.3 of AS 1012.8.1-2014. The moulds were filled in two approximately equal layers with 25 strokes evenly distributed over the mould cross-section. Care was taken to not contact the baseplate and just penetrate the underlying layer (Standards Australia, 2014b). After compaction, the top of each cylinder was struck off, smoothed and a mould cap was installed.

All mixing, rheological testing and casting were conducted with the assistance of laboratory technicians at Wagners Precast Laboratory in Wacol.

3.6.4 Curing Conditions

Initially, all specimens are covered and left undisturbed in the lab environment for no less than 18 hours and no more than 36 hours as per AS 1012.8.1-2014. Compressive specimens were then demoulded and packed for transport with care taken to avoid damage, moisture loss or temperature variations outside those specified (Standards Australia, 2014b). Flexural and tensile specimens remained in their moulds but were similarly packed and transported to the standard moist curing fog room and testing laboratory at the University of Southern Queensland, Toowoomba Campus. The methodology to transport samples over this distance was adopted so that a more appropriate high-capacity pan mixer could be used.

As per AS 1012.8.2-2014 the remaining specimens were demoulded after 48 hours and returned to standard moist curing as soon as possible until testing. The curing environment was 27 degrees centigrade with a relative humidity of 90%, as the literature suggests typical ECC with high fly ash content can benefit from curing at high relative humidity (Xu et al. 2021).

Compressive specimens were removed from standard curing eight days before testing so that GFRP could be wrapped. Unconfined and confined specimens were cured under laboratory conditions until testing.

3.7 Experimental Testing

3.7.1 Assessing Rheological Properties

Testing of rheological properties was completed during, and immediately after the completion of mixing. Samples were taken from the pan according to AS 1012.2-2014. A rheometer was not available for this project, as a result, a mini-slump and modified marsh cone were adopted. The simple testing methods of mini-slump flow and marsh cone time can be used to indicate the yield stress and plastic viscosity of ECC mortar as validated by Yang et al. (2009).

A slump flow test was performed as per AS 1012.3.5-2015 using a setup according to Figure 3.3. The slump flow diameter is related and well correlated to the yield stress of ECC (Ferraris 1999; Saak et al. 2004; Yang et al. 2009; Tan et al. 2017). Therefore, the slump flow test and related mini-slump test were used to assess the potential difference in yield stress between several PET contents.

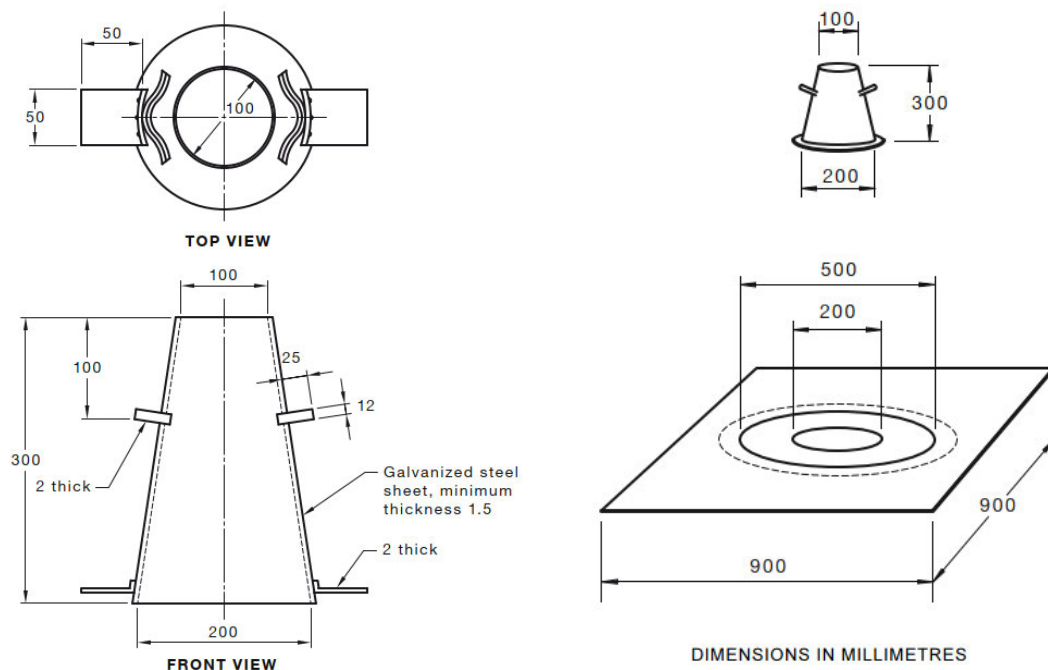


Figure 3.3 – Typical slump flow test (Standards Australia, 2015)

With a clean, level and lightly moistened mould and base plate, the slump cone was filled in one continuous pour until the top edge. The top of the mould was screed, and excess material was carefully removed from the base. The mould was carefully lifted vertically within 3 ± 1 s. The time between cone lift and flow to 500 mm circle represents the t_{500} flow time. Once the

flow was complete, the largest spread diameter (d_1) was measured. A second measurement perpendicular to the first was also taken (d_2). The test was invalid if there was a 50 mm difference between measurements. The mini-slump test was completed in the same manner using a truncated cone with a bottom diameter of 100 mm, top diameter of 70 mm and height of 59 mm as validated by Yang et al. (2009). Slump flow testing using these methods also helps to indicate resistance (or not) to segregation and was reported.

A modified marsh funnel as shown in Figure 3.4 with 850 mL capacity, and an internal orifice diameter of 20 mm indicates the plastic viscosity of ECC mortar as validated by Yang et al. (2009) using twice the volume. The cone was filled with the orifice closed. Once the orifice was opened the time for the entire contents of ECC mortar to flow out was recorded.



Figure 3.4 – Custom made flow funnel used to indicate plastic viscosity

3.7.2 Tensile Testing

Two cylinder specimens from each batch were split in tension concerning AS 1012.10-2000. Using a 2-channel automatic compression machine with a 2000 kN capacity, results were averaged over two tests. Testing was set up as shown in Figure 3.5 and aligned with the procedure detailed in clause 5 of AS 1012.10-2000.

An inspection for defects was firstly undertaken, and a straight edge was used to find the best plane of loading. Specimen diameters (to 0.2 mm) from the average of three measurements and lengths (to 1 mm) from the average of two measurements were determined and recorded. To load the testing machine, bearing strips were placed between the top and bottom platen, aligning the axis of the loading plane centrally and applying a small initial force, to remove side supports. The testing force was then applied without shock at a rate equivalent to 1.5 ± 0.15 MPa per minute until the increasing tensile forces were no longer supported. The maximum force applied was recorded and an image was used to note the appearance and type of fracture. At least one specimen from each batch was broken for further examinations.

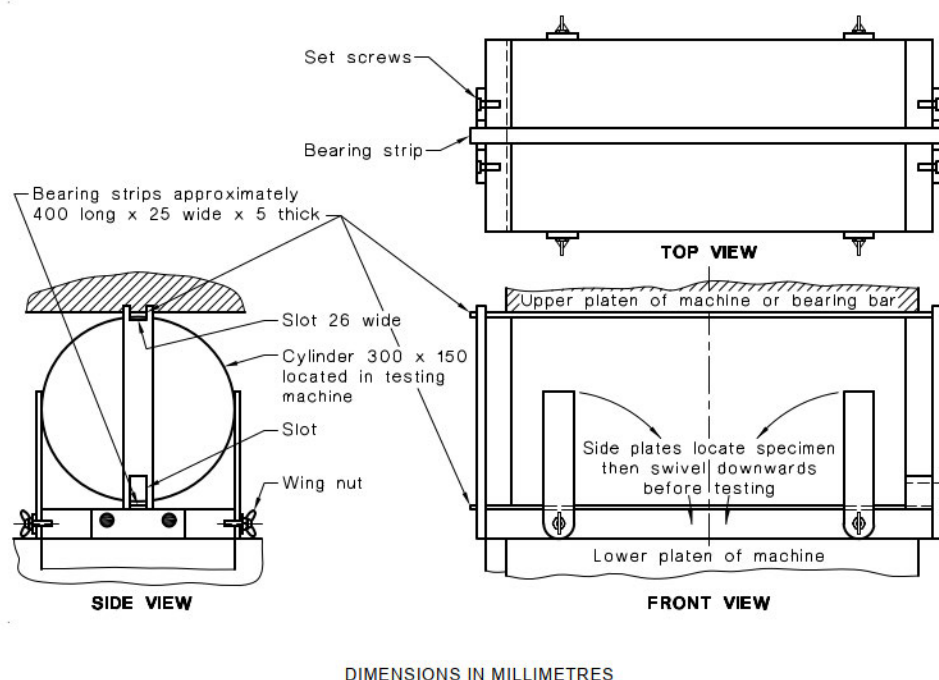


Figure 3.5 – Typical indirect tensile test jig arrangement (Standards Australia, 2000b)

Uniaxial tension testing at the University of Southern Queensland was not possible to Australian Standard for this project. Three briquet specimens for the control and two briquet specimens from each PET-ECC batch were tested in uniaxial tension with reference to the

methods of ASTM C307. Nine 3D printed moulds were available limiting the testing regime. A Hounsfield H5KS testing machine with 2500 N capacity was used to conduct the tests. The project adopted three briquets for the control batch to verify the characteristic ECC tensile strain capacity. Results for PET-ECC were indicated by the average of two tests.

An inspection for defects was first undertaken. Specimen depth from the average of three measurements was recorded. The width at the waist and length of each briquet was determined and recorded. Specimens were loaded centrally in the grips shown in Figure 3.6. A displacement was applied without shock at 1 mm/min and specimens were tested until failure. An image was used to note the appearance of microcracking. Results were inspected against the manually measured residual length of each specimen.



Figure 3.6 – Uniaxial testing apparatus

3.7.3 Flexural Testing

Two beam specimens from each batch were 4-point flexure tested, with reference to AS 1012.11-2000. Using a 2-channel automatic flexure testing apparatus with 2000 kN capacity,

results were averaged over the two tests. Due to resource limitations, two beams were adopted as a compromise to provide indicative results in this project. The apparatus should be set up as shown in Figure 3.7 and in alignment with clause 5 of AS 1012.11-2000, testing was performed in alignment with the procedure detailed in clause 6 of AS 1012.11-2000.

An inspection for defects was firstly undertaken and excess water was removed. Specimen length was measured. Width and depth were determined from the average of three measurements and recorded. Specimens were loaded sideways (with respect to the moulding orientation) onto the testing apparatuses supporting rollers. Loading rollers were then brought into contact with the specimen and their position was marked. The testing force was then applied without shock at a rate of 1 ± 0.1 MPa per minute until failure. The maximum force applied was recorded and cross-section measurements were performed nearest the failure. An image was used to note the appearance and type of fracture.

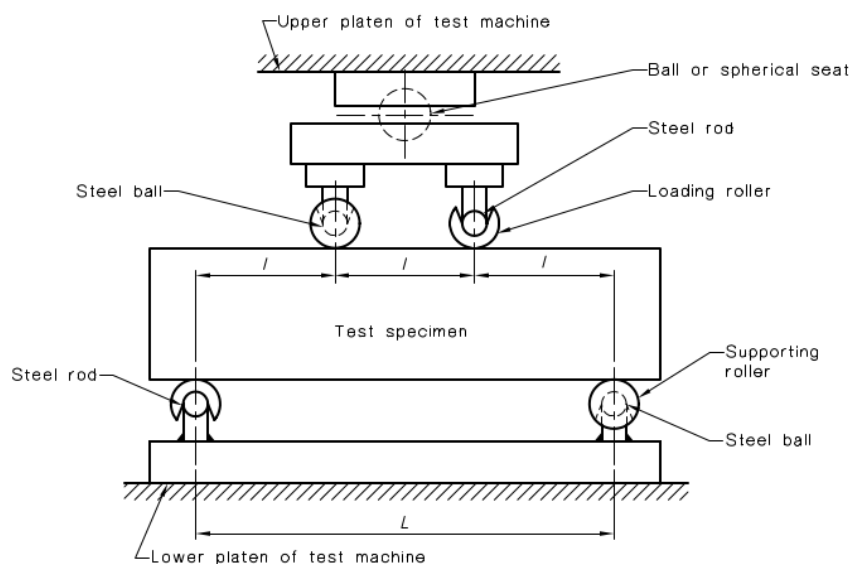


Figure 3.7 – Suitable flexure testing apparatus governed by clause 5 measurements (Standards Australia, 2000a)

3.7.4 Compression Testing

Four specimens from each batch were tested in compression with reference to AS1012.9-2014. Using a 2-channel automatic compression machine, with a 2000 kN capacity, results were averaged over two tests for confined and unconfined PET-ECC. Testing was set up as shown

in Figure 3.8 and conducted with reference to the procedures outlined in clause 8 of AS 1012.9-2014 and AS 1012.17-1997.

An inspection for defects was firstly undertaken and ends ground plane as required. A determination of the specimen height and diameter (to 0.2 mm) from the average of two perpendicular measurements was made and recorded.

Specimens were placed in the machine aligning its axis with the centre of thrust. Recording equipment was set up as shown in Figure 3.8. Testing commenced by bringing the upper platen to the specimen. Force was applied without shock at a rate equivalent to 20 ± 2 MPa per minute for at least 40% of expected compressive strength. The test was paused to remove the linear variable differential transformer (LVDT) compressometer. The deviation from AS 1012.17-1997 to determine an indicative static chord modulus of elasticity and poisons ratio was required due to limited resources in this project. The sample was then tested until the increasing forces were no longer supported as per AS 1012.9-2014. The maximum force applied was recorded and an image was used to note the appearance and type of failure. At least one specimen from each batch was broken for further visual examination.

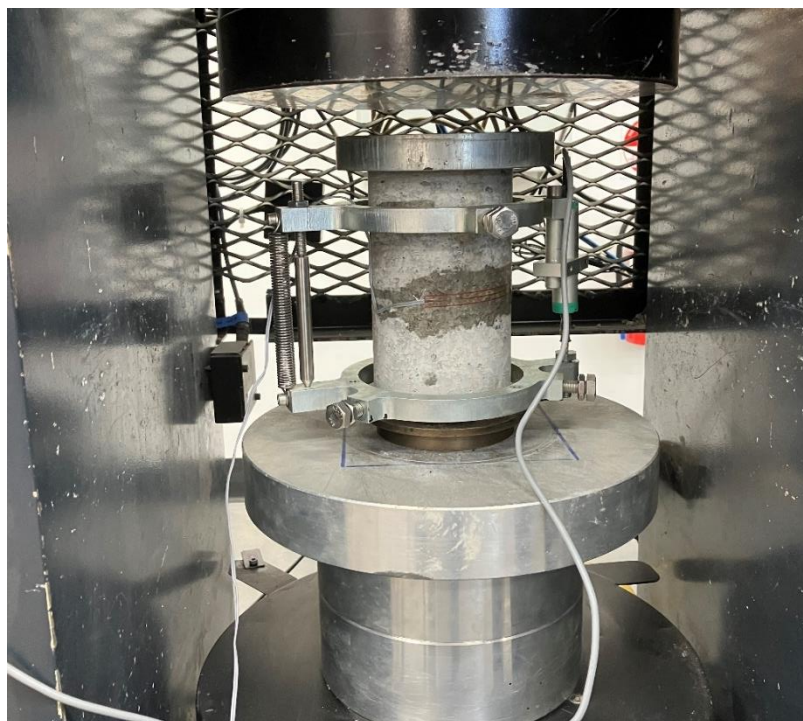


Figure 3.8 – Compression testing setup

3.8 Numerical Modelling

Using the student version of ABAQUS, a FE model was developed for PET-ECC as outlined in Chapter 5. The method of FE modelling for GFRP confined and unconfined compressive samples are well-established and validated by researchers such as Ootom et al. (2021).

The student version is limited to 1000 nodes and limits the analysis potential of the GFRP-confined PET-ECC. By developing a CDP model of the new ECC materials it can demonstrate the potential for further research.

CHAPTER 4. EXPERIMENTAL INVESTIGATION

4.1 Materials

Recycled PET granules were sourced from Kangavar et al. (2022) and Aston Sustainability in Brisbane. The PET is produced using a rotary blade granulator machine which generates relatively smooth sub-rounded particles. Additional processing (multiple runs through the granulator) was not possible for this project. As a result, more than thirty kilograms of material was required to produce the minimum required fine fraction of PET aggregate (Figure 4.1). The granules were observed to be elongated versus sand of the same fraction size. The different coloured particles were noted, and no other differences were identified.



Figure 4.1 – Example particle sizes of the fine PET aggregate fraction

The properties of the PET granules were found as shown in Table 4.1 with reference to the procedures detailed in AS 1141.4-2000 and AS 1141.5-2000.

Table 4.1 – PET granule properties

Apparent particle density (t/m ³)	1.32
Particle density dry basis (t/m ³)	1.32
Particle density SSD basis (t/m ³)	1.32
Bulk density – uncompacted (t/m ³)	0.7
Water Absorption (%)	0.1

RECS 15 fibre (Figure 4.2) was sourced from Domcrete Australia, a local importer. RECS denotes the industrial surface treatment used to tailor the fibre-matrix interface. PVA is hydrophilic and the surface treatment can be beneficial to encourage a uniform distribution and development of robust strain hardening (Li et al. 2002). The standard properties provided by the supplier are shown in Table 4.2.

Table 4.2 – Standard RECS 15 properties

Fiber Diameter (μm)	38
Length (mm)	8
Specific Gravity (g/cm^3)	1.3
Tensile Strength (MPa)	1600
Youngs Modulus (GPa)	40



Figure 4.2 – RECS15 PVA fibre

The remaining materials were graciously supplied by Wagners. This included grade 1 fly ash, medium quartz sand, general-purpose cement and HRWR.

Millmerran grade 1 fly ash (Figure 4.3) was supplied meeting the requirements of AS 3582.1-2016 and the Australian Technical Infrastructure Committee (ATIC) specification SP43. Typical quality parameters from the supplier are shown in Table 4.3 and the results of oxide testing are attached in Appendix D. The fly ash was separated from a bulk supply and not from individual bags.



Figure 4.3 – Grade 1 fly ash

Table 4.3 – Typical Millmerran grade 1 fly ash quality parameters

Fineness (%)	87
Average particle size (µm)	8
LOI (%)	0.2
Relative Density	1.94
Bulk Density (t/m ³)	1
Chloride ion (%)	<0.001
CaO (%)	1.57
Available Alkali (%)	0.3
Relative Strength (%)	105
Relative Water (%)	94

Medium sand from Rockwell Quarries, Southeast Queensland (Figure 4.4) was supplied. The sand is classified as natural quartz sand and has a free silica content of 94%, the grains are subrounded to angular. Further properties were found as shown in Table 4.4 according to the procedures detailed in AS 1141.4-2000 and AS 1141.5-2000.



Figure 4.4 –Rockwell medium quartz sand

Table 4.4 –Medium quartz sand properties

Apparent particle density (t/m ³)	2.64
Particle density dry basis (t/m ³)	2.47
Particle density SSD basis (t/m ³)	2.53
Bulk density – uncompacted (t/m ³)	1.6
Water Absorption (%)	2.3

The sand was observed to be visibly saturated. Further investigation found a moisture content of 4.3%.

A polycarboxylate HRWR with a solids content of 30% has been used to good effect in previous research but was not available for this project. ADVA LS 780, a high-performance polycarboxylic polymer-based HRWR was supplied for use by Wagners. A trial batch was conducted to estimate dosage and check compatibility. Potable water from the laboratory was combined with HRWR to form a uniform solution following the manufacturer's recommendations.

Finally, general-purpose Wagners cement was supplied and separated from a bulk supply and not from individual bags. The GFRP and strain gauges used in this project were kindly supplied by my supervisor Prof. Weena Lokuge.

4.2 Particle Size Distribution

The particle size distribution (PSD) of the sand supplied is shown in Table 4.5. The PET was remixed to approach the PSD of medium sand according to the grading limits of deviation for manufactured fine aggregate according to AS 2758.1-2014. For this project, the submitted grading was taken as the grading for sand and the supplied grading of PET was to be no more than the maximum deviations in the standard.

Table 4.5 – Medium sand PSD and grading limits

AS sieve size (mm)	Per cent passing (%)	Manufactured fine aggregate limits of deviation (%)
4.75	100	±5
2.36	90	±10
1.18	75	±15
0.6	54	±15
0.425	39	±10
0.3	24	±10
0.15	5	±5
0.075	2	±5

PET was initially separated into four parts using large sieves as shown in Figure 4.5. The large sieves available at the University of Southern Queensland Z1 Laboratory were 4.75 mm, 2.36 mm, and 1.18 mm. The large bin was used to collect coarse particles retained on the 4.75 mm sieve. Twenty-litre buckets were used to collect the medium particles retained on the 2.36 mm,

Steve was unavailable for this project and presents a source

Table 4.6 – Fine PET granules PSD

AS sieve size (mm)	Per cent passing (%)
4.75	100
2.36	100
1.18	80
0.6	51
0.425	NA.
0.3	18
0.15	1
0.075	1

The medium and fine portions were then remixed by weight on a case-by-case basis for each batch to ensure the PSD remained constant, these methods have been used by other researchers to limit the grading effect of recycled aggregate (Ghorbani et al. 2019; Kangavar et al. 2022). PET is a manufactured aggregate, and the limits according to AS 2758.1-2014 were accepted for the project given the challenges in acquiring and processing the material. Figure 4.7 shows the higher fraction size of the processed PET is aligned with the lower deviation limit of the medium sand.

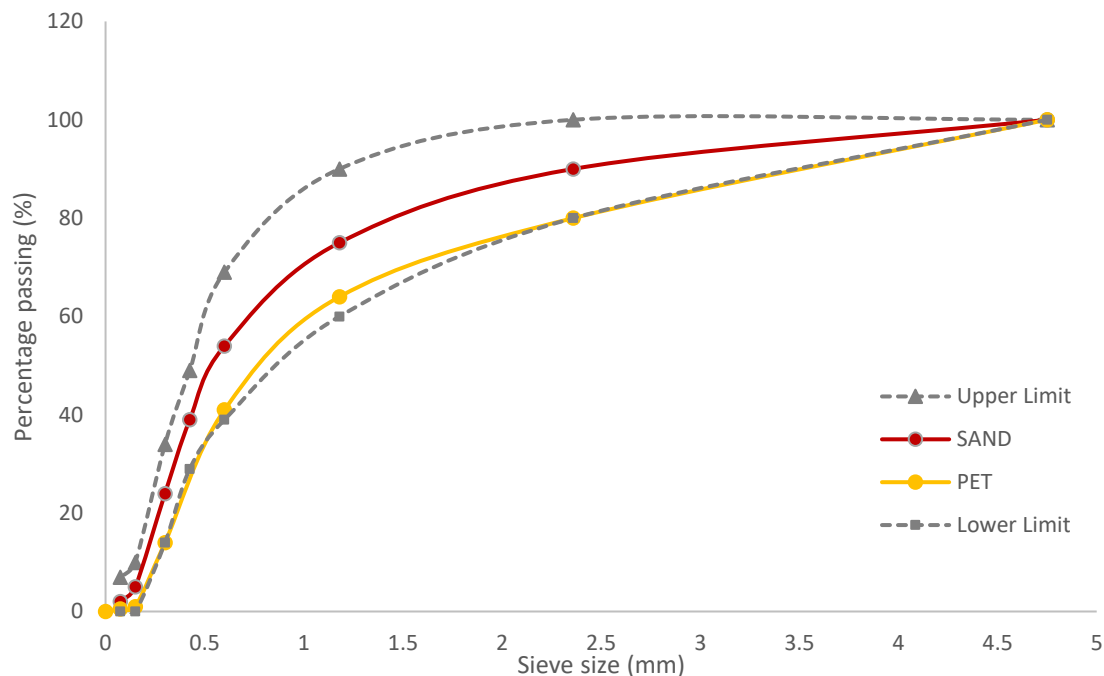


Figure 4.7 – Particle size distribution of PET and medium sand

4.3 Material Quantities

The total required volume of ECC was calculated with 20% wastage as shown in Table 4.7.

Table 4.7 – ECC volume calculations

QTY	Shape	Specimen size (mm)			Volume of each sample (m ³)	Total Volume (m ³)
24	Cylinder		100	200	0.0016	0.0377
8	Beam	450	100	100	0.0045	0.0360
8	Briquette	75	25	40	0.000075	0.0006
					Total fresh volume (m ³)	0.074
					Total including wastage (m ³)	0.089
					Total per batch (m ³)	0.022

HFA-ECC with a fly ash-to-cement ratio of 2.4 and a sand-to-binder ratio of 0.37 was adopted in this project. As validated by Yang et al. (2007) a fly ash content of two to three times cement has the unique potential to improve greenness and develop robust multiple cracking and tensile strain hardening. The low sand-to-binder ratio has many benefits, primarily in this application it was to limit the negative impacts on fibre dispersion and interface bonding (Guan et al. 2019). The mixture proportions adopted after the trial batch are based on the findings of Yang et al. (2007) and are shown in Table 4.8.

Table 4.8 – HFA-ECC mixture proportions

	Weight per unit volume (kg/m ³)
Cement	362
Sand	456
HRWR	7.4
Fly Ash	870
PVA (2% Vol)	26
Water	320

The volumetric replacement of sand within HFA-ECC was based on the apparent particle density of the aggregates. The measured apparent density is similar to the specific gravity but also accounts for any voids present in the materials. The measured apparent particle density of

sand was 2.64 t/m³ and correlated well with the supplied specific gravity of 2.6. For volume substitution, particle density was used, and it is assumed that PET does not contain voids.

The mixture proportions of HFA-ECC were kept constant beside sand in all PET-ECC trials. The replacement proportions of sand to PET in PET-ECC are shown in Table 4.9.

Table 4.9 – PET-ECC mixture proportions

	Constituent	Weight per unit volume (kg/m³)
Batch 1: Control	Sand	456
	PET	0
Batch 2: 10% PET	Sand	410
	PET	23
Batch 3: 30% PET	Sand	319
	PET	69
Batch 4: 50% PET	Sand	228
	PET	114

The total volume of materials required for the project is tabulated in Table 4.10 and is simply the multiplication of the trial proportions to the volume required. The quantities of sand and water are adjusted for a four per cent moisture content. The total volume of materials was confirmed using the absolute volume method.

Table 4.10 – PET-ECC material quantity

	Weight (kg)
Cement	32.3
Sand	32.5
PET	4.6
HRWR	0.66
Fly Ash	77.6
PVA (2% Vol)	2.32
Water	27.6

4.4 Sample Preparation

4.4.1 Trial Batch

A trial batch was firstly performed to assess HRWR dosage and resulting rheological properties. The full-sized pan mixer was not suitable for small mixing quantities and a bucket mixer was utilised. The recommended dosage of ADVA LS 780 ranges from 400 ml - 800 ml per hundred kilograms of binder.

The trial batch used the lowest recommended HRWR dosage and indicated a high plastic viscosity through long flow time. Additionally, the matrix also presented with a low slump flow diameter indicating higher yield stress. After fibre addition and the fibres failed to distribute uniformly, and clumping was evident. Limited segregation was observed. These findings were likely a result of the low power and shearing action of the bucket mixer.

Without the experience or resources to conduct further testing to pinpoint the matrix saturation dosage it was decided to increase the HRWR dosage to approach the maximum dosages available from the literature. As a rheological control, polycarboxylate HRWR has been dosed up to HRWR to binder ratios of 0.5% to 0.75% without the use of a VMA (Yang et al. 2009). From the literature, it was expected that after the saturation dose of HRWR was reached, a slight decline of mechanical properties was possible, but would encourage a uniform fibre distribution.

An HRWR to binder ratio of 0.6% was adopted in this project. This also represented a midrange dosage from the manufacturer. Optimal tailoring of the HRWR was not possible due to the low mixing energy of the trial bucket mixer and further research is required.

4.4.2 Mixing and Casting

Production of PET-ECC specimens was undertaken on 16 August 2022 at Wagners Precast Laboratory in Wacol, Brisbane. Each batch was prepared using a Bennett Equipment planetary pan mixer. The mixing procedure followed Section 3.3 using the proportions described in Section 4.3. However, the final step in the mixing procedure was modified. After visual inspection, the fibres did not appear to be distributed until eleven minutes (for control and 10% PET replacement) and up to thirteen and fifteen minutes of mixing for 30% and 50% PET replacement ratios, respectively. This indicated insufficient mixing energy was available from the pan mixer and highlighted the challenge of ensuring adequate distribution of the fibres.

Assessment of the mortar matrix rheology was performed for each batch using the modified marsh cone and mini-slump tests detailed in Section 3.7. After the addition of fibres, ECC should typically have good self-consolidation behaviour and the deformability factor (r) would be calculated as in Equation 4.1.

$$r = \frac{D_{avg} - D_0}{D_0} \quad (4.1) \text{ (Nawy 2008)}$$

Where D_{avg} is the average flow diameter from two measurements and D_0 is the bottom diameter of the slump cone. However, due to insufficient mixing energy, the consolidation behaviour was very poor with significant segregation. Due to the impact of segregation rheological comparisons were not explored further in this project.

The difference in matrix properties between the control and PET-ECC was apparent and is discussed in Section 6.1. After the addition of fibre, further differences were observed as the PET content increased. The mixture was sticky and extremely hard to work with. The amount of segregation in the slump flow test (Figure 4.8) was significant and the ECC matrix was considerably more stable with 50% PET replacement.



Figure 4.8 – ECC slump flow tests a) 0% PET-ECC, b) 50% PET-ECC

After fresh testing was complete the specimens were cast following the procedure detailed in Section 3.7.2. Standard steel moulds were used for compressive and splitting tensile specimens and a 3D-printed gang mould was used for briquette specimens. Several moulds were custom made from form ply for flexural beams as shown in Figure 4.9.



Figure 4.9 – Flexural specimens cast and covered in custom made form ply moulds

Specimens were then left undisturbed in the lab, as shown in Figure 4.10, for 24 hours.



Figure 4.10 – Cylinder and briquette specimens' initial cure

Several specimens bled, suffering significant paste loss. This is shown on the day of casting by the table in Figure 4.10 and then 24 hours later in Figure 4.11.



Figure 4.11 – Control batch cylinder paste loss and table accumulation

Demoulding of cylindrical specimens was completed after 25 hours. Before standard curing as detailed in Section 3.6.4, each cylinder was individually wrapped in wet material and damp cardboard for transport in sealed twenty-litre buckets. Flexural and briquette specimens were transported in their moulds wrapped in wet material. The transport time from Wagners to the fog room at the University of Southern Queensland, Toowoomba Campus, was two and a half hours with bucket temperatures steady at an average of 22.3 degrees centigrade. No damage from transport was observed and flexural specimens were demoulded after 48 hours and returned to the curing room as soon as possible as shown in Figure 4.12. Care was taken to avoid dry areas.



Figure 4.12 – Several PET-ECC specimens in the UniSQ fog room

4.4.3 End Grinding

Cylinders were removed from the curing environment and heights were measured eight days before testing. The average of two opposing cylinder measurements for the six cylinders in each batch was found. The measurements are presented in Appendix E Table E.1.

Contradicting the noted segregation in slump tests, as the PET replacement ratio increased the amount of bleeding and loss of cylinder height was reduced as shown in Figure 4.13. These findings indicate that the matrix stability of higher PET contents may have also reduced bleeding losses. However, confidence in the control batch is low, and it is possible two steel moulds had excessive gaps.

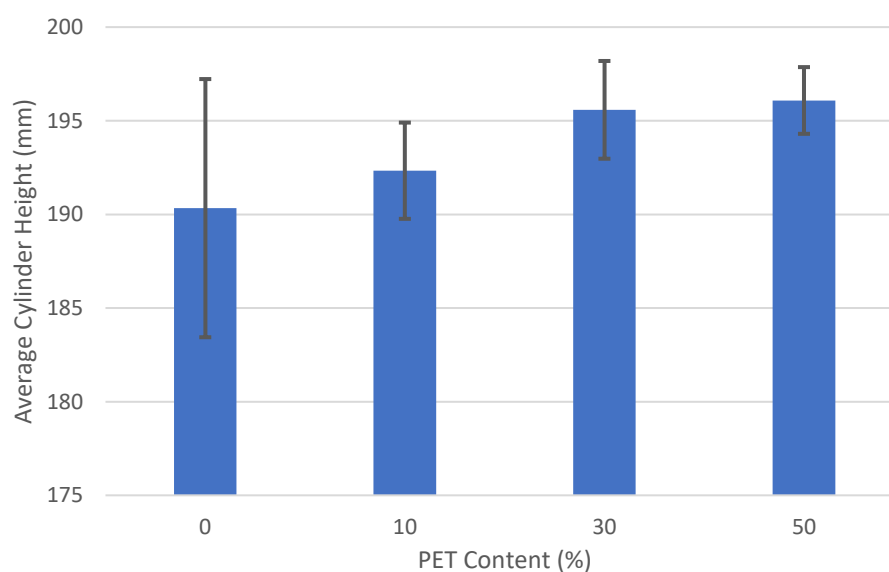


Figure 4.13 – Average cylinder heights and standard deviation before end grinding

Cylinders were all tamped, trowelled level, and capped following the same procedure. Bleeding caused large variations in height and paste distribution throughout the top fibres as shown in Figure 4.14 and Figure 4.15.



Figure 4.14 – Cylinder bleeding defect in 10% PET-ECC



Figure 4.15 – Cylinder height variations in the control batch

A Sherpa concrete saw was used to address this. All cylinders were cut to 170 mm heights as shown in Figure 4.16. Normal concrete can fracture from cutting with this method, a trial cut confirmed this was not the case for PET-ECC, and all edges remained intact. This methodology and deviation from the standard specimen sizes were necessary due to the unforeseen challenges related to casting.



Figure 4.16 – a) top, b) side of all cylinders cut level to 170 mm height

4.4.4 GFRP Wrapping

Confined compressive specimens were allowed to dry and were then wrapped using GFRP. GFRP was cut for a thirty-millimetre hoop overlap. The cylinders were first cleaned to remove dust contaminants.

Existing surface pores were filled and primed with WEST SYSTEM 105 epoxy resin (Table 4.11) following the manufactures recommendations. The priming coat was allowed to go off before wrapping. Equal weights of wrap to laminating resin were applied to each cylinder. To ensure resin uniformity, the glass fibres were fully wet out on a flat surface before wrapping. Approximately five millimetres of the wrap was trimmed below the ends of each cylinder. The wrapped cylinders (Figure 4.17) were allowed to cure with unconfined specimens, for eight days in the lab environment before testing. This method of confinement was adapted from industry advice and the findings of Lokuge and Karunasena (2016) who used GFRP sheets in the confinement of geopolymer concrete.



Figure 4.17 – GFRP wrapped cylinders

Table 4.11 – WEST SYSTEM 105 epoxy resin and 206 slow hardener properties

Compression yield (psi)	11,500
Tensile elongation (psi)	7,300
Flexural strength (psi)	11,800

4.4.5 Attaching Lateral Strain Gauges

Strain gauges were glued onto each cylinder to be tested under compression. Due to resource and time limitations, a single strain gauge was attached to the midsection of each specimen as shown in Figure 4.18. Unconfined specimens were primed with epoxy and sanded to fill pores and insure adhesion.



Figure 4.18 – Compression cylinders ready for testing

4.5 Experimental Testing

Testing of the specimens was carried out over the period of seven days, commencing with flexural testing on 8 September 2022 and compressive and tensile testing on 15 September and 16 September 2022. This represents testing at 23 and up to 31 days since casting. The standard time for testing is 28 days. As laboratory availability was restricted, the variation in age was necessary to complete testing on a large number of specimens.

All testing was conducted with the assistance of laboratory technicians at the University of Southern Queensland, Toowoomba Campus. Several specimens were defective as previously discussed and variations in dimensions and weights were recorded to help provide detail on any affected test results.

4.5.1 Tensile Testing

Splitting tensile testing was performed according to AS 1012.10-2000 using a using 2-channel automatic compression machine with a 2000 kN capacity. The tensile testing of a control specimen is shown in Figure 4.19. The specimens were inspected for defects, weighed, and measured before testing.

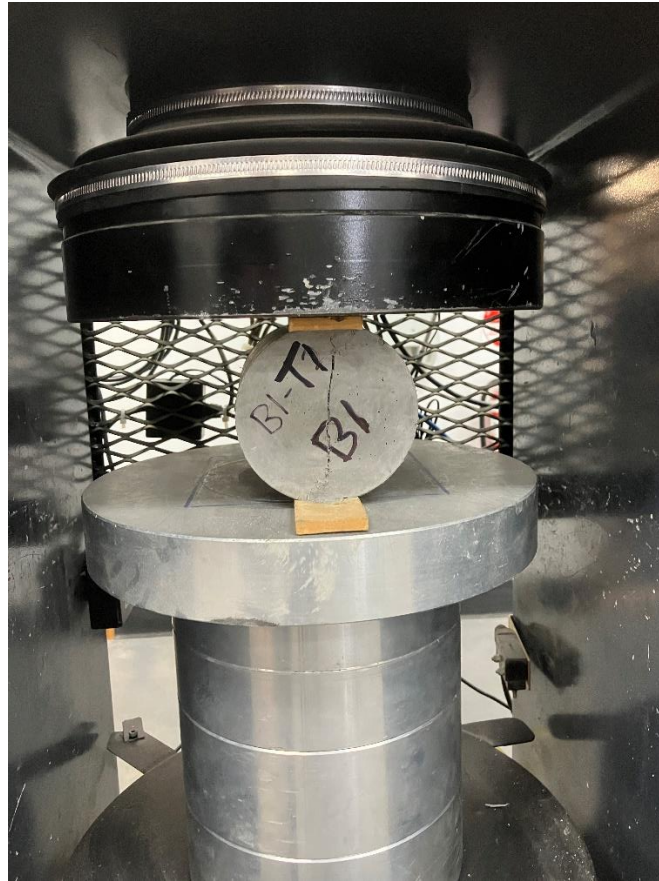


Figure 4.19 – Batch 1 control splitting tensile testing

The indirect tensile strength was calculated using:

$$T = \frac{2000P}{\pi LD} \quad (4.2)$$

Where:

T = the indirect tensile strength (Mpa).

P = the maximum applied force indicated by the testing apparatus (kN).

L = the cylinder length (mm).

D = the cylinder diameter (mm) (Standards Australia 2000c).

Uniaxial tensile testing was conducted using a Hounsfield H5KS testing machine with 2500 N capacity, according to ASTM C307. The force and elongation data were recorded using QMat software on a separate PC as shown in Figure 4.20 and the residual length was manually checked. The specimens were inspected for defects and measured before testing.

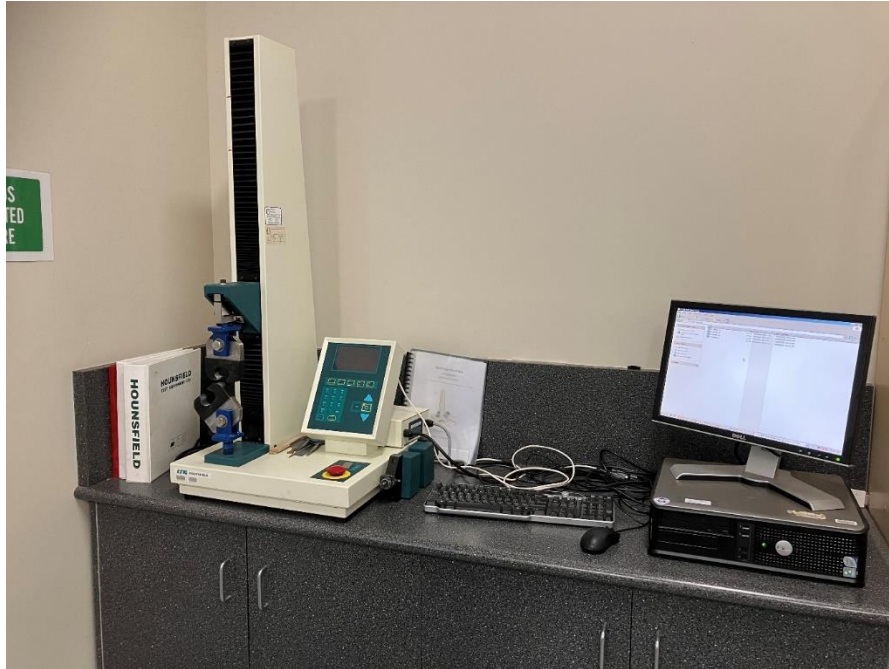


Figure 4.20 – Hounsfield H5KS testing machine

The direct tensile strength is indicated by the stress calculated at maximum load, given by:

$$S = \frac{P}{bd} \quad (4.3)$$

Where:

S = the stress applied to the specimen (MPa).

P = the load at or prior to failure (N).

b = the width at the waist of the briquet specimen (mm).

d = the depth of the briquet specimen (mm) (The American Society for Testing and Materials 1999).

4.5.2 Flexural Testing

Flexural testing was conducted at 21 days using a 2-channel automatic compression machine, with a 2000 kN capacity. Beams were inspected for defects, weighed, and measured before testing.

Two twelve-millimetre-thick slabs were produced for the control and 50% PET replacement ratios. With the assistance of laboratory technical staff, the flexural testing machine was loaded in a similar manner to the planned full-sized beams. Due to limitations with the automatic testing apparatus, loads were applied manually at approximately 0.8 kN per second. Testing of slabs was conducted to confirm data collection methods.

A load cell and platen displacement laser were connected to an HBM Mx 1615 data logger and recorded using a windows PC. Results were obtained that validated the testing setup and data collection methods as shown in Figure 4.22. Both samples demonstrated strain-hardening-like behaviour and smooth plots.



Figure 4.21 – Equipment validation of flexural testing apparatus

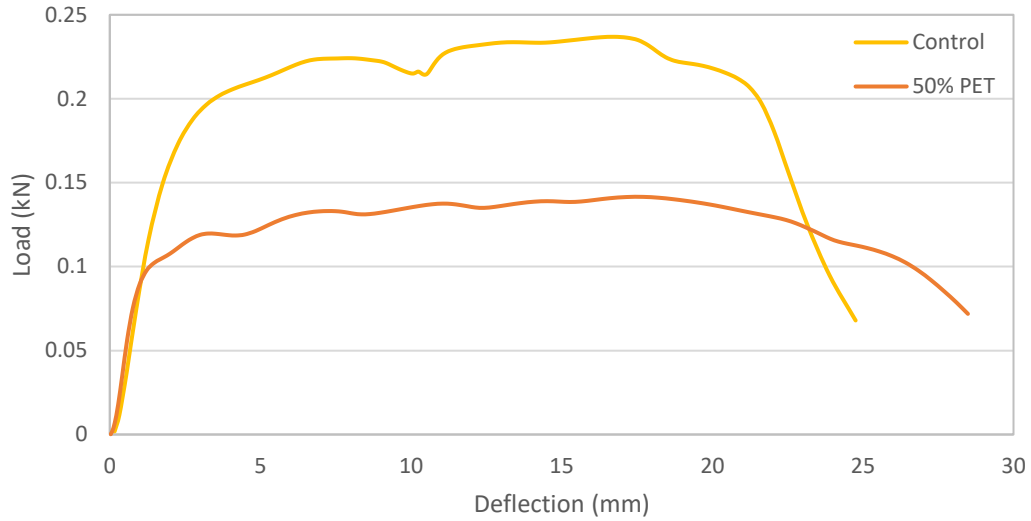


Figure 4.22 – Flexural test data validation

Beams were loaded in a similar manner to the slabs with reference to Section 3.7.3. The flexural apparatus at UniSQ did not have available mounting positions to test the beams as per AS 1012.11 and a modified loading was needed and adopted as shown below.

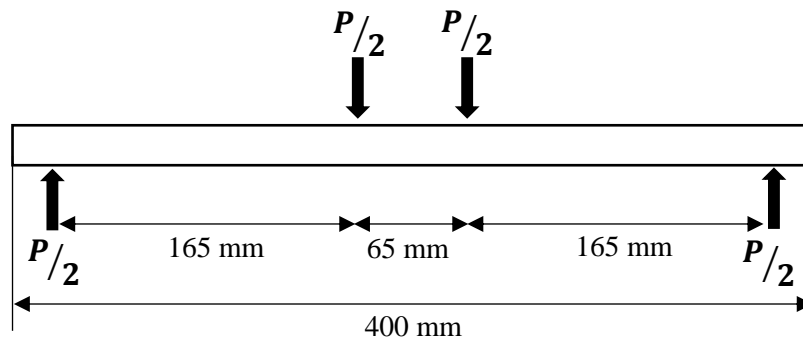


Figure 4.23 – Equilibrium forces acting on beam specimen

The estimated modulus of rupture will now be given by:

$$\sigma = \frac{3P(L-L_i)}{2bd^2} \quad (4.4)$$

Where:

σ = the estimated modulus of rupture (MPa).

P = the load applied (kN).

L = the total length between supports (m).

L_i = the length between applied point loads (m).

b = the average depth (mm).

d = the average width (mm).

4.5.3 Compression Testing

Compression testing was performed using a using 2-channel automatic compression machine, with 2000 kN capacity. An HBM Mx 1615 data logger was used to collect data which was recorded using a windows PC. The specimens were inspected for defects, weighed, and measured before testing.

The static chord modulus of elasticity (E) was firstly estimated using an LVDT compressometer. The static chord modulus was calculated from Equation 4.5 and validated by a linear regression analysis of the elastic stress-strain curve.

$$E = \frac{(G_2 - G_1)}{\epsilon_2 - 0.00005} \quad (4.5)$$

Where:

G_2 = the test load divided by the unloaded cross-sectional area of the specimen (MPa).

G_1 = the applied load at a strain of 50×10^{-6} divided by the unloaded cross-sectional area of the specimen (MPa).

ϵ_2 = the deformation at the test load divided by gauge length (10^{-6} m/m) (Standards Australia 1997).

As shown in Figure 4.24, compression testing to failure was then performed using the platen displacement method.



Figure 4.24 – Control GFRP cylinder under compression with centralized fibre rupture

The compressive strength was calculated by dividing the maximum force by the specimens' measured cross-sectional area (Standards Australia 2014c).

$$C = \frac{4P}{D^2\pi} \quad (4.6)$$

Where:

C = the compressive strength (MPa).

P = the maximum force applied to the specimen (kN).

D = the diameter of the specimen (mm) (Standards Australia 2014c)

While there is little consensus on the best method of estimating a column's ductile performance, the displacement ductility factor is useful (Lokuge & Karunasena 2016). Most GFRP confined composites in this project demonstrated strain softening similar to those of Lokuge and Karunasena (2016) in geopolymer concrete columns. This project adopts the ductility factor definition of Lokuge and Karunasena (2016) as presented below:

$$\mu = \frac{\varepsilon_2}{\varepsilon_1} \quad (4.7)$$

Where:

μ = the displacement ductility factor

ε_1 = an approximation of strain on the limit of elastic behaviour.

ε_2 = the corresponding strain to 85% of the peak stress.

The definitions used for μ in relation to the stress-strain curve are shown in Figure 4.25. The best fit line was found for each specimen through a linear regression analysis of the elastic portion of the stress-strain curve. The line was extrapolated for each specimen to intersect with the peak stress.

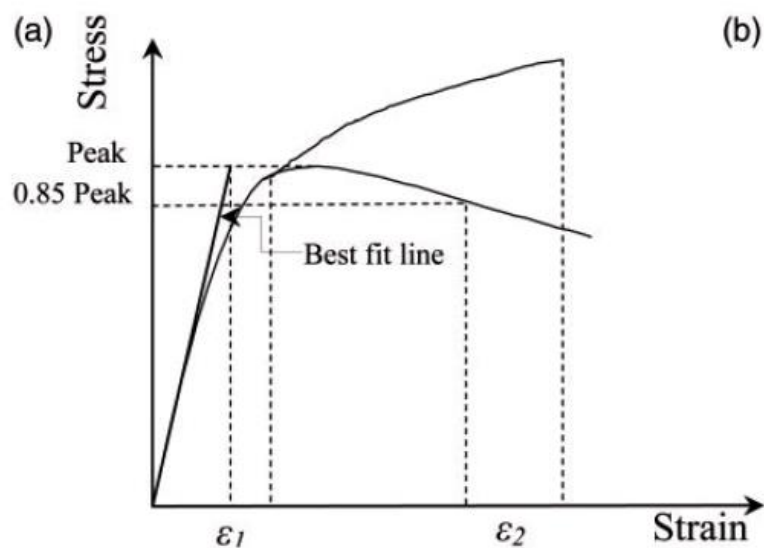


Figure 4.25 – Typical curves for ductility factor measurement (Lokuge & Karunasena 2016)

CHAPTER 5. NUMERICAL INVESTIGATION

A finite element model (FEM) was used to help validate experimental results and demonstrate the potential to predict the behaviour of PET-ECC columns under compression. PET-ECC was modelled using the student version of ABAQUS 2021 and was limited to 1000 nodes. Further research is needed using the commercial version.

5.1 Model Development

Modelling of the ECC cylinders was based on the findings and validation of Ootom et al. (2021) and uses a one-to-two-cylinder height ratio. Due to mesh size limitations, a conventional shell element with reduced integration (S4R) was not considered as shown in Figure 5.1.

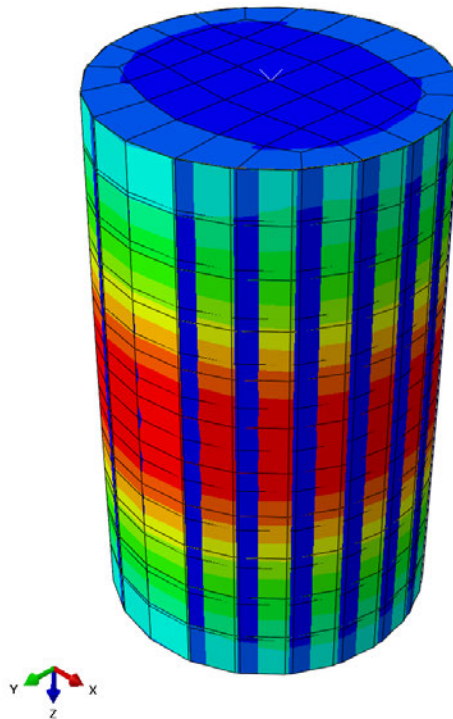


Figure 5.1 – GFRP (S4R) wrapped cylinder with infill protrusion

PET-ECC cylinders and GFRP jackets were to be implemented as solid three-dimensional elements meshed by eight-node brick elements (C3D8R). Due to student version limitations a minimum mesh size of 30 mm was required for GFRP and ECC. A sensitivity analysis was not possible for GFRP-confined models, and this is an area for additional research.

Hourglass control, reduced integration and NLGEOM were activated. The column base is assumed fully restrained; the top is restrained to allow axial displacement loading. Ootom et

al. (2021) utilise a ridged loading plate to avoid scattering of results and provide an even load distribution to the top of the column. This was implemented using the planar shell feature to create a third ridged element. To avoid penetration in the normal direction the interface is assumed to be hard contact between the plate and the top of the column. A frictional contact interface and coefficient of 0.25 was assumed in the tangential direction (Otoom et al. 2021).

Tie constraints can be used to model the interaction of ECC to GFRP. It effectively fuses the elements and has been adopted when debonding failures are not observed (Otoom et al. 2021). The developed model is shown in Figure 5.2.

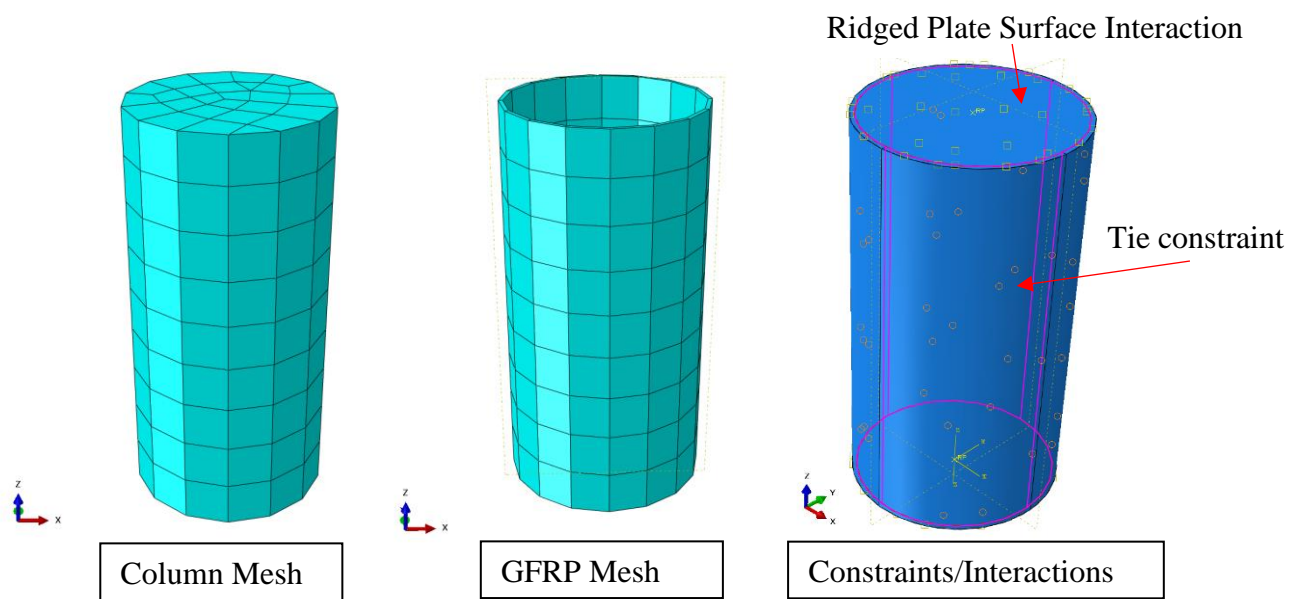


Figure 5.2 – ABAQUS model development

5.2 Material Simulation

No experimental testing of the GFRP wrapping and West System epoxy was conducted. Therefore input parameters were tailored based on the work of Otoom et al. (2021) and the known experimental results of the ECC infill.

5.2.1. Concrete Damaged Plasticity

The concrete damaged plasticity model (CDP) was utilised to model the behaviour of the composites in this project. CDP is a widely applicable and validated method of modelling the

inelastic behaviour of ordinary concrete and composites (Cai et al. 2020; Ootom et al. 2021; Yuan et al. 2021). To limit convergence problems the main plasticity parameters were adapted from the findings of Ootom et al. (2021) and Cai et al. (2020) as shown in Table 5.1.

Table 5.1 – CDP model elasticity input parameters

Parameter	Model Input
Dilation Angle	40
Eccentricity	0.1
Fb0/fc0	1.16
K	0.667
Viscosity Parameter	0.0005

Within the finite element elastoplastic model, CDP allows the use of both tension and compression properties. The uniaxial relationships between compressive and tensile stress-strain as well as damage-strain for the control ECC are shown in Figure 5.3.

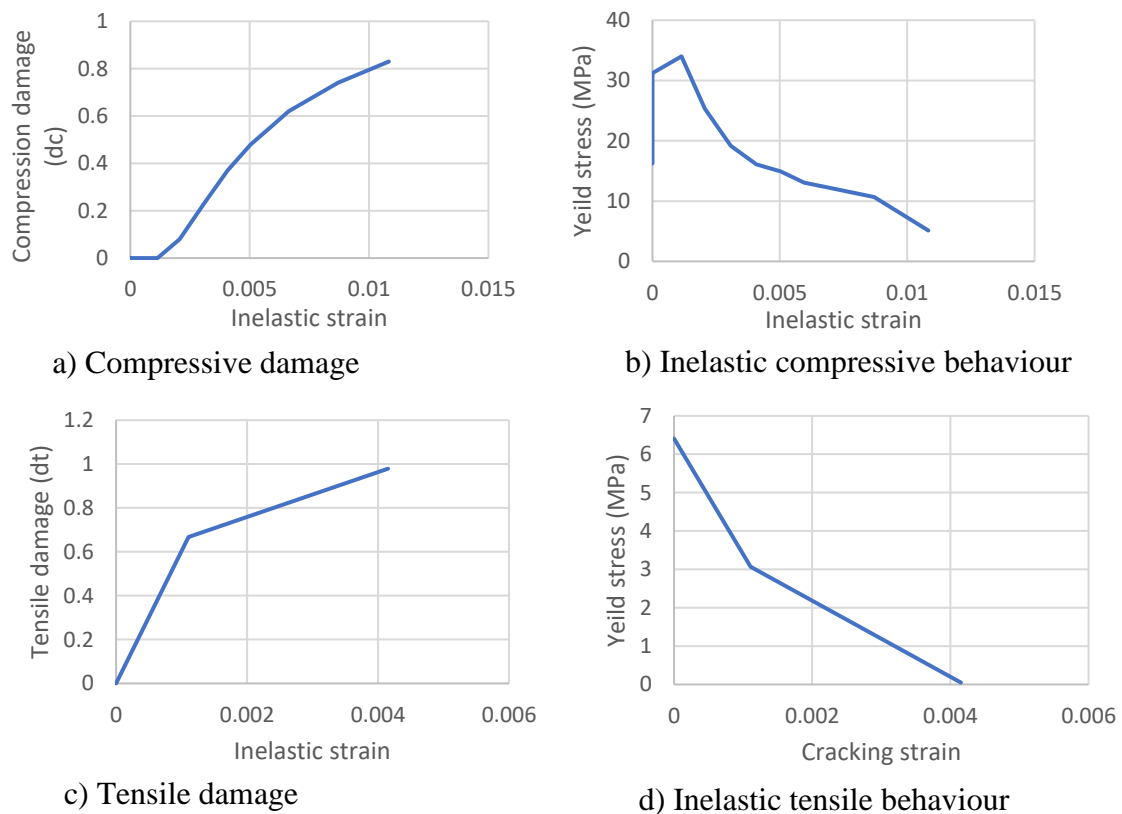


Figure 5.3 – Stress-strain and damage-strain relationships for the control ECC.

The initial FEM elastic behaviour is governed by the modulus of elasticity and Poisson's ratio, and the inelastic behaviour is governed by CDP. The compressive and tensile stresses are defined by ABAQUS according to Equations (5.1) and (5.2) (Otoom et al. 2021).

$$\sigma_c = (1 - d_c)E_0(\varepsilon_c - \varepsilon_c^{pl}) \quad (5.1)$$

$$\sigma_t = (1 - d_t)E_0(\varepsilon_t - \varepsilon_t^{pl}) \quad (5.2)$$

Where, σ is the stress, d_c and d_t are the compressive damage and tensile damage parameters respectively and ε is the respective inelastic and plastic strains. The damage parameters are defined by the uniaxial behaviour of concrete as determined in Equations (5.3) and (5.4) and shown in Figure 5.4.

To achieve this it is assumed the experimental stress-strain curves for tension and uniaxial compression can be converted into stress and plastic strain curves as suggested by Otoom et al. (2021).

$$d_c = 1 - (\sigma_c / \sigma_{cu}) \quad (5.3)$$

$$d_t = 1 - (\sigma_t / \sigma_{t0}) \quad (5.4)$$

Where σ_{cu} and σ_{t0} are the respective ultimate stresses.

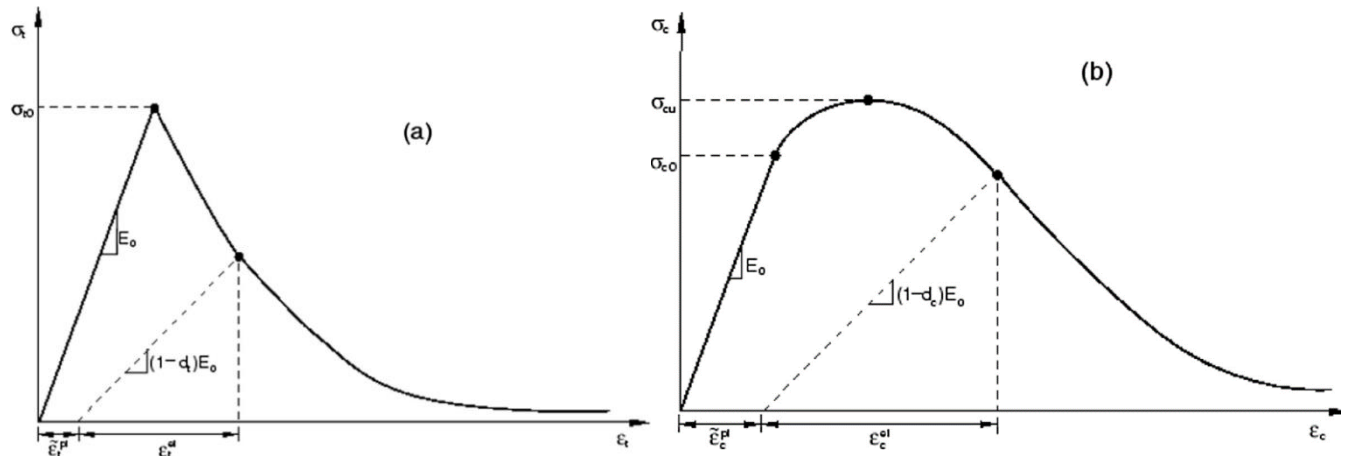


Figure 5.4 – Behaviour of column infill under a) tension and b) compression (Otoom et al. 2021)

CHAPTER 6. RESULTS AND DISCUSSION

6.1 Limitations

The production of ECC in this project was negatively influenced by a lack of mixing energy. While the pan mixer was a planetary unit, it was limited to a single speed and provided insufficient energy to uniformly distribute the fibre reinforcing throughout the matrix. As a result, poor deformability was observed with significant segregation. While the results are still promising, they likely do not reflect the true potential of SEQ-ECC and PET-ECC. Further research is recommended.

6.2 Fresh Concrete Testing

Assessment of the fresh rheological properties of the composites was undertaken following Sections 3.8.1 and 4.4.2. The experimental data is shown in Appendix E Table E.2.

6.2.1 Mortar Rheology

The mortar rheology was found according to Sections 3.7.1 and 4.4.2. In conventional ECC an optimally high plastic viscosity and low yield stress of the mortar are beneficial to encourage a uniform fibre distribution and good hardened properties (Yang et al. 2009; Li & Li 2012). Low yield stress is indicated by high slump flows and high plastic viscosity is indicated by longer modified marsh funnel flow times. As shown in Figure 6.1 the lowest relative yield stress and highest relative plastic viscosity were achieved with 30% PET replacement.

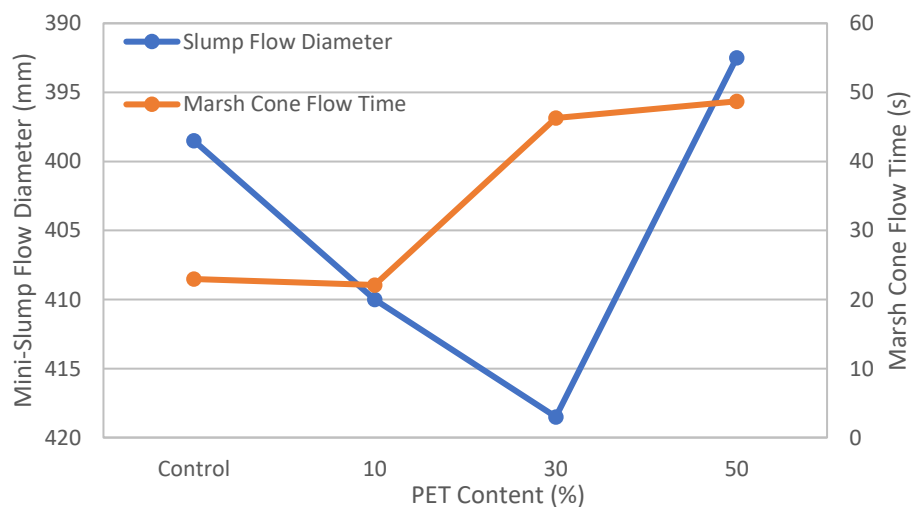


Figure 6.1 – Indicative mortar rheological properties

The mini-slump mortar test indicated that the addition of PET granules initially decreases matrix yield stress at 10% and 30% PET replacement before increasing the yield stress at 50% PET. It was also noted that PET granules slightly decreased the plastic viscosity at 10% PET replacement before it rose significantly. However, while the indicative plastic viscosity was highest for 30% and 50% PET replacement, it was observed that the mortar no longer flowed through the cone as shown in Figure 6.2. The PET granules developed a sticky black residue that did not allow the aggregates to flow through the twenty-millimetre orifice. This is suboptimal in ECC applications.



Figure 6.2 – 50% PET-ECC mortar aggregates stuck in flow cone

The mortar with 50% PET replacement also displayed a significant degree of segregation in the form of a halo. This indicated a large visual change in matrix properties as shown in Figure 6.3. No halo or segregation was present in 0% and 10% PET ratios. This halo indicates that mortar segregation increases with the addition of PET.

In the past PET has been substituted in normal concrete without admixtures. Reductions in workability have been observed to different degrees (Albano et al. 2009; Ferreira et al. 2012; Rahmani et al. 2013; Saikia & de Brito 2014; Almeshal et al. 2020; Dawood et al. 2021; Kangavar et al. 2022). Reductions are largely attributable to increased friction due to the shape of PET particles used. This project has found a similar reduction in plasticity as PET increases. The segregation could then be attributable to the limited absorption of PET aggregate and

reduced HRWR requirements. This indicates the dosage of HRWR could be tailored to obtain more desirable mortar properties for higher PET contents.

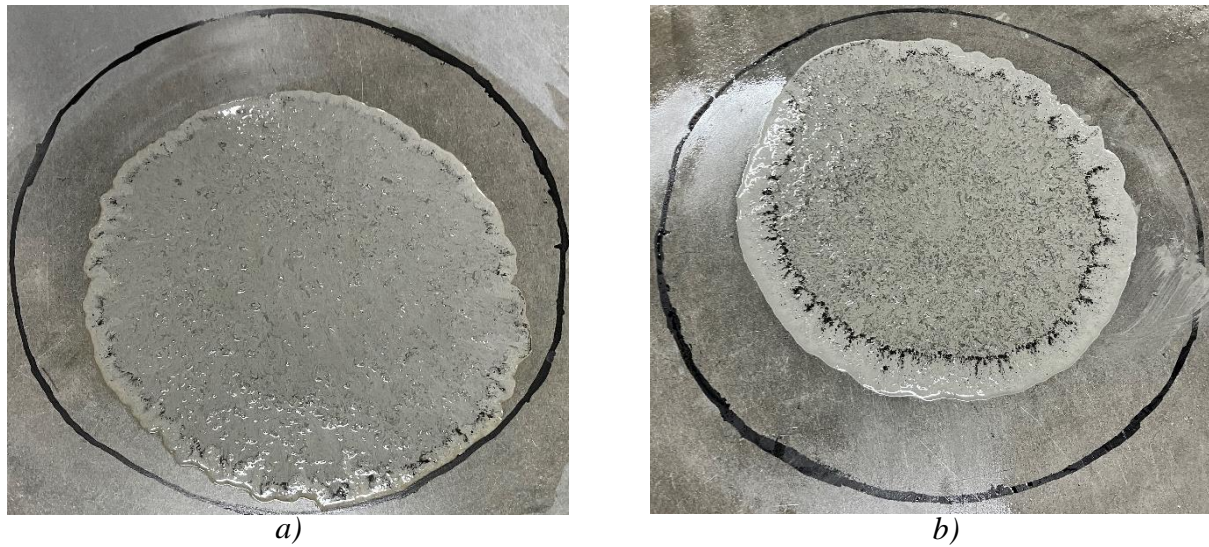


Figure 6.3 – Mortar matrix mini-slump tests: a) 30% PET content, b) 50% PET content

It was also found that there was also significant colour and consistency change between the control, 30% and 50% PET replacement. As shown in Figure 6.4 the surface of the mortar became black with bubbles present. The fly ash is assumed to be constant and has a very low loss on ignition (LOI). Therefore, the colour and rheology change could suggest a chemical reaction occurred between the mixture constituents and the PET aggregate. This was a focus of investigations using scanning electron microscopy (SEM) in Section 6.7.



Figure 6.4 – In pan mortar reaction with 50% PET content

6.2.2 ECC Matrix Rheology

The mini-slump and slump flow tests were used to assess the fresh properties of the ECC matrix following Sections 3.8.1 and 4.4.2. All batches were impacted by significant segregation and had very poor deformability. This was likely attributable to insufficient mixing energy. As highlighted by other researchers this is suboptimal in ECC applications (Yang et al. 2009; Li & Li 2012). No further comparisons such as deformability factor were made due to these issues.

The control had the best deformability and distribution of fibre throughout the matrix but required 11 minutes of mixing to reach this point. In normal ECC production, the mixing time is commonly three to five minutes using smaller planetary mixers (Yang et al. 2009; Li & Li 2012; Li et al. 2020). Pourfalah and Suryanto (2013) explored the use of locally available materials in ECC observing similar segregation. The segregation seen in this project could be caused by the stability of the base ECC matrix as found by Pourfalah and Suryanto (2013) and or insufficient mixing. It is proposed that the mixer was unable to adequately disperse the fibres throughout the matrix and the decreased plasticity because of PET substitution caused additional matrix stability. VMA would be useful to help confirm these issues but was not available for this project and is an area for future research.

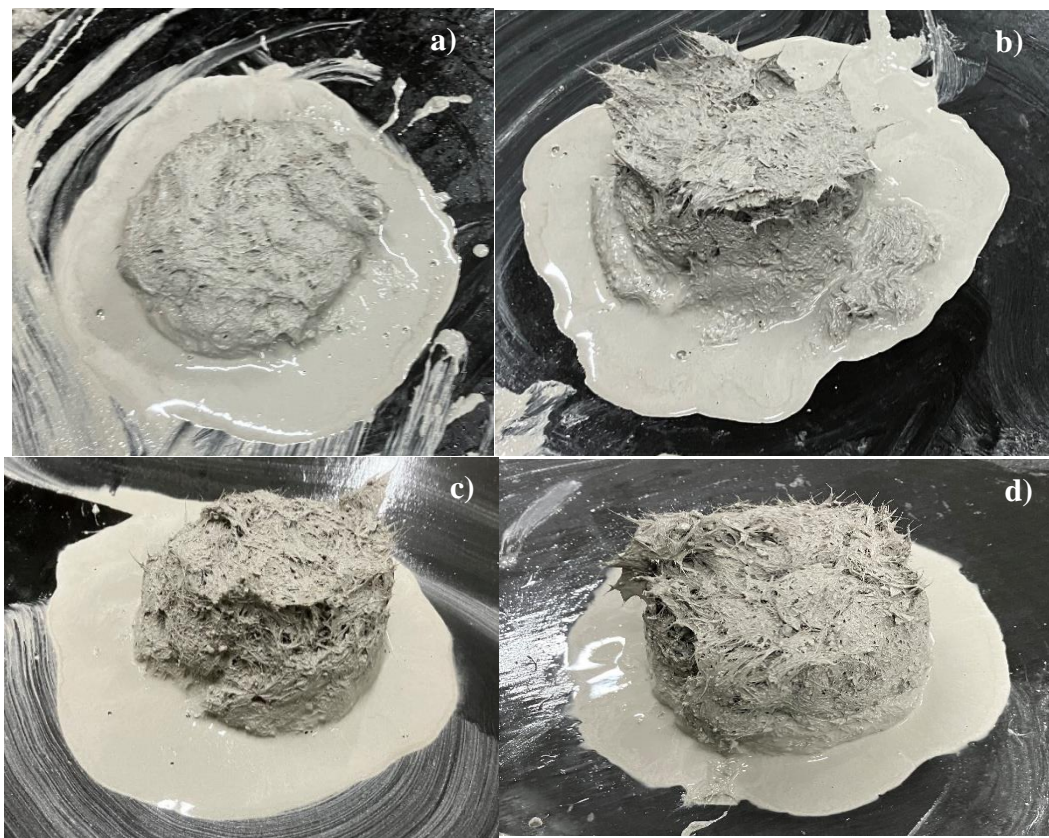


Figure 6.5 – Mini-slump tests: a) control, b) 10%, c) 30% and d) 50% PET

6.3 ECC Density

The test results of hardened cylinder density are presented in Figure 6.6. Specimens were dry and measured prior to testing. As the PET content increases it was found that density decreases. The density of the control was 1804 kg/m³. PET-ECC with 10% and 30% replacement ratios was found to be relatively similar at 1800 kg/m³ and 1768 kg/m³, respectively. Relative to the control, PET-ECC density with 50% PET content was found to decrease by 4.6% to 1723 kg/m³. The findings are aligned and supported by other studies into PET replacement in ordinary concrete (Choi et al. 2005; Rahmani et al. 2013; Almeshal et al. 2020; Kangavar et al. 2022). The reduced impact of PET compared to these studies is due to the smaller ratio of aggregates used in ECC.

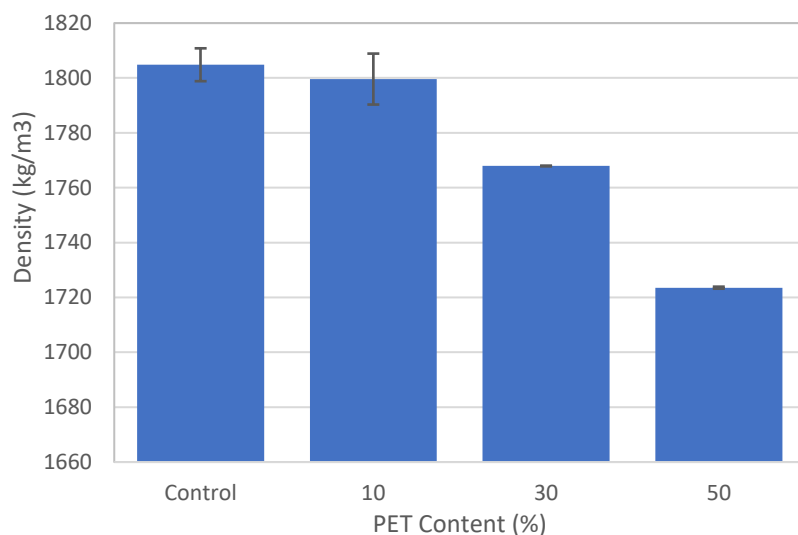


Figure 6.6 – Average density results

6.4 Tensile Testing

6.4.1 Uniaxial Tensile Strength

To characterise the column infill material, uniaxial tension testing was conducted according to the procedures in Sections 3.7.3 and 4.5.1. Two PET-ECC specimens were defective due to bleeding and suffered early failures at less than 1% strain. The results were discarded as recommended by ASTM C307. This left a single specimen for both 10% and 50% PET, making it difficult to draw any substantial PET-ECC conclusions. The results and specimen details are shown in Appendix E Table E.3. This is a novel testing method of ECC, used to overcome the

equipment limitations of this project. While promising, the results obtained require further validation against standard methods.

Figure 6.7 shows the characteristic 28-day tensile stress-strain curves of the control (SEQ-ECC) and PET-ECCs. The scatter in the initial elastic phase highlights the possible limitations of ASTM C307. That is, some of the initial strain variations could be attributable to the movement of the specimen within the grips or differences in fibre distribution throughout the specimen. The project did aim to eliminate movement in the grips, as a result, the movement was not visually apparent.

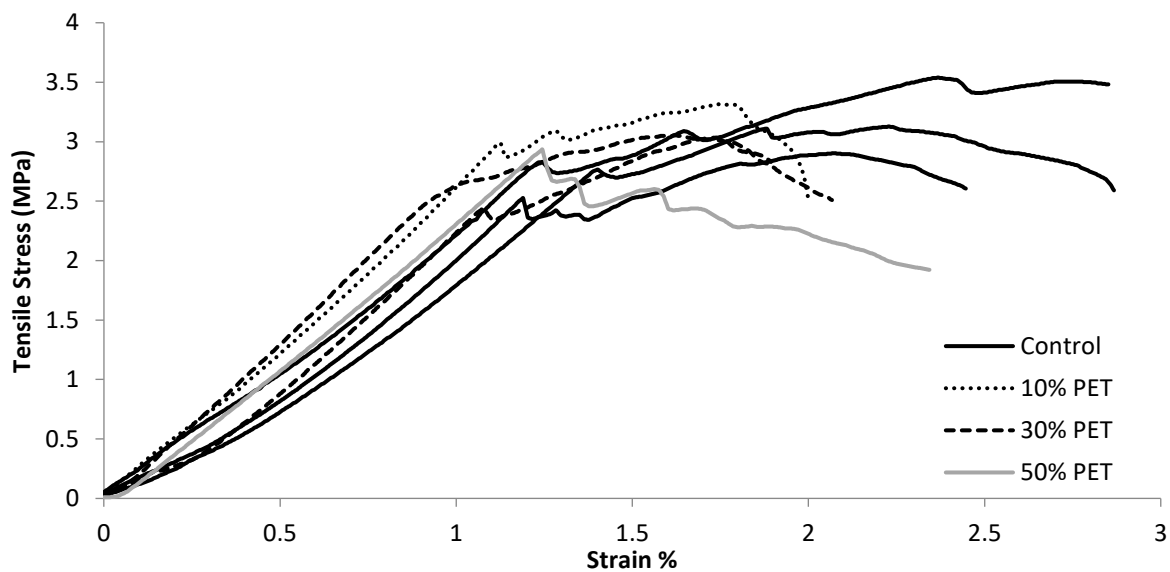


Figure 6.7 – Tensile stress-strain curve of PET-ECC at 28 days

The average tensile strain capacity of the control was found to be 2.4% and in the range of 240 times the ductility of ordinary concrete. This is within the ECC target range of 1-8% (Nawy 2008) and was similar to Yang et al. (2007) who reported a 28-day tensile strain capacity of $2.9 \pm 0.8\%$ using USS in HFA-ECC. However, while a strain-hardening-like behaviour was observed, the capacity from the first crack is significantly reduced compared to Yang et al. (2007).

The tensile strain capacity of the two 30% PET specimens was 1.75%, representing a reduction of approximately 25% from the control. The single results of 10% PET and 50% PET were 1.8% and 1.35% respectively. While more statistically significant research is needed the results indicate a reduction in the tensile strain capacity of PET-ECC as the PET content increases.

The reduction was broadly in line with the expected reductions due to weak PET bonding (Bamigboye et al. 2021; Kangavar et al. 2022) and small specimen size.

It was observed that the first crack of the control specimens occurred at approximately 1% strain. With subsequent multiple cracking as shown in Figure 6.8, specimens developed a strain-hardening-like behaviour. Besides the main failure cracks (1 and 2 in Figure 6.8a) the residual cracks were less than 100 μm as measured using a stereo microscope and barely visible to the naked eye as shown in Figure 6.8b. This indicates a degree of the durability of ECC found by Sahmaran et al. (2007) may also be retained using locally available sand. This is an area for further research.

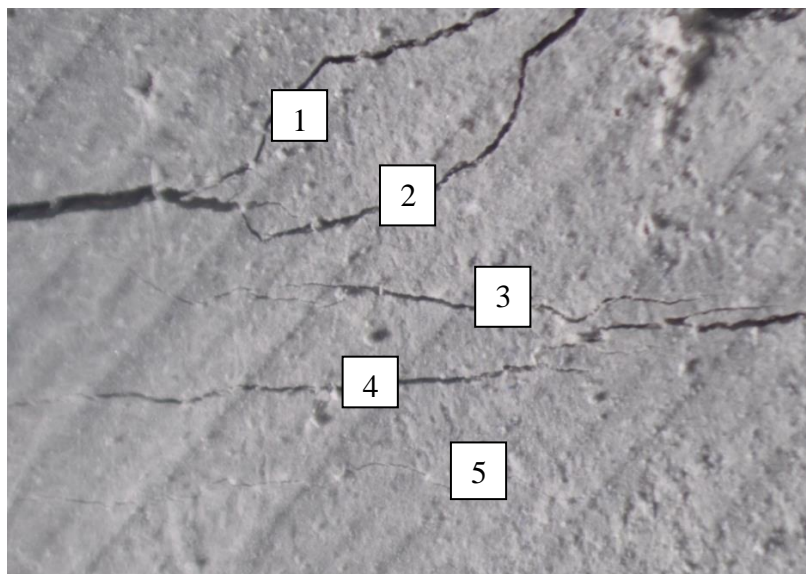


Figure 6.8a – Stereo microscope image of a control briquet with residual cracks highlighted

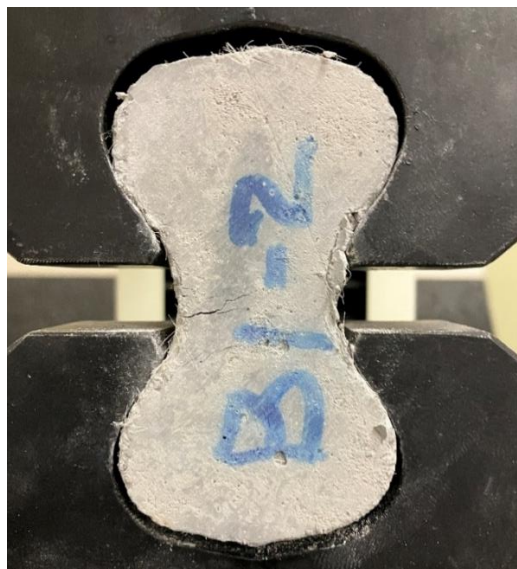


Figure 6.8b – Cracking of a control briquet at failure

By contrast, the cracks on the 50% PET-ECC specimen were visible to the naked eye and normal camera at less ultimate elongation (Figure 6.9). This was expected due to the weakened bonds as reported by Kangavar et al. (2022), among others and suggests PET introduces additional, and larger flaws to the matrix.

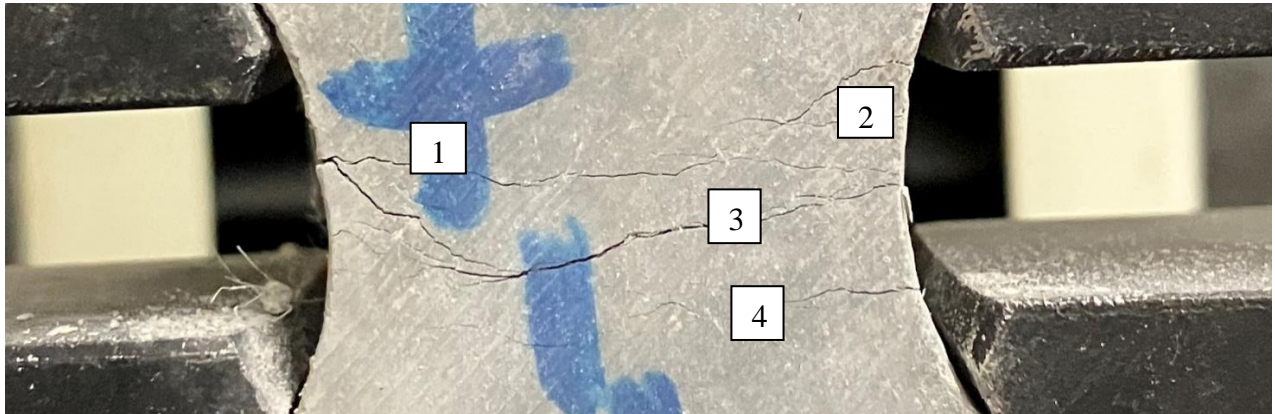


Figure 6.9 – Cracking of 50% PET at failure with visible cracks highlighted

Importantly the results confirm that a degree of the tensile ductility of ECC is retained and validates the potential use of locally available sand and PET granules in HFA-ECC. Further research is needed to tailor the micromechanical properties and optimise the strain-hardening potential of both SEQ-ECC and PET-ECCs.

6.4.2 Splitting Tensile Strength

The splitting tensile strength of the cylinders was tested following the procedures detailed in Sections 3.7.3 and 4.5.1. The results are presented in Figure 6.10 and the details of each specimen are shown in Appendix E Table E.4. All specimens were within the typical ECC target strength of 4-12 MPa (Nawy 2008).

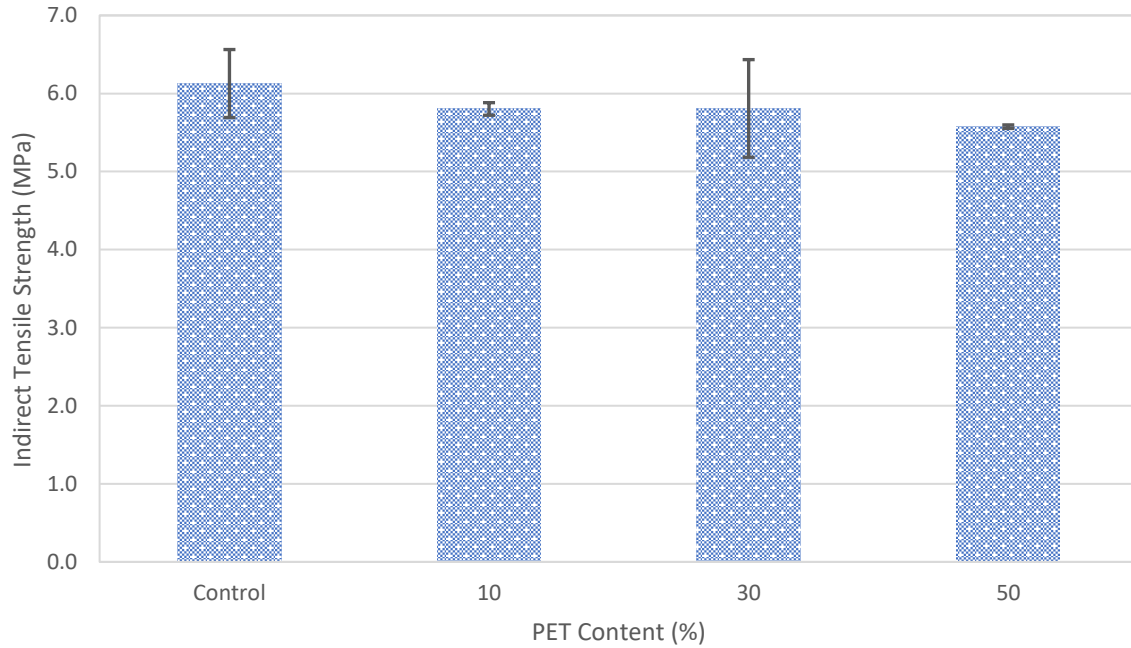


Figure 6.10 – Comparison of splitting tensile strength

A single control beam achieved the optimal splitting tensile strength of 6.4 MPa. A reduction of less than 2% was observed in a single 30% PET-ECC specimen. Compared to the control an average decrease of 5% was observed for 10% and 30% PET replacement ratios. A larger performance deterioration of 8.5% was found for 50% PET content. The results generally align with the behaviour found by Kangavar et al. (2022) and are supported by others (Choi et al. 2009; Saikia & de Brito 2012) substituting PET aggregates in ordinary concrete. The variations in the behaviour of ECC could be attributable to the enhanced adhesion and flexibility of PET granules at lower replacement ratios. However, PET granules tend to separate from the surrounding matrix at ultimate strength leading to reduced performance at higher replacement ratios.

In general, cracking emanated from the centre of the specimens and the strongest specimens resisted crack propagation to the outer surface as shown in Figure 6.11.

Significant variations in the results of 30% PET content were observed. As shown in Figure 6.11 the strongest control and 30% PET-ECC specimen did not develop a crack to the bottom of the cylinder before failure. Compared to the behaviour of weaker specimens this could be attributable to non-uniform fibre distributions and more research is required.

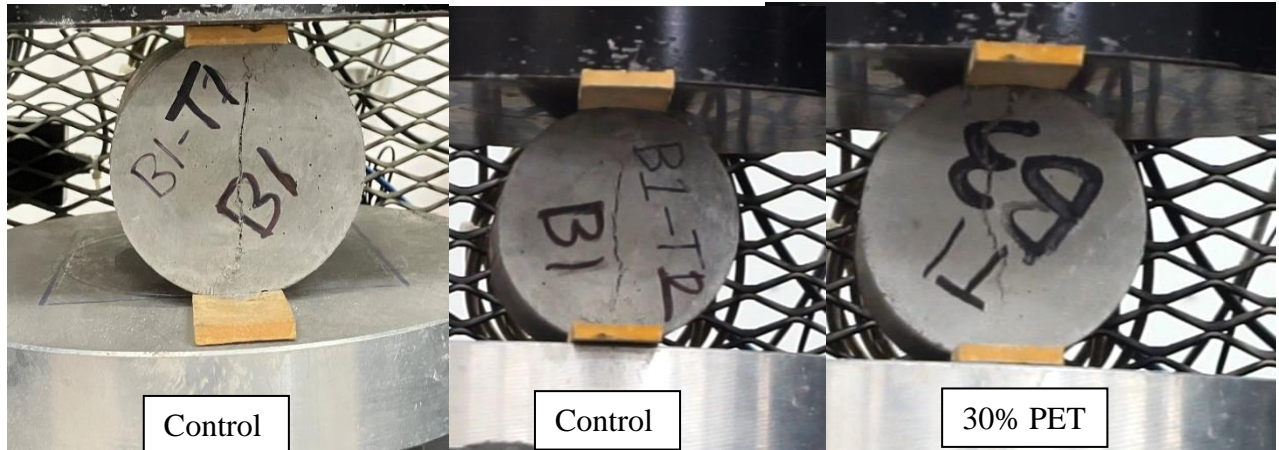


Figure 6.11 – Strongest specimen cracks at failure

6.5 Flexural Strength

Flexural testing was conducted following Sections 3.7.3 and 4.5.2. The experimental data and specimen details are shown in Appendix E Table E-5 and E-6. All specimens fell short of the typical ECC strength range of 10-30 MPa (Nawy 2008) and were not unexpected expected due to insufficient mixing energy and high fly ash content. The data recording rate was accidentally reset between tests and there were issues with laser displacement measurements. These issues impacted the shape of several curves with significant steps in some data points. To best represent the load versus deflection behaviour of the beams, exponential smoothing with a damping factor of 0.85 was used as shown in Figure 6.12. The large scatter between results may then be attributable to non-uniform fibre distributions, reflecting the different behaviour of the matrix as it fractures.

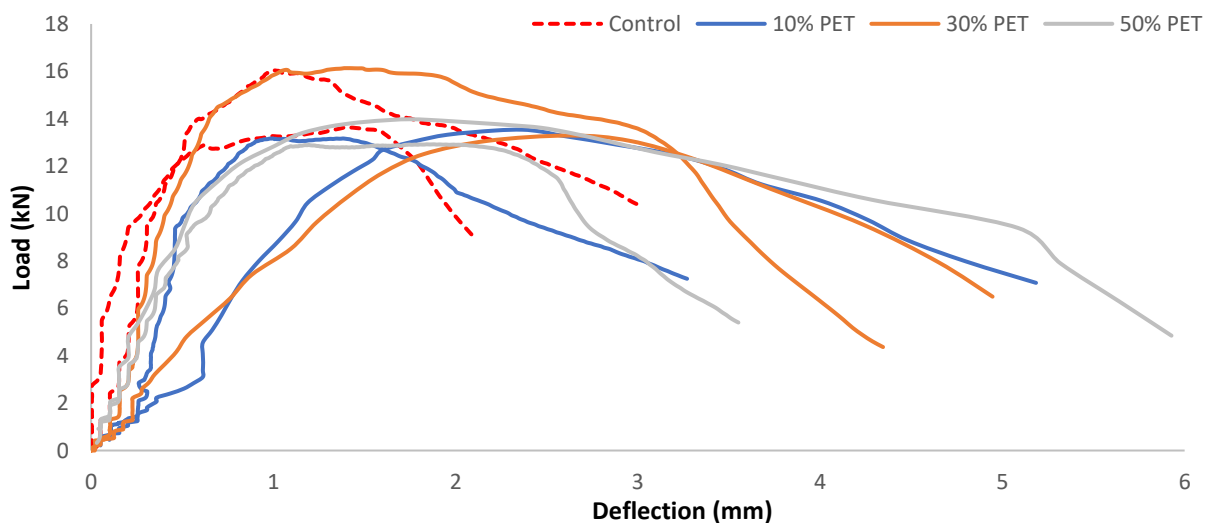


Figure 6.12 – Comparison of all flexural load-deflection behaviours

As shown in Figure 6.13, all beams presented a structurally desirable flexural tension failure. The failure was consistently initiated around the left-hand side loading roller, indicating a potential for uneven loading and a limitation of the testing apparatus. This could not be addressed in this project and was kept constant throughout testing.

It was found that all beams failed in a ductile manner with no concrete crushing. PET-ECC beams appeared to fail more gradually than the control with extended declines in loading and continued deflection. However, the flexural load vs deflection behaviour varied significantly and was not due to visible defects or density. The difference in flexural load between the two control beams was approximately 15%. The difference between the two 30% PET-ECC beams was almost 19%. All beams presented with limited multiple cracking and behaved more like a strain-hardening FRCC than ECC as defined by Ma et al. (2021). The variations in cracking behaviour, deflection and ultimate flexural strength may be partly attributable to poor fibre distribution resulting from insufficient mixing energy.



Figure 6.13 – Characteristic flexural tension failure a) control, b) 30% PET-ECC

A poor fibre distribution could be further indicated by the crack propagation of the two strongest beams as highlighted in Figure 6.14. In both cases, the main failure tension crack begins from the tension side of the beam and was effectively bridged by the fibres with a further crack propagating to cause the ultimate failure of the beam. As found by several researchers, uniform fibre distribution is critical to the ductility and strength of ECC (Sahmaran et al. 2009; Yang et al. 2009; Li & Li 2012; Zhou et al. 2012). It is proposed that adequate mixing and a uniform fibre distribution would encourage the behaviour seen in the strongest two beams.

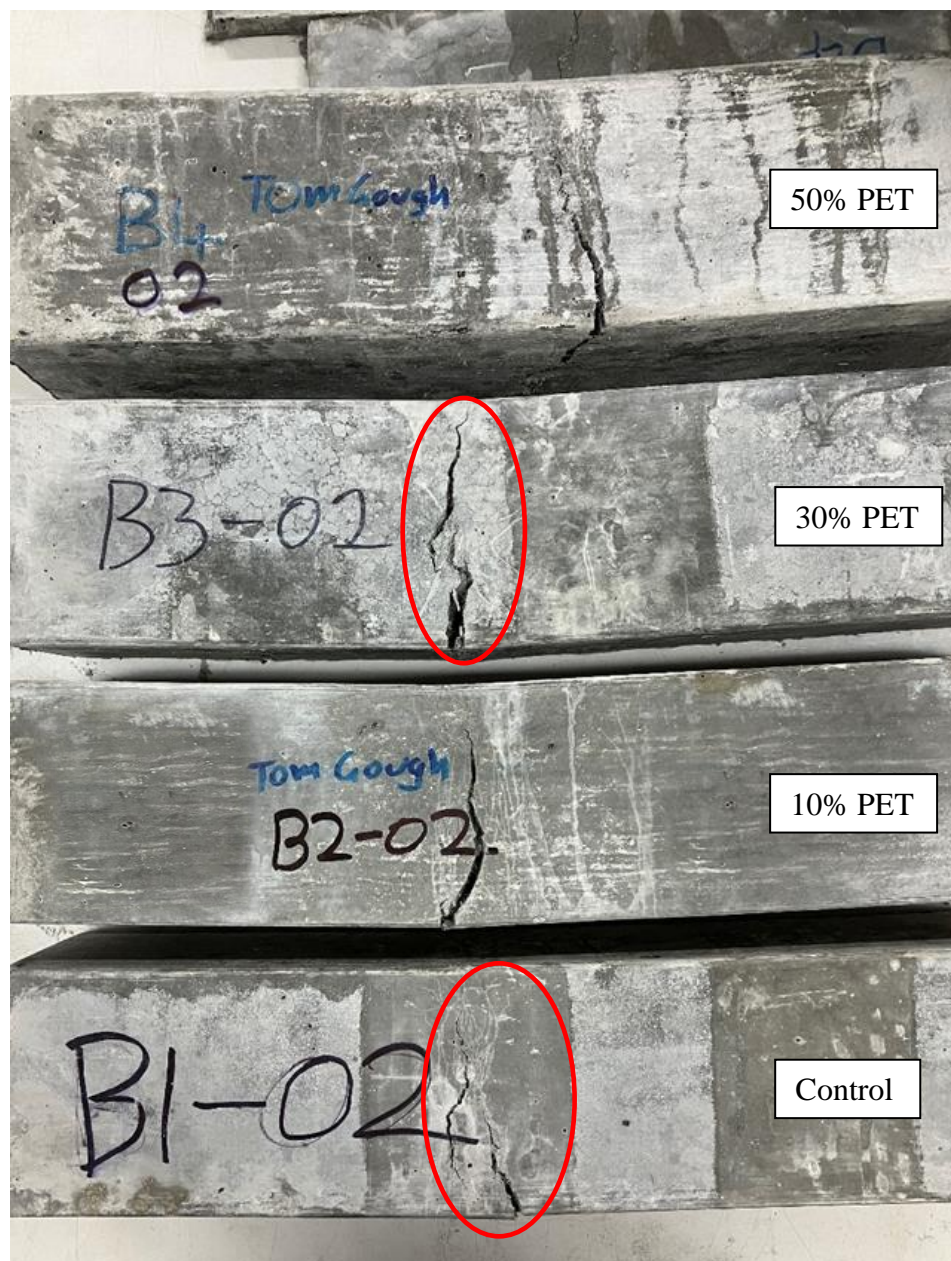


Figure 6.14 – Residual beam failure patterns with fibre bridging highlighted

According to micromechanical design principles, it is also possible that the aggregates in the control and PET-ECC increase the matrix fracture toughness and thus J_{tip} to beyond the complementary energy J_b' , failing the fundamental energy criterion (Equation 2.2). During testing, it was observed that visible cracking formed near maximum loading. This indicates the first cracking strength σ_{fc} of the matrix could also be greater than the maximum fibre-bridging stress σ_0 and fail the fundamental strength criterion (Equation 2.3). The effect of the substituted aggregate on the micromechanical properties of PET-ECC is an area for future research.

Figure 6.15 depicts the MOR results. A single control beam achieved the optimal flexural strength of 8.2 MPa. A reduction of less than 1% was observed in a beam with 30% PET content. All other beam failures featured a single tensile crack and may be impacted by relatively poor fibre distributions.

In general, a reduction in the modulus of rupture was observed. Compared to the control the MOR decreased on average 7.8%, 1.9% and 14.6% respectively for 10%, 30% and 50% PET. The results indicated that the ultimate strength decreases, and ductility typically increases with the addition of PET aggregates. Studies utilising PET aggregates in ordinary concrete also found a similar ductile behaviour (Rahmani et al. 2013; Kangavar et al. 2022) but noted additional flexural strength. More research is required given the mixing limitations of this project.

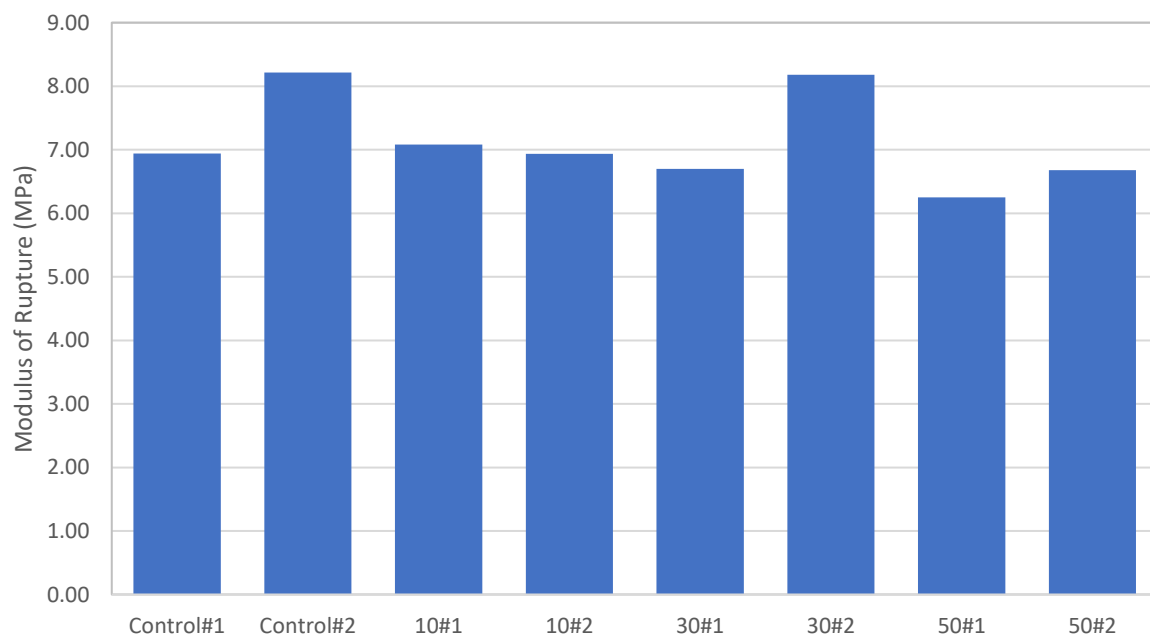


Figure 6.15 – Comparison of all flexural results

When the indirect tensile and flexural strengths are compared as shown in Figure 6.16, we can see there were significant variations in the control and 30% PET specimens using both methods. This highlights the need for more statistically significant testing with adequate mixing.

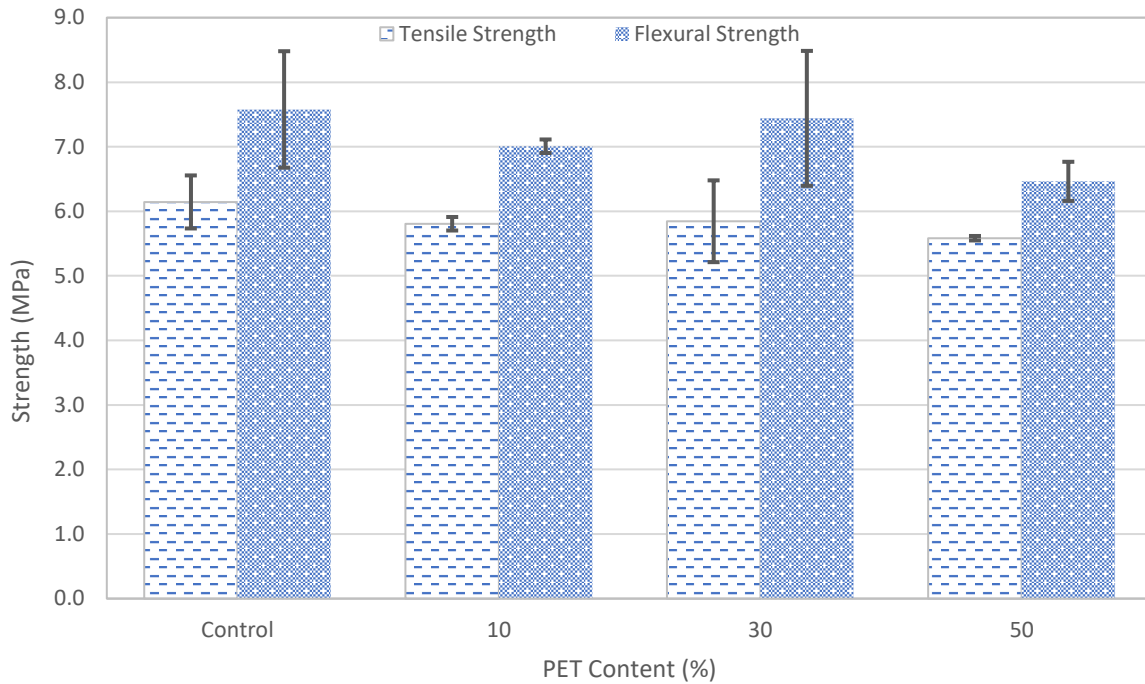


Figure 6.16 – Comparison of indirect tensile and flexural strength

6.6 Compression Testing

6.6.1 Compressive Strength

Compressive testing was conducted according to Sections 3.8.4 and 4.5.3. The results and specimen details are shown in Appendix E Table E-7 and E-8. Figure 6.17 depicts the compressive strength of the control and PET-ECC.

Unlike Kangavar et al. (2022) in ordinary concrete, the compressive strength of the control ECC was found to decrease with any addition of PET granules. The reduced compressive strength for any replacement ratio aligns more closely with the findings of other researchers (Choi et al. 2005; Silva et al. 2013; Saikia & de Brito 2014). It was proposed by Kangavar et al. (2022) that the variations of findings in ordinary concrete could be attributable to different

shapes, particle sizes and w/c ratios. Studying the effects of these parameters on ECC is an area for future research.

Compared to increasing PET substitution ratios in ordinary concrete, a reversing positive trend was observed relative to PET content in PET-ECC. A significant reduction of 31.8% was observed compared to the control for the 10% PET replacement ratio and the compressive strength of 30% and 50% PET replacement ratios decreased by 22.4% and 20.9% respectively from the control. This challenges the generalised behaviour of decreased strength in ordinary concrete for higher PET contents (Choi et al. 2005; Choi et al. 2009; Silva et al. 2013; Saikia & de Brito 2014; Kangavar et al. 2022) suggesting ECC may benefit from PET granule substitution even at 50% replacement. This could be attributable to the relatively low aggregate ratio in ECC, but further research with adequate mixing is required to validate this behaviour.

The decrease of more than 20% for all unconfined PET-ECC specimens could be attributable to insufficient mixing energy and weaker matrix bonding of PET aggregates both negatively impacting compressive strength and is supported by research studying the effects of PET aggregates in ordinary concrete (Choi et al. 2005; Choi et al. 2009; Silva et al. 2013; Saikia & de Brito 2014; Kangavar et al. 2022).

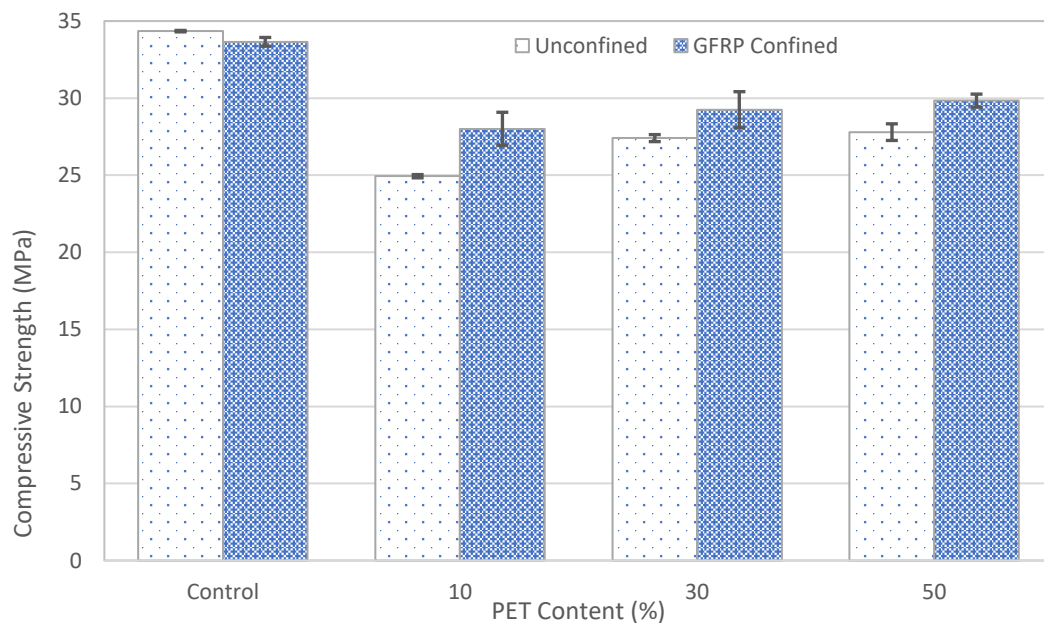


Figure 6.17 – Compressive strength of confined and unconfined short ECC columns

The behaviour of a single layer of GFRP confinement compared to the unconfined specimens marginally decreased the compressive strength of the control by 1.8% and increased the compressive strength by 11.7%, 6.4% and 6.9% respectively for 10%, 30% and 50% PET. These minor increases in ECC compressive strength are supported by (Yuan et al. 2021). The reduced effect of confinement compared to ordinary concrete is postulated to be due to the absence of coarse aggregates and low elastic modulus (Dang et al. 2020; Yuan et al. 2021).

The decrease in compressive strength of the control is not considered significant but still contradicts Yuan et al. (2021) who found a minor increase using a single layer of GFRP. However, compared to Yuan et al. (2021) the control indicated a superior self-confining effect as discussed in Section 6.6.2.

Using USS, Yang et al. (2007) found the compressive strength of HFA-ECC to be 38.4 ± 1.6 MPa. In this project, the unconfined compressive strength of the control using locally available sand showed a reduction of approximately 8% from USS HFA-ECC reported by Yang et al. (2007) and is supported by the findings of Sahmaran et al. 2009 in that particle size may not significantly influence ECC compressive strength. The results justify further research into the potential use of both SEQ-ECC and PET-ECC as viable lightweight concrete construction materials.

6.6.2 Stress-Strain Behaviour

Figures 6.18, 6.20, 6.22 and 6.24 show the confined and unconfined axial stress, axial strain, and lateral strain behaviours for the control and PET-ECC, respectively. Figures 6.19, 6.21, 6.23 and 6.25 show the corresponding cracking behaviour. The capacity for post-peak ductility and toughness of the unconfined control and PET-ECC is far superior to that of ordinary concrete.

The ECC infill governs the initial hardening branch and differences in the matrix are indicated by the stress-strain behaviour in response to matrix fracturing. Matrix fracturing is indicated by a loss of linearity before peak loading. Cracks eventually form from lateral expansion, and because of the fibre bridging ability, a brief period of strain hardening is observed around the peak load. In the case of unconfined columns, the softening branch after peak loading is governed by the ability of the fibres to respond to large cracks and lateral dilation. Some fibres are pulled-out or fractured and others effectively bridge the forming cracks. Even after large declines in bearing capacity all samples remained intact.

For confined columns, the lateral dilation after peak stress is also resisted by the GFRP. Apart from the control, a single layer of GFRP provided enough confinement to extend the strain-softening branch significantly from the peak. The control infill had sufficient self-confining fibre behaviour to initially resist lateral strains with the GFRP providing confinement at a later stage as shown in Figure 6.18. Compared to ECC using granulated slag and USS (Yuan et al. 2021), a single oblique shear failure was not observed in the control allowing more fibres to assist in the self-consolidation behaviour. This beneficial behaviour was also seen to an extent in 30% and 50% PET-ECC and contrasts less desirable failure mechanisms found in other types of ECC (Zhu et al. 2014).

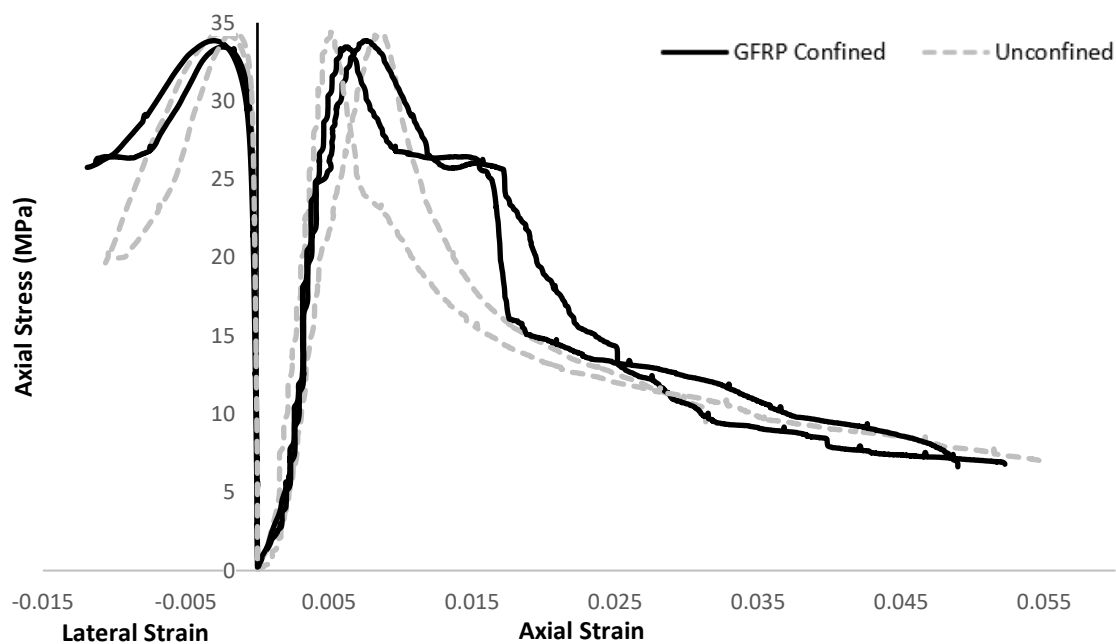


Figure 6.18 – Unconfined and confined control stress-strain behaviour



Figure 6.19 – Unconfined and confined control failure patterns

Generally, multiple diagonal shear cracks developed to failure in both confined and unconfined specimens and the stain gauge commonly failed before GFRP rupture. In all cases, the FRP ruptured in a controlled nonexplosive way.

The results also indicate that PET granules may increase the conversion of shear stresses into tension stresses, a similar behaviour found by Kangavar et al. (2022) when replacing sand with PET in ordinary concrete.

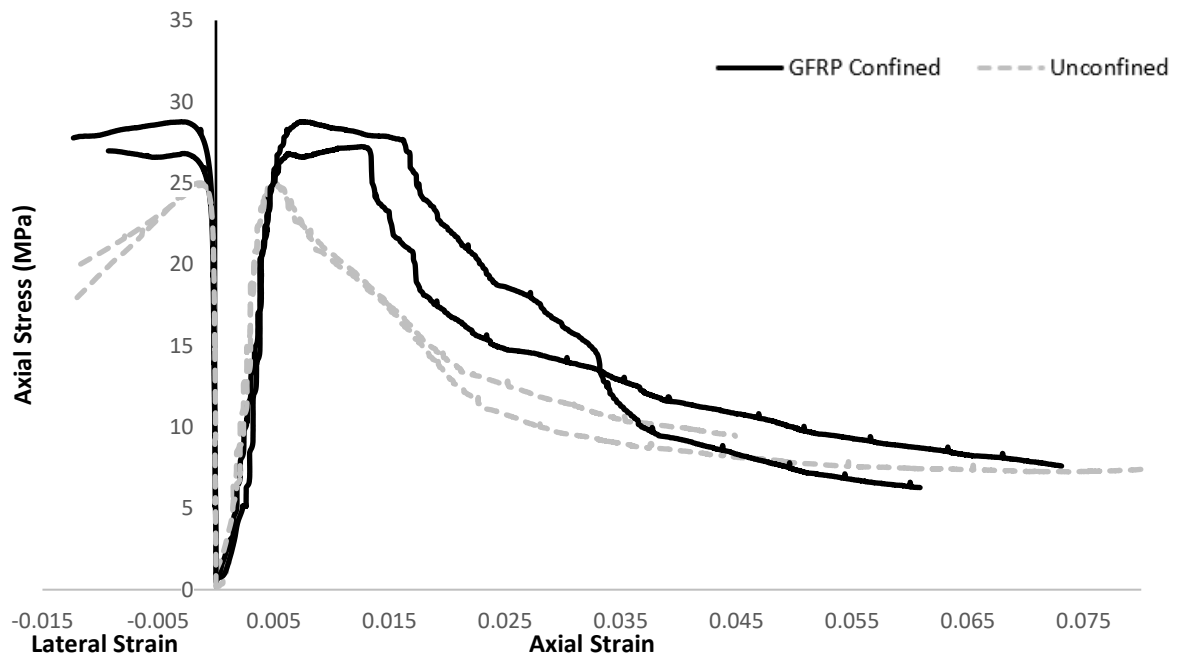


Figure 6.20 – Unconfined and confined 10% PET-ECC stress-strain behaviour

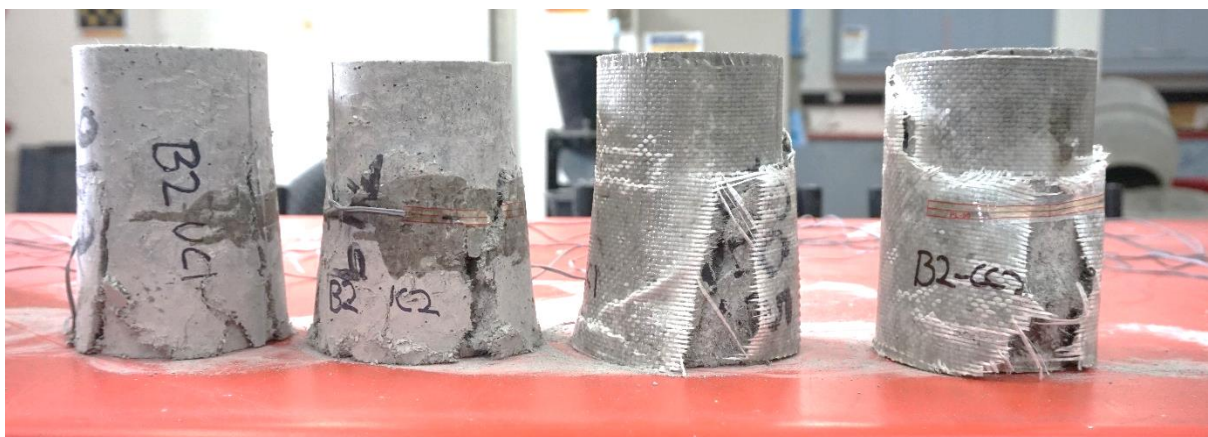


Figure 6.21 – Unconfined and confined 10% PET-ECC failure patterns

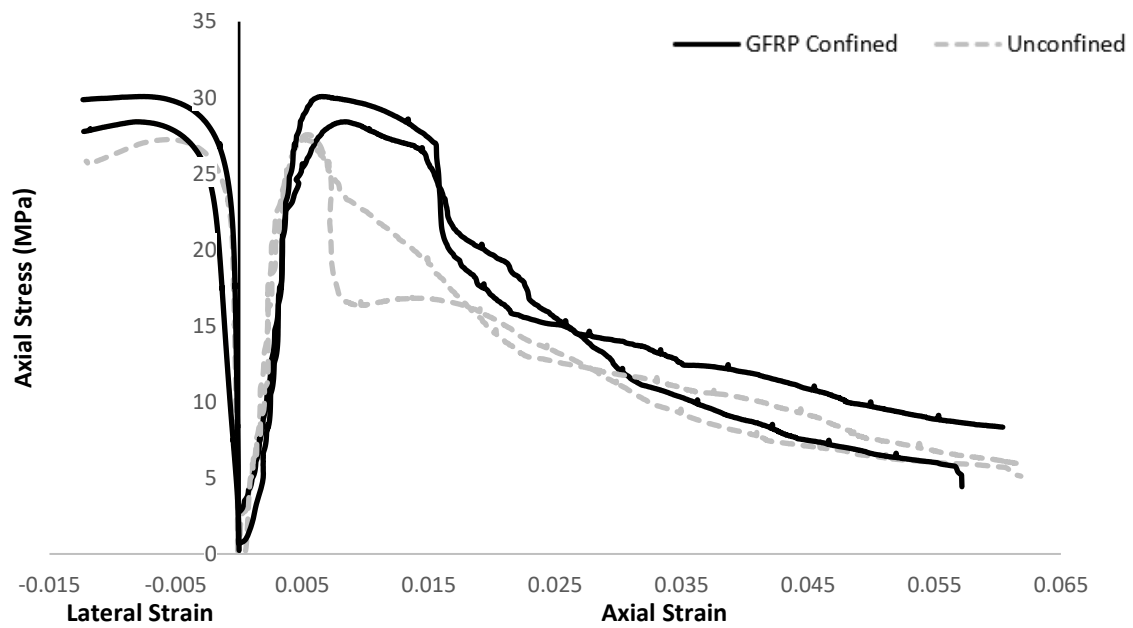


Figure 6.22 – Unconfined and confined 30% PET-ECC stress-strain behaviour



Figure 6.23 – Unconfined and confined 30% PET-ECC failure patterns

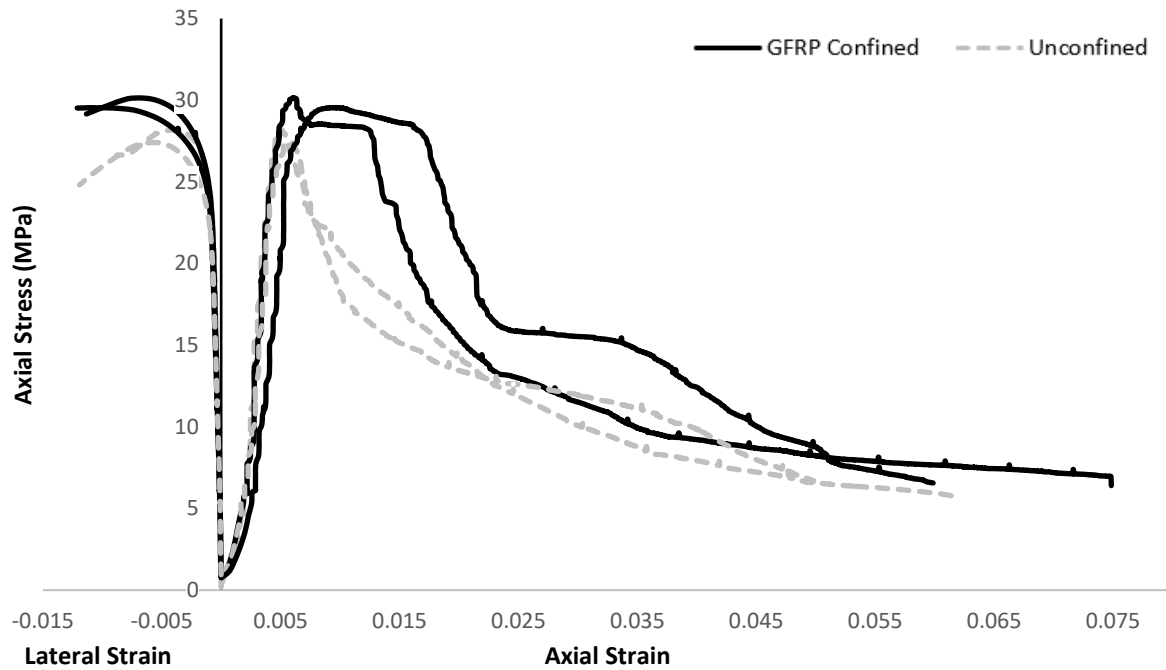


Figure 6.24 – Unconfined and confined 50% PET-ECC stress-strain behaviour



Figure 6.25 – Unconfined and Confined 50% PET-ECC failure patterns

In all cases, a controlled ductile failure was observed with the stress-strain curve approaching a horizontal plane before failure. This behaviour of ECC under compression is supported by past research (Xu & Cai 2010). A comparison of the unconfined behaviour of the control and PET-ECCs is shown in Figure 6.26. While the lateral strain gauge commonly broke at around 10% lateral strain the specimens continued to laterally deform until the fibre reinforcing strength was overcome.

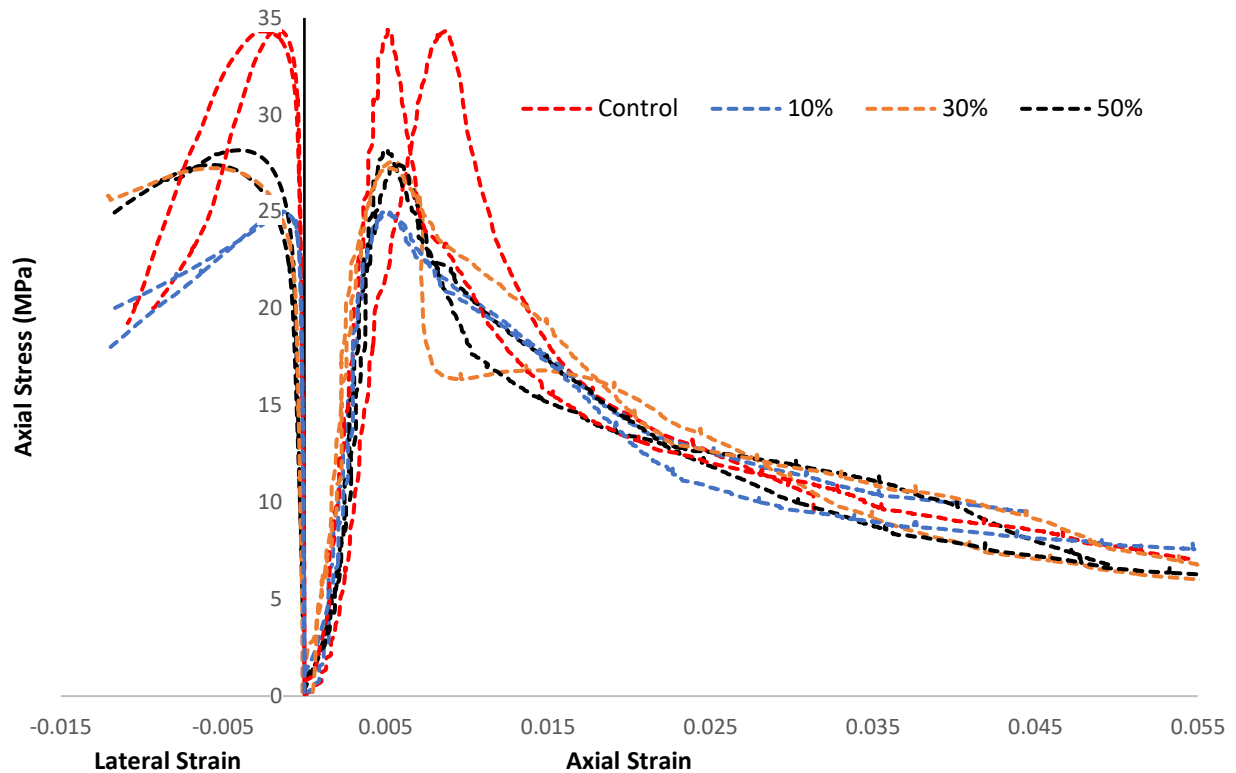


Figure 6.26 – Comparison of all unconfined column tests

As shown in Figure 6.27, except for the 10% PET replacement ratio, diagonal shear cracks typically developed. The low compressive strength and internal cone crushing failure in the bottom two-thirds of the 10% PET-ECC specimens indicates a consistent weakening of the matrix under compression. This behaviour contradicts the expected behaviour of PET in ECC. As there were no obvious visual defects to indicate any casting issues, the difference in behaviour could be attributable to insufficient mixing time relative to the other PET-ECCs as discussed in Section 4.4.2.

FRP is a promising method to provide additional strength in rehabilitation works or new structural applications (Lokuge & Karunasena 2016). The results of this project record the basis compressive behaviour and effect of a single layer of GFRP confinement in new green ECC construction materials. The newly developed ECC provides beneficial and unique characteristics that are lacking in ordinary concrete.

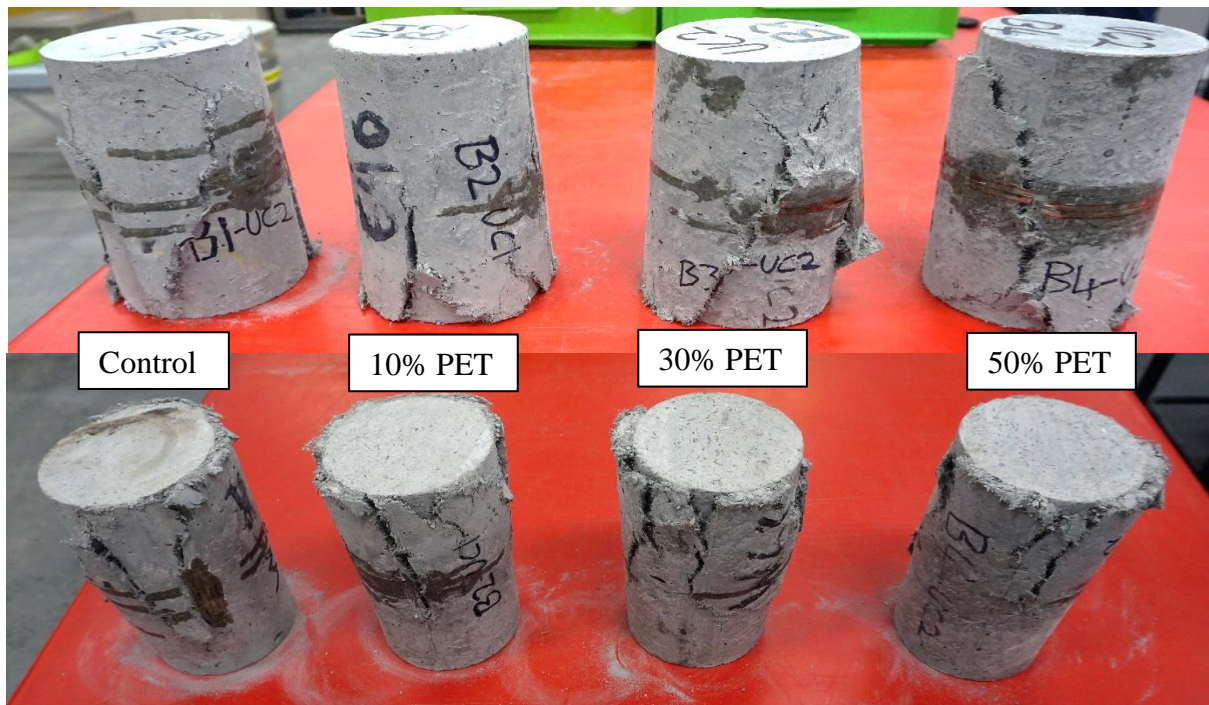


Figure 6.27 – Comparison of unconfined tests

6.6.3 Column Ductility

The column ductility factor was calculated following Section 4.5.3 to assess the ductile performance of the short columns. PET-ECC was found to have a higher ductility than the control with the results shown in Figure 6.28. Generally, one layer of GFRP was strong enough to resist 11% lateral strain and significantly increased the ductility of confined PET-ECC. The GFRP confined control also displayed good ductility as shown in Figure 6.29 but fell below the 85% stress threshold adopted in this project.

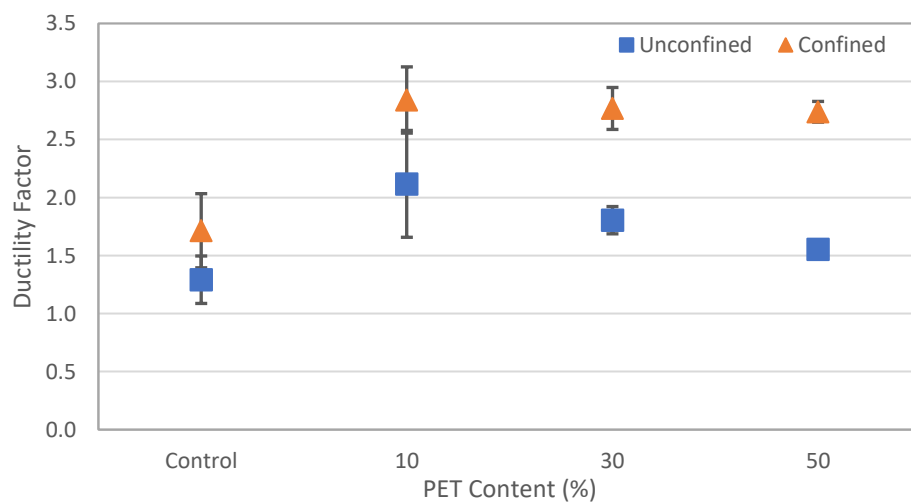


Figure 6.28 – Comparison of column ductility

The highest ductility factor of 2.8 was found for confined 10% PET-ECC. However, the large variation of 10% PET-ECC columns could indicate issues with the matrix fibre distribution of these specimens or premature failure of the GFRP.

The ductility of unconfined columns decreased as the PET replacement ratio increased. Compared to unconfined 10% PET-ECC, the ductility factor of 30% and 50% PET-ECC decreased by 16.2% and 31% respectively. The reduction was significantly less in GFRP-confined PET-ECC. The reduction from 10% PET-ECC was on average 2.8% and 3.7% respectively for GFRP-confined 30% and 50% PET replacement ratios.

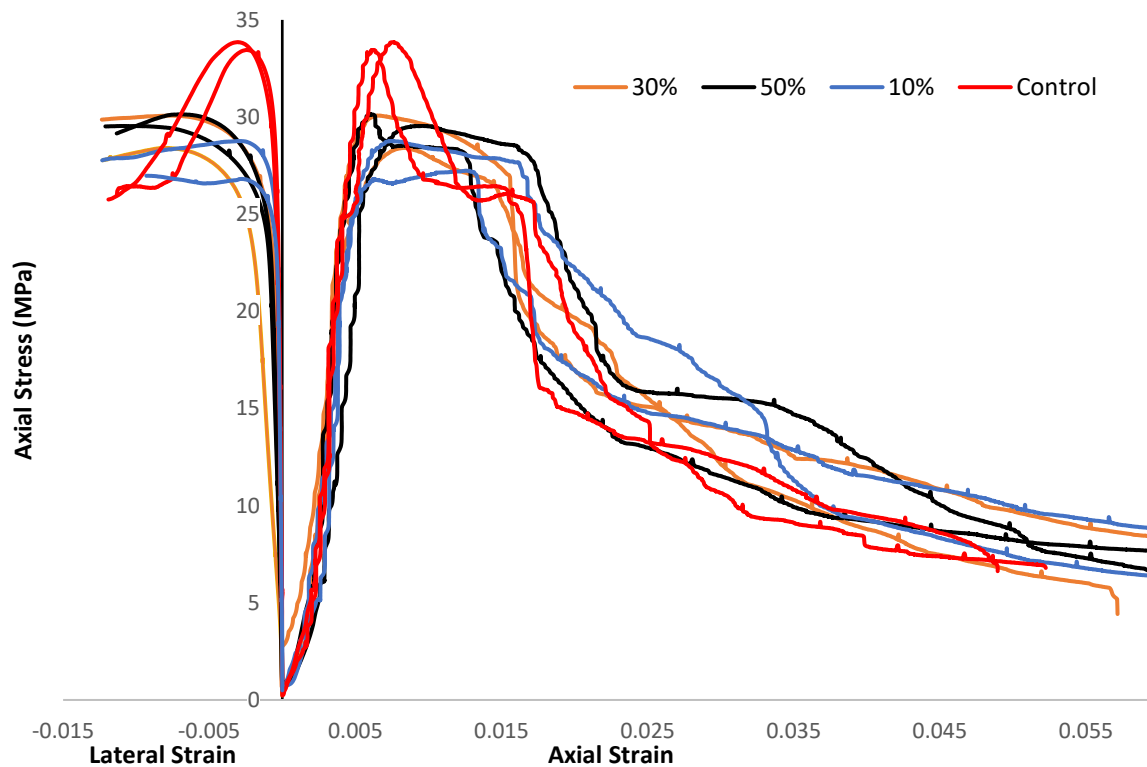


Figure 6.29 – Comparison of all GFRP confined column tests

The increase in PET-ECC ductility could be attributable to the flexible nature and weak bonding of PET granules (Kangavar et al. 2022). The increase in ductility for confined columns is supported by the behaviour found by Lokuge and Karunasena (2016) using the same GFRP on geopolymer concrete and Yuan et al. (2021) using GFRP on ECC. With the basis compressive results reported, the new composites provide viable mechanical properties that would benefit from further investigations of different confinement and mixing methods.

6.6.4 Modulus of Elasticity

The modulus of elasticity was calculated following Section 4.5.3, from the LVDT stress-strain curves. The results are shown in Figure 6.30. The control had an average elastic modulus of 11.7 GPa and significant variations were observed for PET-ECC. Unfortunately, the LVDT was not correctly set up for a 30% PET test and did not record any data.

The control and PET-ECC did not reach the typically reported ECC elastic modulus of 18-34 GPa (Nawy 2008) and no comparison in HFA-ECC was found. The reduction from a typical ECC with high cement content and USS could be attributable to the high fly ash content. The findings are supported by Yuan et al. (2021) who used a high blast furnace slag replacement of cement and reported an elastic modulus of 10.1 GPa. Compared to ordinary concrete with a similar compressive strength, the reductions in the elastic modulus can be attributable to the removal of coarse aggregates.

Results indicate that the modulus of elasticity in PET-ECC is relatively stable at higher replacement ratios compared to studies of PET in ordinary concrete (Kangavar et al. 2022). The findings also contradict the commonly observed behaviour of ECC increasing in elastic modulus with increases in compressive strength (Xu & Cai 2010). However, significant variations were observed in the data of PET-ECC, which could be attributable to insufficient mixing energy and non-uniform fibre distributions. As a result, more research is required. Any conclusions have low statistical significance and degree of confidence.

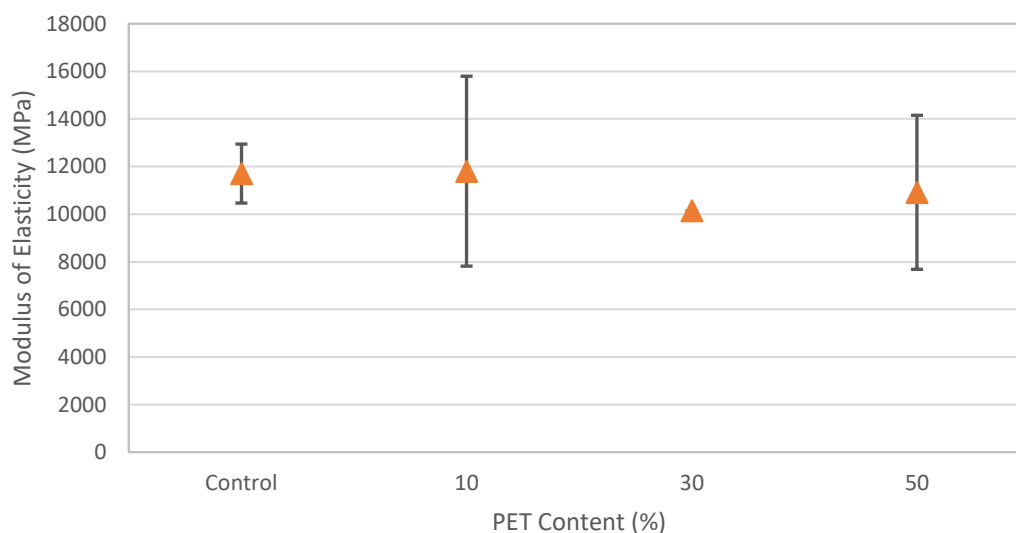


Figure 6.30 – Modulus of elasticity values

6.7 Scanning Electron Microscopy (SEM) Investigation

Samples of 50% PET-ECC were taken from the internal matrix of splitting tensile specimens. The investigation found that the surface of some of the PET granules appeared to have a degraded surface coating as shown in Figure 6.31. This contrasted the surface of other PET granules as shown in Figure 6.32 and may be attributable to different uses during their initial life. Both PET granules shown were white in colour, and not the green particles identified in Section 4.1. The PET granule in Figure 6.32 retained its white colour and the PET granule in Figure 6.31 was dark grey in colour. The different characteristics and coating degradation of the PET could be related to the pan reaction identified in Section 6.2.

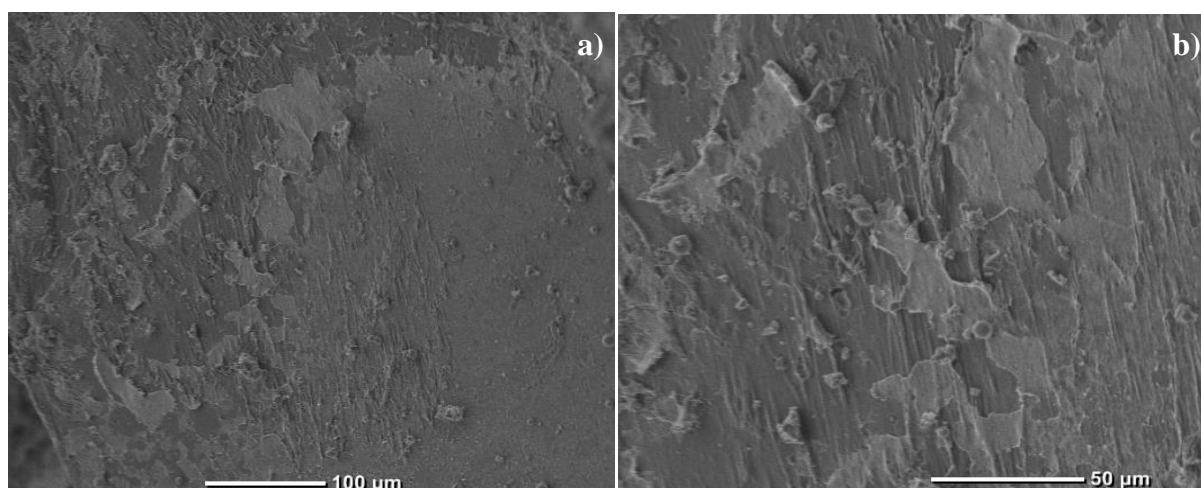


Figure 6.31 – Degraded PET granule surface at: a) 200 times magnification, and b) 500 times magnification

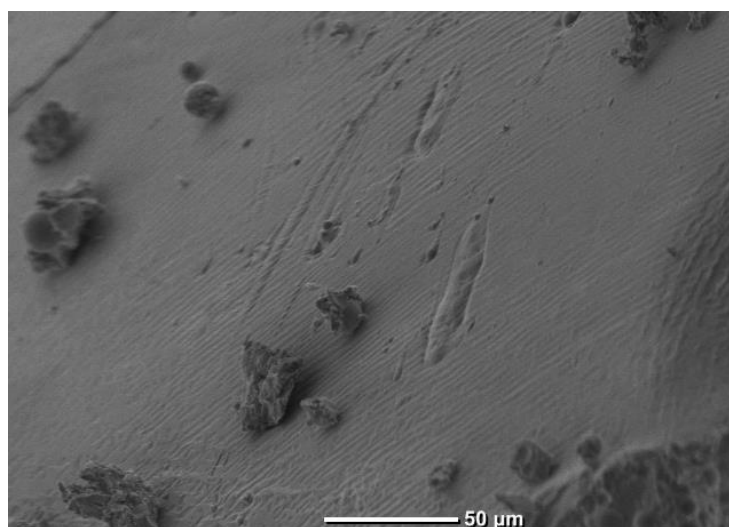


Figure 6.32 – Relatively smooth and intact PET surface at 300 times magnification

The investigation highlights issues of surface variability in PET recycled aggregates that have not been widely recognised in recent research (Bamigboye et al. 2021; Chithambar Ganesh et al. 2021; Dawood et al. 2021; Kangavar et al. 2022). In the development of ECC, this variability is problematic, and more research is required to ensure the consistency and reactivity of PET granules, particularly when using chemical admixtures.

Similar to Yang et al. (2007) it was found that many un-hydrated fly ash particles were distributed throughout the matrix as an inert filler and densely packed the interface zone between the fibre and aggregates. In Figure 6.33 the fly ash is shown by the smooth spherical particles surrounding the groove left by the fibre (removed before investigation). This indicates the fibre-to-matrix interface could have a strong holding force due to fly ash increasing the compactness of the ITZ as reported by Yang et al. (2007).

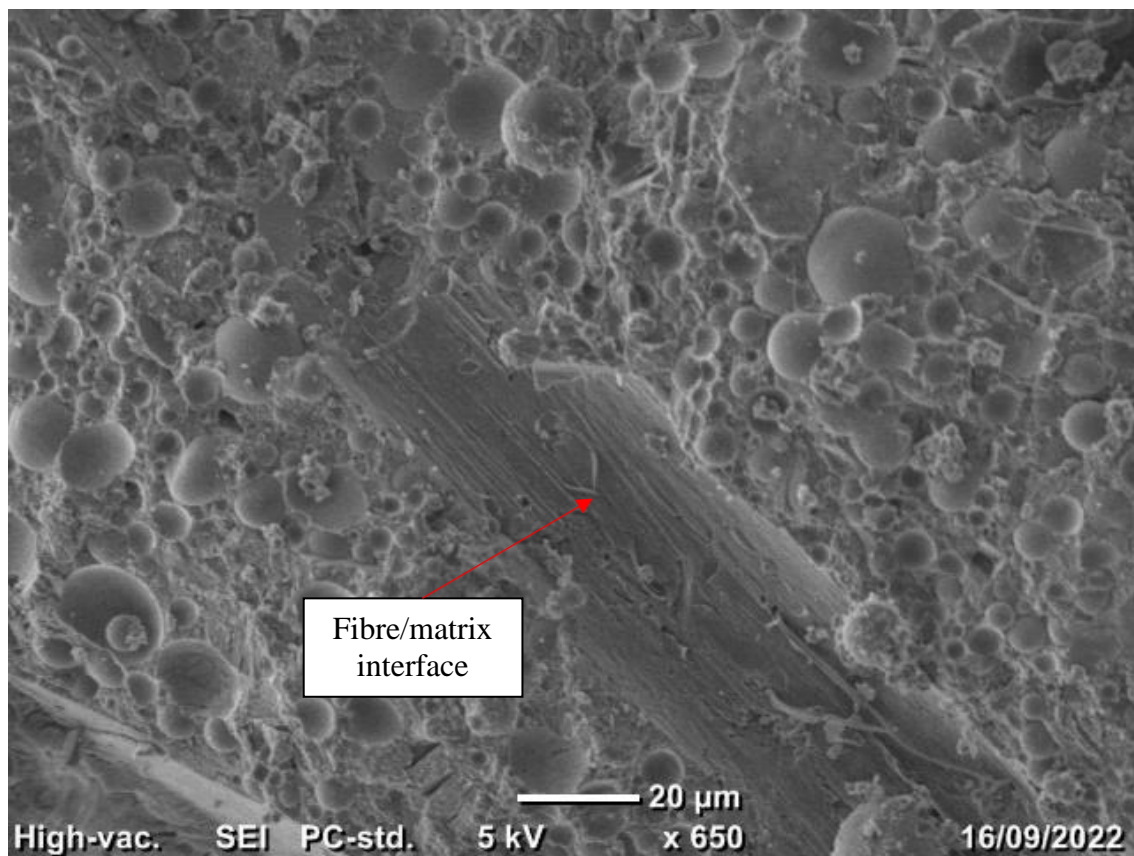


Figure 6.33 – Fibre matrix interface of 50% PET-ECC at 32 days

In Figure 6.34 an undamaged PET granule was removed with ease to show the relatively smooth, fractured interface of the surrounding matrix. This indicates the strength of PET aggregates exceeds the bonding strength of the matrix. As a result, PET granules may provide beneficial flaws to the matrix that could encourage strain-hardening potential with adequate mixing and fibre distribution (Li et al. 2020). More research is needed to micromechanically tailor PET-ECC to utilise the additional flaws.

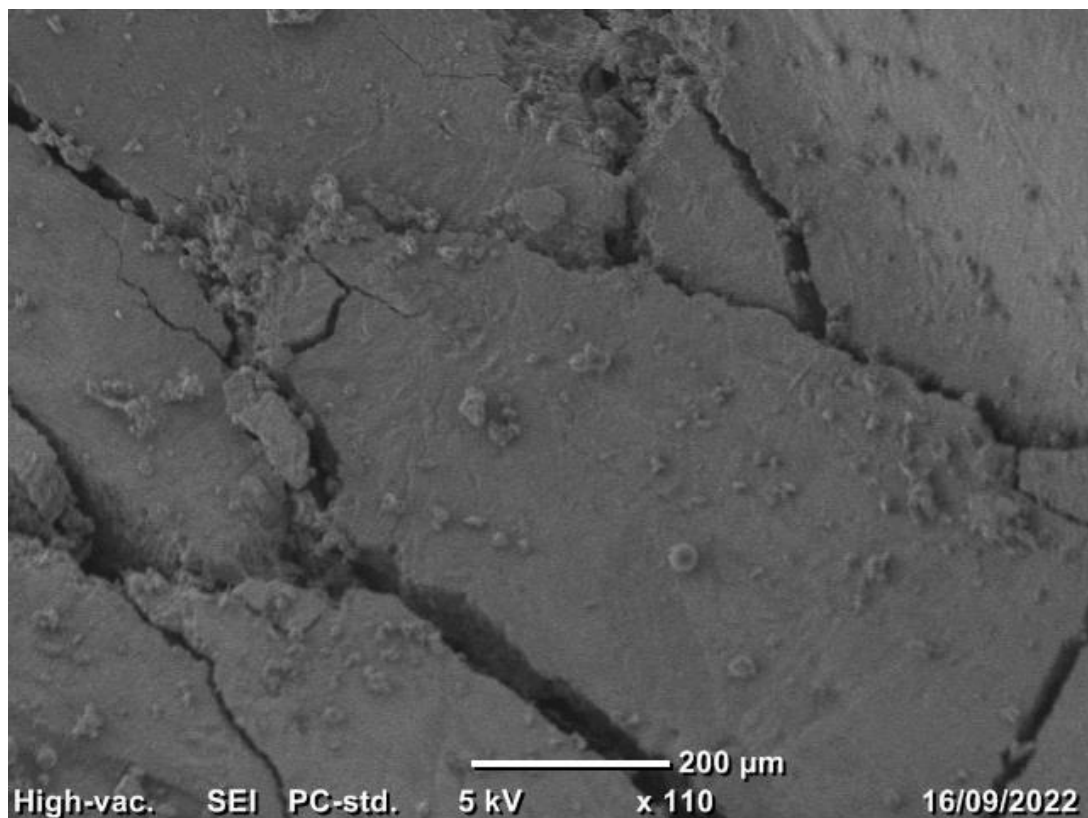


Figure 6.34 – PET matrix interface of 50% PET-ECC at 32 days

6.8 Numerical Investigation

The FEM produced in ABAQUS according to Chapter 5 was validated against the unconfined experimental data. Figure 6.35 displays the experimental and numerical simulation results for unconfined control columns. While the model material characteristics were developed on a limited set of highly variable data it shows a similar relationship between the numerical and experimental results. The FE results initially showed a high modulus of elasticity up to 13 MPa stress. The following branch to the peak stress of 34.9 MPa mimicked the average of the hardening and softening seen in the two experimental specimens. The model peak stress and the strain were closely aligned with the experimental data with a ratio (EXP/FE) of 0.98 and 1.08, respectively. More work is needed to tailor the post-peak behaviour of the model once the mixture of SEQ-ECC and PET-ECC is optimised, and a uniform fibre distribution is achieved.

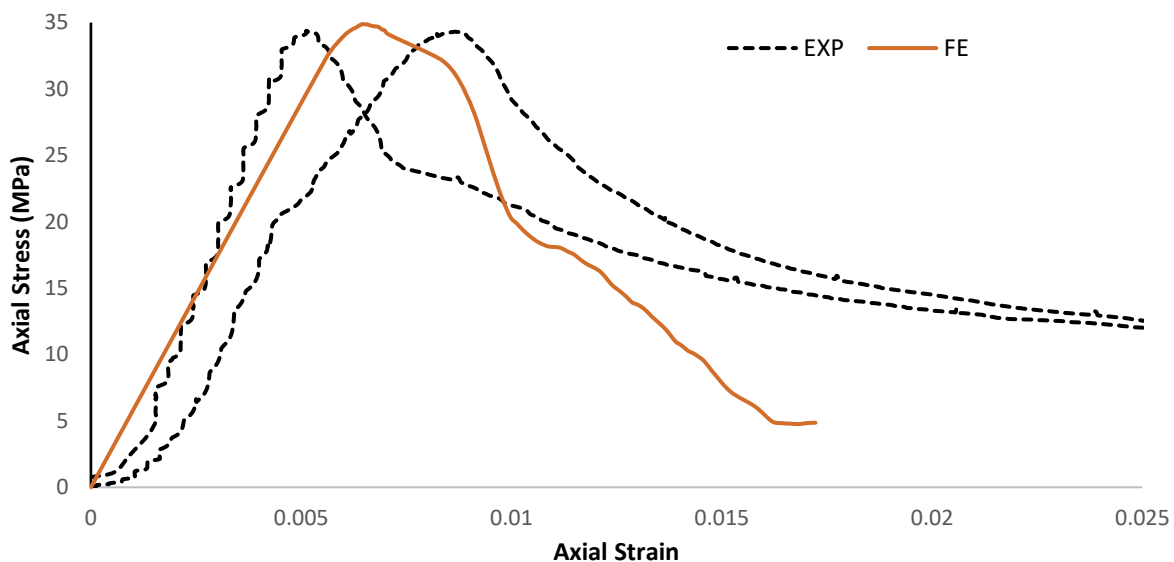


Figure 6.35 – Control stress-strain FE model validation

Further research is needed to investigate the material properties of the GFRP wrapping system used in this project. The findings of Ootom et al. (2021) in Pilemedic™ GFRP composites were unable to be tailored to estimate the experimental results of this study.

The results demonstrate the potential for a CDP FEM to predict the unconfined behaviour of SEQ-ECC. However, due to the limitations of this project more research is required to develop more accurate material characteristics.

CHAPTER 7. CONCLUSION

7.1 Summary

SEQ-ECC using locally available medium quartz sand was developed within the uniaxial tensile strain target range. PET-ECC was then developed by replacing sand with PET granules by 10%, 30% and 50% volume. Extensive material characterisation of the new composites was completed with a particular focus on the unconfined and confined compressive behaviour of short columns. ECC mixing quality assurance challenges were realised in this project.

Based on the results the following conclusions have been made:

1. Locally available medium quartz sand can be used in HFA-ECC as it develops a tensile strain capacity greater than 1% with a reduction in compressive strength of less than 10% with multiple shear cracking. The true strength of the new SEQ-ECC may not be realised due to insufficient mixing.
2. Recycled PET granules can be used in SEQ-ECC, but as found in SEM investigations, care to avoid a chemical reaction should be taken. While the mechanical strength was generally poorer for PET-ECC, it should not inhibit further research given the superior ductility. PET-ECC would benefit from adequate mixing and tailoring of HRWR dosage.
3. The use of PET granules negatively impacted the deformability of the fresh matrix which was inversely proportional to the increase of PET granules. Due to the lighter weight of PET granules compared to sand, the density was also reduced from 1804 kg/m³ by 0.3%, 2.0% and 4.6% as PET content increased.
4. The splitting tensile strength of PET-ECC was up to 9% lower than SEQ-ECC at a 50% PET replacement ratio. SEQ-ECC and PET-ECC developed strain hardening-like behaviour under uniaxial tension, with the tensile strain capacity reducing but up to 25% for 30% PET content. The larger residual cracks and lower capacity of PET-ECC suggested additional matrix flaws are introduced by PET granules.

5. The flexural strength results highlighted fibre mixing challenges with only two beams demonstrating multiple flexural cracking behaviours. The fibres used in the composites meant all samples failed in a ductile manner with PET-ECC beams exhibiting a more gradual failure with extended declines in loading and continued deflection. Compared to SEQ-ECC a reduction in flexural strength of 7.8%, 1.9% and 14.6% was found for 10%, 30% and 50% PET replacement, respectively.
6. The unconfined compressive strength of SEQ-ECC short columns was more than 34 MPa and decreased significantly with PET granules. Reductions of 31.8%, 22.4% and 20.9% were found for 10%, 30% and 50% replacement ratios, respectively. Typically, diagonal shear cracks developed and were resisted by fibres to fail in a controlled and ductile manner. All specimens had a compressive strength greater than 25 MPa and could fulfil the requirements of structural lightweight concrete according to AS 2758.1 (Standards Australia, 2014b).
7. A single layer of GFRP confinement did not increase the compressive strength of SEQ-ECC but the compressive strength of confined PET-ECC increased by 11.7%, 6.4% and 6.9% respectively for 10%, 30% and 50% PET content.
8. The ductility factor of PET-ECC was greater than SEQ-ECC with unconfined 10% PET increasing by a significant 48.7%. The ductility of unconfined PET-ECC short columns decreased inversely proportional to PET content. With GFRP confinement, the ductility factor of PET-ECC was equalised at 2.8 ± 0.05 for all PET contents compared to 1.7 for SEQ-ECC. This represents a significant ductility factor increase of 48.9% for PET-ECC with up to 50% PET content.
9. The results of the FEM showed that the unconfined compression behaviour of SEQ-ECC columns can be predicted with good precision using the CDP model. The peak stress and strain ratio of experimental to numerical results were 0.98 and 1.08, respectively.

This work has added to the collective knowledge of recycled and greening aggregates in ECC. By characterising the basis material properties of the new composites, this study has helped to fill the knowledge gap on the effects of PET granules in ECC. The results demonstrate the

possibility for lightweight and ductile short columns to be produced from unconfined and GFRP-confined PET-ECC with up to 50% of sand replaced. ECC benefits from mixture tailoring according to micromechanics, and the tensile strain capacity, flexural strength and multiple cracking behaviour could be optimised to utilise the flaws created by PET granules.

7.2 Future Research

To realise the full potential of PET-ECC, the following is a list of identified key research opportunities. List items should not be considered exhaustive and are derived from the results and investigations of this project:

1. Building on the findings of this study, investigations of SEQ-ECC and PET-ECC with adequate mixing are required. The composites should be developed with excellent deformability and no segregation, this may require specialist mixing equipment and VMA. Research to identify the optimal rheological properties of the mortar prior to fibre addition could also further increase the confidence in mixing quality control.
2. Variations in the surface, shape and type of recycled PET granules could influence the fresh and hardened properties of ECC. The characteristics of different sources of recycled PET granules should be investigated and possible reactions with different chemical HRWR identified.
3. Investigate the use of different types of fibres on the mechanical properties of PET-ECC and SEQ-ECC. This could assist in further reducing the environmental impacts and costs of ECC. Different types of fibre may also require different levels of mixing energy to achieve uniform distribution, knowledge of the suitable types and dosage of fibre could be used to optimise available mixing equipment.
4. Evaluate the effect of fibre dosage, HRWR dosage, rheological properties and curing regimens on the mechanical characteristics of PET-ECC. This would assist in optimising the properties of PET-ECC.

5. Investigate and isolate the micromechanical changes due to larger sand and PET granules concerning ECC design theory. This would assist in mixture designs and tailoring material behaviour in a range of structural applications.
6. Examine the effect of additional types and layers of confinement on the composites. This could provide further desirable properties to a lightweight, ductile, and durable structural concrete material.
7. Validate the use of briquette specimens to test the uniaxial tensile strength of ECC according to ASTM C307.

LIST OF REFERENCES

- Adesina, A & Das, S 2021a, 'Sustainable utilization of recycled asphalt as aggregates in engineered cementitious composites', *Construction and Building Materials*, vol. 283, p. 122727.
- Adesina, A & Das, S 2021b, 'Development of Sustainable Engineered Cementitious Composites Using Recycled Concrete Aggregates— Feasibility Study Based on Mechanical Properties', *ACI Materials Journal*, vol. 118, no. 4, pp. 97-107.
- Albano, C, Camacho, N, Hernández, M, Matheus, A & Gutiérrez, A 2009, 'Influence of content and particle size of waste pet bottles on concrete behavior at different w/c ratios', *Waste Management*, vol. 29, no. 10, pp. 2707-16.
- Almeshal, I, Tayeh, BA, Alyousef, R, Alabduljabbar, H & Mohamed, AM 2020, 'Eco-friendly concrete containing recycled plastic as partial replacement for sand', *Journal of Materials Research and Technology*, vol. 9, no. 3, pp. 4631-43.
- Andrew, RM 2018, 'Global CO₂ emissions from cement production, 1928–2017', *Earth Syst. Sci. Data*, vol. 10, no. 4, pp. 2213-39.
- Ataei, H, Anaraki, KK & Ma, R 2017, 'Mechanical Properties of Polyethylene Terephthalate Particle-Based Concrete: A Review', in *Airfield and Highway Pavements 2017*, pp. 57-68.
- Bamigboye, GO, Tarverdi, K, Umoren, A, Bassey, DE, Okorie, U & Adediran, J 2021, 'Evaluation of eco-friendly concrete having waste PET as fine aggregates', *Cleaner Materials*, vol. 2, p. 100026.
- Bin Ahmed, F, Abid Ahsan, K, Shariff, T & Rahman Meem, S 2021, 'Formulation of polynomial equation predicting the splitting tensile strength of concrete', *Materials Today: Proceedings*, vol. 38, pp. 3269-78.
- Cai, J, Pan, J, Tan, J, Vandevyvere, B & Li, X 2020, 'Nonlinear analysis of ECC-encased CFST columns under axial compression', *Journal of Building Engineering*, vol. 31, p. 101401.
- Cai, XR & Xu, S 2010, 'Study on corresponding relationships between flexural load-deformation hardening curves and tensile stress-strain hardening curves of UHTCC', *Gongcheng Lixue/Engineering Mechanics*, vol. 27, pp. 8-16.
- Chithambar Ganesh, A, Deepak, N, Deepak, V, Ajay, S, Pandian, A & Karthik 2021, 'Utilization of PET bottles and plastic granules in geopolymer concrete', *Materials Today: Proceedings*, vol. 42, pp. 444-9.
- Choi, Y-W, Moon, D-J, Chung, J-S & Cho, S-K 2005, 'Effects of waste PET bottles aggregate on the properties of concrete', *Cement and Concrete Research*, vol. 35, no. 4, pp. 776-81.
- Choi, YW, Moon, DJ, Kim, YJ & Lachemi, M 2009, 'Characteristics of mortar and concrete containing fine aggregate manufactured from recycled waste polyethylene terephthalate bottles', *Construction and Building Materials*, vol. 23, no. 8, pp. 2829-35.

Code of Ethics and Guidelines on Professional Conduct, 2019, Engineers Australia, viewed 25 May 2022, <<https://www.engineersaustralia.org.au>>.

Dang, Z, Feng, P, Yang, J-Q & Zhang, Q 2020, 'Axial compressive behavior of engineered cementitious composite confined by fiber-reinforced polymer', *Composite Structures*, vol. 243, p. 112191.

Dawood, AO, Al-Khazraji, H & Falih, RS 2021, 'Physical and mechanical properties of concrete containing PET wastes as a partial replacement for fine aggregates', *Case Studies in Construction Materials*, vol. 14, p. e00482.

Ferraris, CF 1999, 'Measurement of the rheological properties of high performance concrete: State of the art report', *Journal of research of the National Institute of Standards and Technology*, vol. 104, no. 5, pp. 461-78.

Ferreira, L, de Brito, J & Saikia, N 2012, 'Influence of curing conditions on the mechanical performance of concrete containing recycled plastic aggregate', *Construction and Building Materials*, vol. 36, pp. 196-204.

Frigione, M 2010, 'Recycling of PET bottles as fine aggregate in concrete', *Waste Management*, vol. 30, no. 6, pp. 1101-6.

Gagg, CR 2014, 'Cement and concrete as an engineering material: An historic appraisal and case study analysis', *Engineering Failure Analysis*, vol. 40, pp. 114-40.

Ghorbani, S, Sharifi, S, Ghorbani, S, Tam, VWY, de Brito, J & Kurda, R 2019, 'Effect of crushed concrete waste's maximum size as partial replacement of natural coarse aggregate on the mechanical and durability properties of concrete', *Resources, Conservation and Recycling*, vol. 149, pp. 664-73.

Godat, A, Chaallal, O & Obaidat, Y 2020, 'Non-linear finite-element investigation of the parameters affecting externally-bonded FRP flexural-strengthened RC beams', *Results in Engineering*, vol. 8, p. 100168.

Guan, X, Li, Y, Liu, T, Zhang, C, Li, H & Ou, J 2019, 'An economical ultra-high ductile engineered cementitious composite with large amount of coarse river sand', *Construction and Building Materials*, vol. 201, pp. 461-72.

Guan, Y, Yuan, H, Ge, Z, Huang, Y, Li, S & Sun, R 2018, 'Flexural Properties of ECC-Concrete Composite Beam', *Advances in Civil Engineering*, vol. 2018, p. 3138759.

Hadigheh, SA & Kashi, S 2018, 'Effectiveness of vacuum consolidation in bonding fibre reinforced polymer (FRP) composites onto concrete surfaces', *Construction and Building Materials*, vol. 187, pp. 854-64.

Hadigheh, SA, Gravina, RJ & Smith, ST 2017, 'Effect of acid attack on FRP-to-concrete bonded interfaces', *Construction and Building Materials*, vol. 152, pp. 285-303.

Hanson, J 1968, 'Effects of curing and drying environments on splitting tensile strength of concrete', *Journal Proceedings*, pp. 535-43.

Kanda, T & Li, VC 1999, 'New Micromechanics Design Theory for Pseudostrain Hardening Cementitious Composite', *Journal of engineering mechanics*, vol. 125, no. 4, pp. 373-81.

Kangavar, ME, Lokuge, W, Manalo, A, Karunasena, W & Frigione, M 2022, 'Investigation on the properties of concrete with recycled polyethylene terephthalate (PET) granules as fine aggregate replacement', *Case Studies in Construction Materials*, vol. 16, p. e00934.

Kissman, V & Sundar, L 2020, 'An experimental study on strengthening of RC column with GFRP', *Materials Today: Proceedings*, vol. 21, pp. 278-85.

Li, M & Li, VC 2011, 'High-Early-Strength Engineered Cementitious Composites for Fast, Durable Concrete Repair-Material Properties', *ACI Materials Journal*, vol. 108, no. 1, pp. 3-12.

Li, M & Li, VC 2012, 'Rheology, fiber dispersion, and robust properties of Engineered Cementitious Composites', *Materials and Structures*, vol. 46, no. 3, pp. 405-20.

Li, VC 2003, 'On Engineered Cementitious Composites (ECC) A Review of the Material and Its Applications', *Journal of Advanced Concrete Technology*, vol. 1, no. 3, pp. 215-30.

Li, VC, Wang, S & Wu, C 2001, 'Tensile strain-hardening behavior of polyvinyl alcohol engineered cementitious composite (PVA-ECC)', *ACI Materials Journal*, vol. 98, no. 6, pp. 483-92.

Li, VC, Wu, C, Wang, S, Ogawa, A & Saito, T 2002, 'Interface tailoring for strain-hardening polyvinyl alcohol-engineered cementitious composite (PVA-ECC)', *ACI Materials Journal*, vol. 99, no. 5, pp. 463-72.

Li, Y, Guan, X, Zhang, C & Liu, T 2020, 'Development of High-Strength and High-Ductility ECC with Saturated Multiple Cracking Based on the Flaw Effect of Coarse River Sand', *Journal of Materials in Civil Engineering*, vol. 32, no. 11.

Liu, H, Zhang, Q, Gu, C, Su, H & Li, VC 2016, 'Influence of micro-cracking on the permeability of engineered cementitious composites', *Cement and Concrete Composites*, vol. 72, pp. 104-13.

Lokuge, W & Karunasena, W 2016, 'Ductility enhancement of geopolymer concrete columns using fibre-reinforced polymer confinement', *Journal of composite materials*, vol. 50, no. 14, pp. 1887-96.

Ma, H, Yi, C & Wu, C 2021, 'Review and outlook on durability of engineered cementitious composite (ECC)', *Construction and Building Materials*, vol. 287, p. 122719.

Marzouk, OY, Dheilly, RM & Queneudec, M 2007, 'Valorization of post-consumer waste plastic in cementitious concrete composites', *Waste Management*, vol. 27, no. 2, pp. 310-8.

The American Society for Testing and Materials 1999, *Standard test method for Tensile strength of chemical-resistant mortar, grouts, and monolithic surfacings*, Standard test method, ASTM C307-99, The American Society for Testing and Materials, West Conshohocken.

- Mirmiran, A, Shahawy, M, Samaan, M, Echary, HE, Mastrapa, JC & Pico, O 1998, 'Effect of Column Parameters on FRP-Confined Concrete', *Journal of composites for construction*, vol. 2, no. 4, pp. 175-85.
- Mohammed, AA, Manalo, AC, Maranan, GB, Zhuge, Y & Vijay, PV 2018, 'Comparative study on the behaviour of different infill materials for pre-fabricated fibre composite repair systems', *Construction and Building Materials*, vol. 172, pp. 770-80.
- Nawy, EG 2008, *Concrete construction engineering handbook*, 2nd ed. edn, CRC Press, Boca Raton.
- Nicolaides, D, Kanellopoulos, A, Petrou, M, Savva, P & Mina, A 2015, 'Development of a new Ultra High Performance Fibre Reinforced Cementitious Composite (UHPFRCC) for impact and blast protection of structures', *Construction and Building Materials*, vol. 95, pp. 667-74.
- Nobis, R 2022, *The Long Road to Today's Portland Cement*, World Cement Association, viewed 15 May 2022, <<https://www.worldcementassociation.org/about-cement/our-history>>.
- O'Farrell, K 2020, *2018–19 Australian Plastics Recycling Survey*, National Report, Department of Agriculture, Water and the Environment, viewed 10 May 2022, <<https://www.awe.gov.au/sites/default/files/documents/australian-plastics-recycling-survey-report-2018-19.pdf>>.
- Ohno, M & Li, VC 2018, 'An integrated design method of Engineered Geopolymer Composite', *Cement and Concrete Composites*, vol. 88, pp. 73-85.
- Otoom, OF, Lokuge, W, Karunasena, W, Manalo, AC, Ozbakkaloglu, T & Thambiratnam, D 2021, 'Experimental and numerical evaluation of the compression behaviour of GFRP-wrapped infill materials', *Case Studies in Construction Materials*, vol. 15, p. e00654.
- Pourfalah, S & Suryanto, B 2013, *Development of engineered cementitious composite mixtures using locally available materials in the UK*.
- Rahmani, E, Dehestani, M, Beygi, MHA, Allahyari, H & Nikbin, IM 2013, 'On the mechanical properties of concrete containing waste PET particles', *Construction and Building Materials*, vol. 47, pp. 1302-8.
- Ranade, R, Zhang, J, Lynch, JP & Li, VC 2014, 'Influence of micro-cracking on the composite resistivity of Engineered Cementitious Composites', *Cement and Concrete Research*, vol. 58, pp. 1-12.
- Raza, A, Rehman, Au, Masood, B & Hussain, I 2020, 'Finite element modelling and theoretical predictions of FRP-reinforced concrete columns confined with various FRP-tubes', *Structures*, vol. 26, pp. 626-38.
- Ribeiro, F, Sena-Cruz, J, Branco, FG & Júlio, E 2018, 'Hybrid effect and pseudo-ductile behaviour of unidirectional interlayer hybrid FRP composites for civil engineering applications', *Construction and Building Materials*, vol. 171, pp. 871-90.
- Saak, AW, Jennings, HM & Shah, SP 2004, 'A generalized approach for the determination of yield stress by slump and slump flow', *Cement and Concrete Research*, vol. 34, no. 3, pp. 363-71.

Sahmaran, M, Li, M & Li, VC 2007, 'Transport properties of engineered cementitious composites under chloride exposure', *ACI Materials Journal*, vol. 104, no. 6, pp. 604-11.

Sahmaran, M, Lachemi, M, Hossain, KMA, Ranade, R & Li, VC 2009, 'Influence of aggregate type and size on ductility and mechanical properties of engineered cementitious composites', *ACI Materials Journal*, vol. 106, no. 3, pp. 308-16.

Şahmaran, M & Li, VC 2008, 'Durability of mechanically loaded engineered cementitious composites under highly alkaline environments', *Cement and Concrete Composites*, vol. 30, no. 2, pp. 72-81.

Saikia, N & de Brito, J 2012, 'Use of plastic waste as aggregate in cement mortar and concrete preparation: A review', *Construction and Building Materials*, vol. 34, pp. 385-401.

Saikia, N & de Brito, J 2014, 'Mechanical properties and abrasion behaviour of concrete containing shredded PET bottle waste as a partial substitution of natural aggregate', *Construction and Building Materials*, vol. 52, pp. 236-44.

Shanmugasundaram, N & Praveenkumar, S 2021, 'Influence of supplementary cementitious materials, curing conditions and mixing ratios on fresh and mechanical properties of engineered cementitious composites – A review', *Construction and Building Materials*, vol. 309, p. 125038.

Shoji, D, He, Z, Zhang, D & Li, VC 2022, 'The greening of engineered cementitious composites (ECC): A review', *Construction and Building Materials*, vol. 327, p. 126701.

Siad, H, Lachemi, M, Sahmaran, M, Mesbah, HA, Anwar Hossain, KM & Ozsunar, A 2017, 'Potential for using recycled glass sand in engineered cementitious composites', *Magazine of concrete research*, vol. 69, no. 17, pp. 905-18.

Silva, RV, de Brito, J & Saikia, N 2013, 'Influence of curing conditions on the durability-related performance of concrete made with selected plastic waste aggregates', *Cement and Concrete Composites*, vol. 35, no. 1, pp. 23-31.

Standards Australia 2000, *Method 11: Determination of the modulus of rupture*, Methods of testing concrete, AS 1012.11:2000, Standards Australia, Sydney.

Standards Australia 2000a, *Method 5: Particle density and water absorption of fine aggregate*, Method for sampling and testing aggregates, AS 1141.5:2000, Standards Australia, Sydney.

Standards Australia 2000b, *Method 10: Determination of indirect tensile strength of concrete cylinders ('Brazil' or splitting test)*, Methods of testing concrete, AS 1012.10:2000, Standards Australia, Sydney.

Standards Australia 2000c, *Method 4: Bulk density of aggregate*, Method for sampling and testing aggregates, AS 1141.4:2000, Standards Australia, Sydney.

Standards Australia 2014a, *Method 8.1: Method for making and curing concrete - Compression and indirect tensile test specimens*, Methods of testing concrete, AS 1012.8.1:2014, Standards Australia, Sydney.

Standards Australia 2014b, *Part 1: Concrete aggregates*, Aggregates and rock for engineering purposes, AS 2758.1:2014, Standards Australia, Sydney.

Standards Australia 2014c, *Method 8.2: Method for making and curing concrete - Flexure test specimens*, Methods of testing concrete, AS 1012.8.2:2014, Standards Australia, Sydney.

Standards Australia 2014d, *Method 2: Preparing concrete mixes in the laboratory*, Methods of testing concrete, AS 1012.2:2014, Standards Australia, Sydney.

Standards Australia 2015a, *Method 3.1: Determination of properties related to the consistency of concrete - Slump test*, Methods of testing concrete, AS 1012.3.5:2015, Standards Australia, Sydney.

Standards Australia 2015b, *Method 3.5: Determination of properties related to the consistency of concrete - Slump flow, T500 and J-ring test*, Methods of testing concrete, AS 1012.3.5:2015, Standards Australia, Sydney.

Tan, Z, Bernal, SA & Provis, JL 2017, 'Reproducible mini-slump test procedure for measuring the yield stress of cementitious pastes', *Materials and Structures*, vol. 50, no. 6, p. 235.

Tayeh, BA, Almeshal, I, Magbool, HM, Alabduljabbar, H & Alyousef, R 2021, 'Performance of sustainable concrete containing different types of recycled plastic', *Journal of Cleaner Production*, vol. 328, p. 129517.

van Zijl, G & Stander, H 2005, 'The effect of admixtures on the fresh and consolidated behaviour of ECC', *Advanced Cement-Based Materials: Proceedings of the Advanced Cement-Based Materials* Denmark University of Technology, Denmark

Wang, S & Li, VC 2007, 'Engineered Cementitious Composites with High-Volume Fly Ash', *ACI Materials Journal*, vol. 104, no. 3, pp. 233-41.

Xin, H, Mosallam, A, Liu, Y, Wang, C & Zhang, Y 2017, 'Analytical and experimental evaluation of flexural behavior of FRP pultruded composite profiles for bridge deck structural design', *Construction and Building Materials*, vol. 150, pp. 123-49.

Xu, M, Yu, J, Zhou, J, Bao, Y & Li, VC 2021, 'Effect of curing relative humidity on mechanical properties of engineered cementitious composites at multiple scales', *Construction and Building Materials*, vol. 284, p. 122834.

Xu, S-L & Cai, X-R 2010, 'Experimental Study and Theoretical Models on Compressive Properties of Ultrahigh Toughness Cementitious Composites', *Journal of Materials in Civil Engineering*, vol. 22, no. 10, pp. 1067-77.

Yan, D & Lin, G 2006, 'Dynamic properties of concrete in direct tension', *Cement and Concrete Research*, vol. 36, no. 7, pp. 1371-8.

Yang, E-H, Yang, Y & Li, VC 2007, 'Use of High Volumes of Fly Ash to Improve ECC Mechanical Properties and Material Greenness', *ACI Materials Journal*, vol. 104, no. 6, pp. 620-8.

Yang, E-H, Wang, S, Yang, Y & Li, V 2008, 'Fiber-Bridging Constitutive Law of Engineered Cementitious Composites', *Journal of Advanced Concrete Technology*, vol. 6, pp. 181-93.

- Yang, E-H, Sahmaran, M, Yang, Y & Li, VC 2009, 'Rheological Control in Production of Engineered Cementitious Composites', *ACI Materials Journal*, vol. 106, no. 4, pp. 357-66.
- Yu, J, Yao, J, Lin, X, Li, H, Lam, JYK, Leung, CKY, Sham, IML & Shih, K 2018, 'Tensile performance of sustainable Strain-Hardening Cementitious Composites with hybrid PVA and recycled PET fibers', *Cement and Concrete Research*, vol. 107, pp. 110-23.
- Yu, K, Wang, Y, Yu, J & Xu, S 2017, 'A strain-hardening cementitious composites with the tensile capacity up to 8%', *Construction and Building Materials*, vol. 137, pp. 410-9.
- Yuan, W-Y, Han, Q, Bai, Y-L, Du, X-L & Yan, Z-W 2021, 'Compressive behavior and modelling of engineered cementitious composite (ECC) confined with LRS FRP and conventional FRP', *Composite Structures*, vol. 272, p. 114200.
- Zhang, P, Gao, Z, Wang, J, Guo, J, Hu, S & Ling, Y 2020, 'Properties of fresh and hardened fly ash/slag based geopolymers concrete: A review', *Journal of Cleaner Production*, vol. 270, p. 122389.
- Zhou, J, Pan, J & Leung, CKY 2015, 'Mechanical Behavior of Fiber-Reinforced Engineered Cementitious Composites in Uniaxial Compression', *Journal of Materials in Civil Engineering*, vol. 27, no. 1, p. 04014111.
- Zhou, J, Qian, S, Ye, G, Copuroglu, O, van Breugel, K & Li, VC 2012, 'Improved fiber distribution and mechanical properties of engineered cementitious composites by adjusting the mixing sequence', *Cement and Concrete Composites*, vol. 34, no. 3, pp. 342-8.
- Zhu, Y, Zhang, Z, Yang, Y & Yao, Y 2014, 'Measurement and correlation of ductility and compressive strength for engineered cementitious composites (ECC) produced by binary and ternary systems of binder materials: Fly ash, slag, silica fume and cement', *Construction and Building Materials*, vol. 68, pp. 192-8.

APPENDIX A – PROJECT SPECIFICATION

ENG4111/4112 Research Project

Project Specification

For: Tom Gough

Title: Compressive behaviour of short ECC columns containing recycled PET aggregate

Major: Civil Engineering

Supervisors: Weena Lokuge

Enrolment: ENG4111 – ONC S1, 2022

ENG4112 – ONC S2, 2022

Project Aim: This project aims to evaluate the mechanical properties of engineered cementitious composite (ECC) if sand is partially substituted by volume with polyethylene terephthalate (PET) granules. The project will test glass fibre reinforced polymer (GFRP) confined and unconfined short ECC columns with 10%, 30% and 50% volume of fine aggregate replaced with PET granules.

Programme: Version 2, May 2022

1. Conduct initial background research on the properties and behaviour of concrete, fibre reinforced polymer (FRP), PET granules and ECC. Evaluate types of PET particles and PET substitution in ordinary concrete and ECC.
2. Plan experiments and source material by identifying suitable a testing methodology.
3. Prepare short-column test samples. Both unconfined and confined by GFRP wrapping. Conduct mechanical testing at 28 days. Study samples using advanced techniques (I.e., microstructural observations).
4. Analyse results and evaluate the use of PET granules.
5. Complete a numerical investigation to aid in result validation.
6. Present findings at the ENG4903 project conference. Prepare and submit USQ honours project thesis.

If time and resources permit:

7. Develop samples for flexural testing.

APPENDIX B – RISK MANAGEMENT

To enable proactive management of foreseeable hazards or impacts on the project a risk assessment was conducted using the definitions of Table B-1. The experimental risk assessment (Ref No: 1554) is available through UniSQ Safe Track System and is shown in Table B-2. The results of events impacting project risk are presented in Table B-3.

Table B-1 – Risk matrix

		Consequence				
		Insignificant (1) No injuries/ insignificant financial loss	Minor (2) First aid/ minimal financial loss	Moderate (3) Medical treatment/ Medium financial loss	Major (4) Hospitalisation/ large financial loss	Catastrophic (5) Death/massive financial loss
Likelihood	Almost Certain (5) Often occurs	Moderate (5)	High (10)	High (15)	Extreme (20)	Extreme (25)
	Likely (4) Could easily happen	Moderate (4)	Moderate (8)	High (12)	Extreme (18)	Extreme (20)
	Possible (3) Could happen	Low (3)	Moderate (6)	Moderate (9)	High (12)	High (15)
	Unlikely (2) Known to have happened	Low (2)	Moderate (4)	Moderate (6)	Moderate (8)	High (10)
	Rare (1) Possible but unlikely	Low (1)	Low (2)	Low (3)	Moderate (4)	Moderate (5)

Table B-2 – Experimental risk assessment


NUMBER	RISK DESCRIPTION	TREND	CURRENT	RESIDUAL
1554	Assessment of the risks associated with laboratory testing		Low	Low
RISK OWNER	RISK IDENTIFIED ON	LAST REVIEWED ON	NEXT SCHEDULED REVIEW	
Tom Gough	30/08/2022	30/08/2022	30/08/2023	
RISK FACTOR(S)	EXISTING CONTROL(S)	PROPOSED CONTROL(S)	OWNER	
Injury due to falling materials	<p>Control: ECC is lighter than conventional concrete which lessens the hazard.</p> <p>Control: Use mechanical aids where possible to isolate hazard.</p> <p>Control: Laboratory safety induction has been provided. Follow safe work procedures and seek assistance from technical staff when preparing specimens and equipment for testing.</p> <p>Control: I will wear closed in safety boots at all times, above the lab requirements of closed in shoes.</p>	No Control:		
Strain injuries from lifting and loading specimens to be tested.	<p>Control: ECC is lighter than conventional concrete which lessens the hazard.</p> <p>Control: Use mechanical lifting aids where possible to isolate hazard.</p> <p>Control: Employ correct methods while lifting and shifting as outlined in Safety Central training videos. Seek assistance and never lift more than you are comfortable with.</p>	No Control:		
Injury from operating Z104 MTS machine in tension.	<p>Control: Testing is conducted in tension rather than compression reducing chances of projectiles.</p> <p>Control: Suitably trained technical staff will operate the MTS machine, controlling injuries from movement related crushing and pinching points.</p> <p>Control: Slide protective screens into place prior to loading any specimens. Safety boots will be worn at all times.</p>	No Control:		
Injury from operating Z1 Concrete Tester (In compression and flexure)	<p>Control: Laboratory safety induction has been provided. Trained technical staff will operate the testing apparatus and supervise loading and unloading of the specimens to ensure the machine does not move and cause crushing injury.</p> <p>Control: Safety boots will be worn, and safety screens will be in place during testing.</p>	No Control:		
Injury from operating Z1 concrete cutter	<p>Control: Suitably trained technical staff will operate the concrete cutter.</p> <p>Control: Safety glasses will be worn at all times in the work area following the PPE requirements of the safe work procedure.</p>	No Control:		
Noise exposure from operating Z1 concrete cutter	<p>Control: Seek assistance from technical staff and always wear tight fitting/protective clothing with no loose or jewelry items.</p> <p>Control: Hearing protection will be worn when the concrete cutter is in use following the PPE requirements of the safe work procedure.</p>	No Control:		

Table B-3 – Project risk assessment

Risk	Current Risk Level	Response	New Risk Level
Overuse Injury	Moderate (8)	Hourly breaks, correct workstation setup and regular daily exercise.	Low (3)
Loss of internet or illness resulting in delays	Moderate (6)	Allow enough time to be flexible as required.	Low (2)
Lab booking and equipment issues	High (12)	Allow enough time to be flexible as required. Negotiate access to utilise the most suitable equipment.	Moderate (4)
Failure and or loss of experimental data	High (12)	Follow suggested techniques and methods from literature and standards to the best of my ability. Ensure samples are sufficiently labelled and stored during curing.	Low (2)
Materials are not readily available	High (12)	Secure materials as early and practicable in the project to provide enough time to find alternatives as required.	Moderate (4)
Insufficient time to analyse results	Low (3)	Time management through the life cycle of the project	Low (1)
Insufficient time to prepare presentation	Low (3)	Time management, summarise information for the 10-minute presentation window.	Low (1)

APPENDIX C – CONSEQUENCES AND ETHICS

The project seeks to provide base knowledge in the development of a more sustainable construction material. Successful results may encourage future researchers to study the use of a more environmentally friendly ECC. High fly ash ECC can divert the coal by-product from landfill and provide a construction material with superior ductility. Locally available sand and recycled PET could help to further reduce the environmental and economic impacts of conventional high fly ash ECC. The use of locally available sand removes the need and transport of processed ultrafine silica sand (USS) and PET substitution can reduce the quarrying needs of sand while diverting PET plastics from landfill.

As a future engineering professional, it is important to demonstrate integrity, practise competently, exercise leadership and promote sustainability (Code of Ethics and Guidelines on Professional Conduct, 2019). Ethical issues in this project can be avoided by:

Demonstrating Integrity – By presenting all findings, conclusions, and recommendations as the result of the author’s own work unless properly recognised. The project seeks to conduct research objectively and in a professional manner while adhering to the UniSQ academic integrity policy.

Practising Competently – By developing the testing methodology from past literature and relevant professionals. All work, conclusions and interpretations from the project should not be misrepresented as anything but those of the student engineer.

Exercising Leadership – By making reasonable efforts to communicate honestly.

Promoting Sustainability – By carrying out the project and objectively evaluating the mechanical performance of a new ECC containing locally available and recycled materials.

APPENDIX D – MATERIAL TEST REPORT



**MILLMERRAN
FLYASH**
SUSTAINABLE STRENGTH

STANDARD FLY ASH CERTIFICATE

FINAL
Prior Reports: None

Independent Flyash Brokers Pty Ltd
Head Office
431 Moffatt Reserve
Millmerran QLD 4357
Tel : (07) 4695 6033
Fax: (07) 4695 6133
www.mflyash.com.au

Product being certified: Independent Flyash Broker Monthly Grab Fly Ash

Product sample date: 18-Jul-2022

Sample Identification: Sample Code: 22070960

Source Power Station: Millmerran Power Station

Sample Condition: Tested as Received. Testing Commenced on 22-Jul-2022

Certifying Laboratory: Cement Australia - Darra Laboratory,
18 Station Avenue, Darra Queensland 4076 Australia.

Certificate Number: CERT223391

Issued: 08 August 2022

Test Results

Test	Moisture %	Fineness @ 45 micron % Passed	Loss on Ignition %	Sulfuric Anhydride %	Available Alkali %	Chloride Ion %	Chemical Composition %
Result	< 0.1	85	0.2	0.1	Not Tested	< 0.002	94.5
Test Method	AS3583.2	AS3583.1	AS3583.3	AS2350.2	AS3583.12	AS3583.13	AS2350.2
AS 3582.1	0.5 % Maximum	75% Minimum	4.0 % Maximum	3.0 % Maximum	-	0.1 % Maximum	70% Minimum

Test	Relative Density	Relative Water Requirement %	Strength Index 7 Day Acc. %	Reference Cement Details
Result	1.98	95	91	Identification: 22071012 Source: Goliath GP
Test Method	AS3583.5	AS3583.6	AS3583.6	Product Type: Type GP
AS 3582.1	-	-	75% Minimum	Sample Date: 25-Jul-22

Additional Testing - Oxides

Test	CaO by XRF %	SiO ₂ by XRF %	Al ₂ O ₃ by XRF %	Fe ₂ O ₃ by XRF %	SO ₃ by XRF %	MgO by XRF %	Na ₂ O by XRF %
Result	1.6	59.1	32.5	2.9	0.1	1.3	0.39
Test Method	AS2350.2	AS2350.2	AS2350.2	AS2350.2	AS2350.2	AS2350.2	AS2350.2

Test	K ₂ O by XRF %	SrO by XRF %	TiO ₂ by XRF %	P ₂ O ₅ by XRF %	Mn ₂ O ₃ by XRF %	Total Alkali (NaEQ) %
Result	0.68	<0.1	1.6	0.2	< 0.1	0.84
Test Method	AS2350.2	AS2350.2	AS2350.2	AS2350.2	AS2350.2	AS2350.2

This sample grade conforms to the following requirements of AS 3582.1:2016


Special	Grade 1	Grade 2
	X	

Approved Signatory



A Prem
Signatory - Cement Australia
Chemical Testing
Construction Materials Testing

Accredited for compliance with ISO/IEC 17025 - Testing
NATA is a signatory to the ILAC Mutual Recognition
Arrangement for the mutual recognition of the
equivalence of testing, medical testing, calibration,
inspection, proficiency testing scheme providers and
reference materials producers reports and certificates.



NATA
WORLD RECOGNISED
ACCREDITATION

Laboratory accreditation number: 188
Laboratory accreditation number: 187

Notes:



Figure D-1 – Millmerran fly ash testing report

APPENDIX E – EXPERIMENTAL DATA

Table E.1 – Cylinder height results

Batch	Cylinder ID	Height (mm)		Averaging			Trimmed Height (mm)
B1	T1	180	180	180			170 ± 2
	T2	185	180	182.5			
	UC1	195	197	196			
	UC2	195	195	195			
	CC1	193	194	193.5	6.89312	ST.DEV	
	CC2	195	195	195	190.333	AVG	
B2	T1	194	192	193			
	T2	193	195	194			
	UC1	190	197	193.5			
	UC2	195	193	194			
	CC1	190	190	190	2.57023	ST.DEV	
	CC2	189	190	189.5	192.333	AVG	
B3	T1	195	194	194.5			
	T2	192	190	191			
	UC1	198	197	197.5			
	UC2	197	196	196.5			
	CC1	199	195	197	2.60971	ST.DEV	
	CC2	198	196	197	195.583	AVG	
B4	T1	195	193	194			
	T2	195	195	195			
	UC1	194	197	195.5			
	UC2	198	195	196.5			
	CC1	197	198	197.5	1.78164	ST.DEV	
	CC2	198	198	198	196.083	AVG	

Table E.2 – Fresh testing

		Mix ID			
		B1 Control	B2 10%	B3 30%	B4 40%
Date		16/08/2022	16/08/2022	16/08/2022	16/08/2022
Lab Temp		21.0	23.1	20.7	22.8
Conc. Temp		22.4	22.1	22.00	22.3
Matrix mini - slump	d1= mm	395	408	415	385
	d2= mm	402	412	422	400
Matrix cone flow time	= s	22.96	22.1	46.3 (STUCK)	48.7 (STUCK)
ECC Matrix + PVA					
Fibre Dist. Time (Mixing Minutes)		11	11	13	15
ECC mini -slump	d1= mm	180	190	125	143
	d2= mm	175	185	123	146
ECC slump flow	d1= mm	525	555	530	530
	d2= mm	530	550	540	530
	t500= s	22.1	15.8	12.2	11

Table E.3 – Uniaxial tensile test data

		Waist Cross Section		Length	Residual Length	First Crack	Strain Capacity
Batch	ID	mm		mm	mm	MPa	%
B1	#1	21	25	74.9	76.3	2.8	2.2
	#2	21	25	74.7	76.2	2.8	2.8
	#3	21	25	74.8	76.1	2.5	2.1
B2	#1	21	25	75.5	75.9	3	1.8
	(Defective) #2	21	18	74.8	NA	NA	NA
B3	#1	21	24	75.5	77.3	2.4	1.8
	#2	21	25	76.5	77.1	2.7	1.7
B4	#1	21	25	76.5	76.8	2.9	1.2
	(Defective) #2	21	17	75.5	NA	2.3	0.8

Table E.4 – Splitting tensile test data

Batch	ID	AVG. DIA.	Length (mm)	Weight (Kg)	Tensile Strength (MPa)
B1-	T1	99.97	169	2.40	5.9
	T2	100.10	170	2.40	6.4
B2-	(Defect) T1	100.18	168	2.35	5.7
	T2	100.01	170	2.40	5.9
B3-	T1	100.04	170	2.40	6.3
	T2	99.91	167	2.30	5.4
B4-	T1	100.06	169	2.30	5.6
	T2	100.10	169	2.30	5.6

Table E.5 – Flexural beam properties

		Cross Section (mm)								
Batch	ID	LHS		Centre		RHS		Length (mm)	Weight (Kg)	Density
B1	Control#1	98	98	100	98	100	98	445	8.10	1870
	Control#2	100	97	100	97	100	97	445	8.00	1853
B2	10#1	95	102	95	102	95	102	445	7.65	1774
	10#2	97	99	98	100	100	100	445	8.05	1846
B3	30#1	97	103	98	103	98	103	446	8.10	1805
	(Defect) 30#2	100	101	100	101	95	101	446	7.80	1761
B4	50#1	100	100	101	101	102	100	446	7.80	1726
	50#2	102	101	101	101	100	101	446	8.25	1813

Table E.6 – Flexural beam test data

Batch	ID	Ultimate Load (kN)	Flexural Strength (MPa)	Average Strength (MPa)	ST.DEV.
B1	Control#1	16.0	8.22		
	Control#2	13.6	6.94	7.58	0.90
B2	10#1	13.2	7.08		
	10#2	13.5	6.93	7.01	0.10
B3	30#1	13.3	6.70		
	30#2	16.1	8.18	7.44	1.05
B4	50#1	12.9	6.25		
	50#2	13.9	6.68	6.5	0.30

Table E.7 – Compressive column properties

Batch	ID	AVG. DIA.	Length	Weight	Density
B1	UC1	99.98	169	2.4	1809
	UC2	100.21	169	2.4	1801
	CC1	101.04	168	2.45	
	CC2	100.55	170	2.45	
B2	UC1	100.06	169	2.4	1806
	UC2	100.13	170	2.4	1793
	CC1	100.49	170	2.5	
	CC2	100.41	169	2.5	
B3	UC1	100.07	169	2.35	1768
	UC2	100.08	169	2.35	1768
	CC1	100.55	169	2.4	
	CC2	100.70	169	2.45	
B4	UC1	99.97	170	2.3	1724
	UC2	99.98	170	2.3	1723
	CC1	101.22	170	2.4	
	CC2	100.95	170	2.4	

Note: Column weight includes GFRP wrap for confined compression (CC) specimens

Table E.8 – Compression testing results and analysis

Ductility Factor (GFRP CONFINED)						GFRP Confined			
Batch	No.	e1	e2	u	S.Dev; AVG	Batch	No.	Comp. Strength (Mpa)	S.Dev; AVG
0% PET	#1	0.006240	0.012105	1.940	0.319	0% PET	#1	33.854	0.284
	#2	0.005507	0.008194	1.488	1.714		#2	33.452	33.653
10% PET	#1	0.005689	0.015011	2.639	0.285	10% PET	#1	27.242	1.078
	#2	0.005933	0.018050	3.042	2.841		#2	28.766	28.004
30% PET	#1	0.006170	0.016287	2.640	0.181	30% PET	#1	28.415	1.174
	#2	0.005474	0.015850	2.896	2.768		#2	30.075	29.245
50% PET	#1	0.005056	0.013527	2.676	0.089	50% PET	#1	30.138	0.422
	#2	0.006636	0.018596	2.802	2.739		#2	29.541	29.839
Ductility Factor (UNCONFINED)						Unconfined			
Batch	No.	e1	e2	u	S.Dev; AVG	Batch	No.	Comp. Strength (Mpa)	S.Dev; AVG
0% PET	#1	0.007085	0.010176	1.436	0.204	0% PET	#1	34.312	0.048
	#2	0.005508	0.006319	1.147	1.292		#2	34.380	34.346
10% PET	#1	0.003902	0.009534	2.443	0.460	10% PET	#1	25.009	0.106
	#2	0.004564	0.008180	1.792	2.118		#2	24.859	24.934
30% PET	#1	0.004307	0.007415	1.721	0.118	30% PET	#1	27.568	0.228
	#2	0.004808	0.009076	1.888	1.805		#2	27.245	27.406
50% PET	#1	0.004777	0.007652	1.602	0.065	50% PET	#1	28.175	0.541
	#2	0.005143	0.007762	1.509	1.555		#2	27.411	27.793

The project plan was delayed by the availability of materials and Laboratory access. See below Table F-1, the initial plan with the additional time required.

[illegible]